ABSTRACT

TAO WU. Formation and properties of surface-anchored polymer assemblies with tunable physico-chemical characteristics. (Under the direction of Dr. Jan Genzer)

We describe two new methodologies leading to the formation of novel surface-anchored polymer assemblies on solid substrates. While the main goal is to understand the fundamentals pertaining to the preparation and properties of the surface-bound polymer assemblies (including neutral and chargeable polymers), several examples also are mentioned throughout the Thesis that point out to practical applications of such structures.

The first method is based on generating assemblies comprising anchored polymers with a gradual variation of grafting densities on solid substrates. These structures are prepared by first covering the substrate with a molecular gradient of the polymerization initiator, followed by polymerization from these substrate-bound initiator centers ("grafting from"). We apply this technique to prepare grafting density gradients of poly(acryl amide) (PAAm) and poly(acrylic acid) (PAA) on silica-covered substrates. We show that using the grafting density gradient geometry, the characteristics of surface-anchored polymers in both the low grafting density ("mushroom") regime as well as the high grafting density ("brush") regime can be accessed conveniently on a single sample. We use a battery of experimental methods, including Fourier transform infrared spectroscopy (FTIR), Near-edge absorption fine structure spectroscopy (NEXAFS), contact angle, ellipsometry, to study the characteristics of the surface-bound polymer layers. We also probe the scaling laws of neutral polymer as a function of grafting density, and for weak polyelectrolyte, in addition to the grafting density, we study the affect of solution ionic strength and pH values.

In the second novel method, which we coined as "mechanically assisted polymer assembly" (MAPA), we form surface anchored polymers by "grafting from" polymerization initiators deposited on elastic surfaces that have been previously extended uniaxially by a certain length increment, Δx. Upon releasing the strain in the substrate after completion of polymerization, we show the grafting density of the polymers grafted to flexible substrates can be tuned as a function of Δx.

Formation and properties of surface-anchored polymer assemblies with tunable physico-chemical characteristics

by

Tao Wu

A dissertation submitted to the Graduate Faculty of

North Carolina State University

in partial fulfillment of the requirements for the Degree of

Doctor of Philosophy

Chemical Engineering

Raleigh

2003

APPROVED BY:

Christine S. Grant	Saad A. Khan	Richard J. Spontak

Christopher B. Gorman	Jan Genzer
	Chair of Advisory Committee

This thesis is dedicated to my parents,

my brother Lin Wu,

my son David Sun Wu, and

especially to my wife, Xaiolei Sun,

for all their love and support

BIOGRAPHY

Tao Wu was born in Lishui, China on June 13, 1973, the second child of Changshu Wu and Lamei Liu. He attended Beijing University of Chemical Technology (BUCT) in Beijing, China in 1990, where he completed his B.S. degree in July, 1994, and M.S. degree in July, 1997, majoring in chemical engineering. The following fall, he enrolled in the M.S. program in the Department of Chemistry at California State University, Fresno in California, and transferred to the Department of Chemical Engineering at North Carolina State University (NCSU) in Raleigh, North Carolina in Aug. 1998. At NCSU, he began his Ph.D. research under the direction of Dr. Jan Genzer.

Tao met Dr. Xiaolei Sun, currently working at Akzo Nobel chemical company, in 1990. They were married in 1997, after nearly 7 years as classmates in BUCT. Their son, David Sun Wu, was born on Nov. 14, 2002 in Raleigh, North Carolina.

ACKNOWLEDGMENTS

First, I would like to acknowledge Dr. Jan Genzer, who provided his academic and technical expertise, financial resources, advice and comments throughout my Ph.D. research, and also helped me on a personal level.

I also would like to acknowledge:

Dr. Christine S. Grant, Dr. Saad A Khan, Dr. Richard J. Spontak, and Dr. Christopher B. Gorman who served as my Advisory Committee;

Dr. Petr Vlcek and Dr. Vladimír Šubr (Institute of Macromolecular Chemistry in Prague) for their assistance with the size exclusion chromatography measurements;

Dr. Sadd A Khan, for providing the access to FTIR apparatus;

Dr. Stefan Franzen group, for teaching me how to use FTIR-ATR;

Dr. Kirill Efimenko, for carrying out NEXAFS analysis;

Dr. Daniel Fischer (NIST) for his assistance during the course of the NEXAFS experiments;

Kit Yeung for his terrific mechanical expertise, for all the repair work has done for my experimental instruments;

I am equally grateful to James Semler, Rajendra Bhat, Bin Wei, Michael Tomlinson and other lab colleagues, who shared wonderful time and experiences with me.

Finally, I am eternally thankful and lucky for Dr. Xiaolei Sun, - my lovely wife, for all the love and support she has given to me over the years. Her encouragement, her patience, her positive and joyful life attitude gave me strength and confidence whenever I needed them.

TABLE OF CONTENTS

LIST OF TABLES

PAGE

LIST OF FIGURES

PAGE

Chapter 1

Introduction and thesis goal

1.1 Introduction

Over the past several years, the modification of solid surfaces with polymeric materials has received tremendous interests in a wide range of interdisciplinary fields, including chemistry, physics, biology, and nanotechnology.[1] Systems, in which molecularly thin polymeric coatings are covalently attached to surfaces, are very interesting for basic scientific studies because the properties of polymers in such a confined geometry greatly differ from those of bulk materials. If, for example, the polymer chains are tethered with one end to a surface and if the distance of the anchored polymer molecules is smaller than 2 times the radius of gyration, the conformation of the polymer molecules at the surface is completely different from that of "unperturbed" polymer molecules in solution, as first shown by Alexander and de Gennes[2] and more recently by a large number of other groups.[3,4] From a technological point of view, polymer-coated surfaces are of great interest because of their widespread use in many processes and formulations, including cosmetics, paints, paper, and water purification.[5] In recent years a rapidly growing area of research has been directed toward the development of devices that make use of a combination of the interactions between biological systems and synthetic materials to produce so-called "biosensors".[6,7]

Grafted polymer materials could be either non-charged (neutral) or charged polymers, so-called polyelectrolytes. During the last several decades, much research has been dedicated to study both theoretically and experimentally the behavior and properties of both neutral and chargeable polymers, which are either physically or chemically bound to substrates. Not surprisingly, the behavior of polyelectrolyte molecules was found to be fundamentally different from that of non-charged polymers.

1.2 Thesis goal

In this Thesis, several methodologies are developed to produce surface-anchored polymer assemblies on solid substrates. As will be demonstrated, with these techniques one can obtain material structures with tunable physico-chemical characteristics, which will be used to study the interfacial properties of surface-anchored neutral polymers and polyelectrolytes. While the emphasis of our work is to understand the fundamentals pertaining to the preparation and properties of the surface-bound polymer assemblies, several examples will also be mentioned throughout the Thesis that will point out to practical applications of such structures.

1.3 Overview of thesis

In Chapter 2 of this Thesis we will provide a review of previous studies pertaining to surface-tethered neutral polymers. Some theoretical models of surface-anchored polymers are briefly introduced, followed by the description of computer simulations and experiments using a variety of techniques. In the second part of Chapter 2, selected studies on tethered polyelectrolytes will also be summarized. Polyelectrolytes could be categorized to two subgroups: strong (quenched) or weak (annealed) polyelectrolytes. Since their behavior differs slightly, studies of their properties will be also reviewed separately. A brief description of theories on polyelectrolyte brushes is also included. Various experimental probes that have been used to probe the properties of surface-anchored polymers will also be

reviewed. The final part of Chapter 2 includes the background of ellipsometry, the chief interfacial tool used in our work, and the data analysis.

In Chapter 3 we outline the methodologies used to prepare systems comprising surface anchored polymers. Several different methods ranging from physisorption to chemisorption (so-called "graft onto" methodologies) will be described and their advantages and disadvantages will be discussed. The central part of this Thesis is to develop techniques leading to the preparation of surface-anchored polymer assemblies with tunable physico-chemical characteristics. These are all based on so-called "grafting from" techniques, which have recently been used widely to prepare tethered polymers. Using the "grafting from" methodology, tethered polymers are formed by direct polymerization from the surface to give the covalently attached polymer brushes with moderate graft densities and high molecular weights. In Chapter 3 we will outline the conventional polymerization methods used in the "grafting from" processes. Special emphasis will be given to the living radical polymerizations, as one of them, so-called atom transfer radical polymerization (ATRP), is the method of choice for all polymerization experiments described in this Thesis. We will demonstrate that due to its simplicity, robustness and the ability to synthesize polymer brushes with narrow molecular weight distributions, the ATRP is a convenient method for preparing surface-anchored polymer assemblies.

One of the goals of the Thesis is to prepare assemblies comprising surface-tethered polymers with a gradual variation of their grafting densities on solid substrates. Chapter 4 will provide a review of methodologies used to prepare such surface-bound molecular gradients. After the description of the gradient preparation techniques, we will describe experimental probes used to characterize such gradients. We will also discuss several

examples that utilize the gradually varying surface properties in templating, materials transport, studying the phase behavior in liquid mixtures, etc.

In Chapter 5, the newly-developed method for preparing gradient polymer brushes of poly(acryl amide) (PAAm) on silica-covered substrates with a gradual variation of grafting density will be described. We will demonstrate that using this technique the transition from the mushroom (low grafting density) to brush (high grafting density) regime of PAAm can be studied on one single sample. The mushroom and brush behavior will be characterized using existing scaling theories of polymer brushes.

Chapter 6 extends the finding reported for neutral brushes to situations involving surface-grafted weak polyelectrolyte, polyacrylic acid (PAA). We will show that due to the complexity of the PAA interfacial behavior, which arises from the appearance of electrostatic interactions in a charged brush, the parameter space widens relatively to neutral surface-anchored polymers. Specifically, in addition to the molecular weight and the grafting density of the polymer on the substrate, the behavior of PAA depends on the solution pH and the amount of the external salt. We will discuss the effects of the various parameters on the interfacial properties of the PAA and demonstrate that the "gradient grafting density geometry" offers a convenient means to completely probing the behavior in such complex systems.

In contrast to the situations described in Chapters 5 an 6, where the grafting density of the surface anchored polymer is tuned by using position-dependent surface gradient, the experiments described in Chapter 7 will report on yet another methodology, termed mechanically assisted polymer assembly (MAPA), which is capable of fine tuning the grafting density of surface-grafted polymer assemblies. In MAPA, poly(dimethyl siloxane)

(PDMS) network is strained and its surface is decorated with ATRP initiators followed by "grafting from" polymerization of PAAm. After the polymerization, the strain is released from the substrate, which returns to its original size, causing the grafted PAAm to form a densely packed layer. By controlling the strain on the PDMS substrate and the chemistry of the grafted polymer layer, the barrier and wetting properties of these organic substrates can be gradually changed over a wide range.

Finally, Chapter 8 provides outlook for future research and outlines possible applications of the structures, whose preparation and properties are discussed in this Thesis.

References

[1] Fleer, G. J.; Cohen Stuart, M. A.; Scheutjens, J. M. H. M.; Cosgrove, T. and Vincent, B. *Polymers at interfaces*; Chapman & Hall: London, 1993.

[2] deGennes, P. G., *J. Physique* **37**, 1445 (1976); *Macromolecules* **13**, 1069; (1980)**,** Alexander, S., *J. Physique* **38**, 983 (1977).

[3] Milner, S. T. *Science* **251**, 905 (1991).

[4] Halperin, A; Tirrell, M. and Lodge, T. P. *Adv. Poly. Sci.* **100**, 31 (1992).

[5] Dautzenberg, H.; Jaeger Halperin, A; Tirrell, M. and Lodge, T. P. *Adv. Poly. Sci.* **100**, 31 (1992).

[6] Göpel, W.; Jones, T. A.; Kleitz, M.; Lundström, J.; Seiyama, T. *In sensors, a comprehensive survey*, Göpel, W.; Hesse, J.; Zemel, J. N.; Eds.; VCH: Weinheim, 1992; Vol. 3.

[7] Ratner, B. D.; Hoffman, A. S.; Schoen, F. J.; Lemons, J. E. *Biomaterials Science, an introduction to materials in medicine*, Academic press: San Diego, 1996.

Chapter 2

Behavior of surface-anchored polymers

Polymer "brushes" are long-chain polymer molecules attached by one end to a surface or interface by some means, with a density of attachment points high enough so that the chains are obliged to stretch away from the interface much further than the typical unstretched size of an isolated chain. This situation, in which polymer chains stretch along the direction normal to the grafting surface (like the bristles in a brush, hence the name), is quite different from the typical behavior of flexible polymer chains in a solution, where the long molecules adopt random-walk configurations.[1]

The tethered polymer layers are widely used for the purpose of colloid stabilization.[2] Other applications such as adhesion,[3] lubrication,[4] tribology,[5] chromatography,[6] and rheology[7] have also been put forward. In recent years, surface-anchored polymers have also been utilized in a rapidly growing area of research directed toward the development of devices that make use of a combination of the interactions between biological systems and synthetic (or modified natural) materials to produce a so-called "biosensor".[8,9]

This chapter provides a brief review of theoretical and experimental studies of tethered polymers.

2.1 Neutral surface-anchored polymers in good solvents

Polymer brushes, with some important variations, are one central model in many important problems in polymer science, and are relevant even in biophysics and surfactant science (where the chains in questions are only marginally long enough to be called

polymers). One of the most important variations among brushes is the presence or absence of solvent for the polymer chains. With solvent present, the physical reason for the chains stretching away from the interface to which they are attached is their affinity for the solvent (and/or dislike of each other). For melt conditions (no solvent present), the chains must stretch away from the interface to avoid overfilling space (since the matter of which the chains are made is approximately incompressible).

The interface to which the chains in the brush are attached may be a solid substrate or the interface between two solvents, between solvent and air, or between melts or solutions of homopolymers. The mechanism by which the chains are attached to the interface varies depending on the nature of the interface. For solid substrates, the chain ends may be chemically bonded to the substrate or the chains may be terminated by a special chemical group that physically adsorbs onto the surface. This end group may be either a small molecule that is strongly attracted to the surface, or a long copolymer adsorbing block, each monomer of which experiences a relatively weak attraction to the substrate. For interfaces between fluids, the attachment may be achieved by similar adsorption mechanisms in which the end group of the chain prefers one medium and the chain prefers the other. Finally, the chain may be attached to a "substrate" that is the narrow interface between microdomains in a melt or concentrated solution of diblock copolymers (two dissimilar polymers joined end to end) when the two blocks of the copolymer are strongly segregated.

2.1.1 Theoretical models and simulations

Theoretical analysis of polymer brushes grafted onto a flat surface and immersed in a good solvent was first carried out independently by Alexander[10] and de Gennes[11]. For tethered chains in a good solvent, the interplay of two terms, the interaction energy per chain, F_{int} and the elastic free energy, F_{el}, sets the equilibrium thickness of the layer[12]. By stretching the chains along the normal to the grafting sites thus increasing the layer thickness, H, polymers lower the monomer concentration in the layer (F_{int} decreases) at the price of a higher F_{el}.

The Alexander model considers a flat, nonadsorbing surface bearing monodisperse tethered chains of N monomers, each of diameter a. The average separation between chains at the tethering surface, d, is much smaller than the radius of a free, undeformed chain. The free energy per chain comprises two terms:

$$F = F_{\text{int}} + F_{el} \tag{2.1}$$

The Alexander model[10] is based on two assumptions that enable simple expressions for these two terms: (1) The concentration profile of the layer is step-like. (2) The chains are uniformly stretched. By employing the Flory argument, the first term F_{ini} accounts for binary interactions between monomers, while the second F_{el} for the elasticity of the Gaussian chains. By minimization of F with respect to wet thickness, this model gives:

$$w\sigma h^2 / N \sim (N\sigma / h)^2 \text{ or } H \sim N(w\sigma)^{1/3} \tag{2.2}$$

where h is the dry brush height, H is the equilibrium wet brush height, σ the surface grafting density (= number of polymer chains per unit area), and w the excluded-volume parameter.

The deGennes approach[11] accounts for the effects of the excluded volume correlations and self-avoidance by use of scaling arguments. The polymer layer is envisioned as a close-packed array of blobs of a uniform size $\xi \sim \sigma^{-1/2}$ normal to the grafting surface, as shown in figure 2.1.

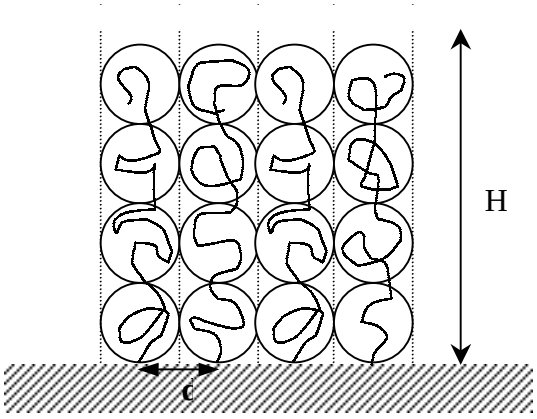

Figure 2.1 Schematic of a flat, tethered layer. H is the average layer thickness while d is the average spacing between chain graft points on the surface.[12]

The radius, ξ, of correlations of the blobs in the stretched, semidilute solution must be on the order of the distance between grafting points, in the limit $R_g \sim N^{1/2} >> \sigma^{-1/2}$, under good solvent conditions. Each blob is assigned a free energy of kT. In this view, F_{ini}/kT equals the number of blobs per chain, where each blob contains $g \sim \xi^{5/3}$ monomers. The elastic free energy is modified as well by recognizing that in a semidilute solution, the chain is Gaussian at large scales, but with the subunits being the excluded volume blobs. Consequently, the F_{el}

term is concentration dependent, in contrast to the Flory argument. This model leads to the following scaling for H:

$$H \sim N\sigma^{1/3} \tag{2.3}$$

The Flory argument is expected to be valid for a high density of weakly interacting chains; scaling conditions obtain in the opposite limit or a semidilute solution. Both the Flory and the scaling arguments suggest a step-function density profile for the brush: each assumes that any chain behaves in a manner identical with every other. More recent work[13,14,15] has shown that these simple scaling arguments miss several important features of the brush, namely, (1) the conformations of different chains in the brush are not necessarily similar, nor is a particular chain uniformly stretched, (2) the density profile, rather than being nearly a step function as was suggested, is instead parabolic, and (3) because the density profile goes continuously to zero at the outer extremity of the brush, the force to compress the brush slightly is weaker (by one power of the strain) than calculated by using a step-function ansatz profile.

Theoretical studies of surface-anchored polymers with self-consistent field (SCF) approximation[15] are more realistic relative to the scaling methodologies. This method makes no assumption about the monomer density profile, but determines it self-consistently. In their model, Milner et al exploited the fact that the chains are strongly stretched to find the exact asymptotic density profile in the limit of long chains. In contrast to the step function profile predicted by the scaling models, the SCF brush profile is found to be parabolic. Moreover, the free ends of the chains are distributed through the entire height of the brush, rather than confined to a narrow zone at the outer extremity, as postulated by the scaling

models. In spite of these difference between the scaling and SCF models, the scaling laws connecting molecular weight and graft density with the brush height determined by the SCF approach are similar to those offered by the simpler scaling methodologies:

$$H = (\frac{12}{\pi^2})^{1/3}(\sigma w)^{1/3} N \text{ or } H \sim N(\sigma w)^{1/3} \quad . \tag{2.4}$$

This corresponds to a polymer brush profile:

$$\phi(z) = (B/w)(H^2 - z^2) \tag{2.5}$$

where $B=\pi^2/8N^2$.

Recent studies[16,17,18,19,20] with SCF theory give more details on the structure of polymer brushes, scaling behavior and other properties, as a function of the grafting density and solvent conditions.

Computer simulations have also been performed to explore and test the density profile of terminally anchored polymer chains. With molecular dynamics simulation, Murat and Grest[21,22] studied the behavior of end-grafted polymer brushes in good solvents for a range of surface coverage. They found that while for intermediate values of the surface coverage the monomer concentration profile approached a parabolic form, increasing the coverage led to flattening of the density profile relative to the simple parabola.

Monte Carlo simulations of Chakrabarti and Toral[23] examined the density profile of grafted polymer chains on a three-dimensional lattice for several different values of the surface coverage and the chain length. They found that for monodisperse chains density profile showed a depletion layer near the grafting plane, in agreement with

phenomenological theories. Beyond this depletion layer, the density profile can be represented by parabolic form, in agreement with SCF calculation.

The scaling laws mentioned above are applicable in situations that involve relatively concentrated polymer brushes, where the mean distance d or $\sigma^{-1/2}$ between anchor points is smaller than the Flory radius, ξ. This regime is so-called brush regime. However, when the mean distance d is large compare to the Flory radius, or at the very low surface grafting density, the chains enter so-called "mushroom" regime. For surface polymers in the mushroom regime, the interactions between polymers are negligible and the polymer thickness is independent of the chain graft density. In a good solvent, the scaling law becomes:

$$H \sim R_g = a\left(\frac{N}{6}\right)^{3/5} \sim \sigma^0 \tag{2.6}$$

The scaling arguments have been used to distinguish between these two regimes. Moreover, an "extended mushroom" conformation was observed even at very low grafting densities, with a broad mushroom-to-brush transition. Recently, Rex et al.[24] combined affinity of binding measurements and Monte Carlo simulations to study the structure of poly(ethylene glycol) (PEG) layers. They have concluded that the chains are in the mushroom regime even when the distances between the grafting points are well below the Flory radius, a finding that seems to support the existence of a broad mushroom-to-brush transition.

Compared to high molecular weight polymers, which have been used mostly in previous theoretical studies, surface grafted short chain polymers have also been studied. Kuhl et al.[25] have modeled force profiles between two PEG-containing bilayers using the

Dolan and Edwards[26] theory for the "dilute mushroom" regime and the Alexander-de Genes model for the brush regime and concluded that these theories could be applied to systems of short chains. Szleifer argued that the analytical self-consistent mean field and the scaling theories are not valid for systems of short chains. His theoretical single-chain, mean field calculations have shown that the brush thickness agrees with the predictions of the analytical theories, probably due to lack of sensitivity to the assumption of infinitely long chains. However, these predications do not hold to other thermodynamic properties, such as osmotic pressure in the layer.

Polymer brush profile studies with direct numerical solution of the mean-field equation of Dolan and Edwards have also been extensively performed by Scheutjens and Fleer[27] and collaborators[28] and other groups[29,30]. The theory of Scheutjens and Fleer (SF)[27,31] is potentially the most comprehensive and wide ranging in its applicability, such as curved geometries, polydisperse chains, brushes in presence of homopolymer, adsorbing copolymers, and other problems.

2.1.2 Experimental probe of equilibrium polymer brushes

Properties of polymer brush, including thermodynamic, kinetic, structure and dynamic, are commonly investigated in both theoretical and experimental studies[32]. Due to the specific interests of this thesis, the following review will mainly focus on experimental systems involving end-grafted polymer brushes at equilibrium in good solvent conditions.

A typical system of this kind comprises three components: polymer, solvent, and the surface. There are several ways of forming an interfacial polymer layer between the solvent and the surface. These include 1) physisorption of either homopolymers or block copolymers, where one block is strongly adsorbed to the surface and the other block forming the brush layer[33]; 2) "grafting-onto" techniques, in which end-functionalized polymers are adsorbed from solutions and reacted with appropriate surfaces sites[34]; and 3) "grafting-from" techniques, in which the polymers are generated from polymerization initiators residing directly at the surface[35]. More detailed review about these different techniques will be introduced in chapter 3.

2.1.3 Selected experimental studies

Surface force measurement

The force-balance technique by using the surface forces apparatus developed by Israelachvili and Adams[36] represents a powerful and straightforward method for probing the structure of brushes. With this instrument, forces are measured between two cylindrically curved sheets of musco-size mica (radius of curvature ≈1 cm), the cylinders being oriented at right angles to one another. The Derjaguin approximation[37] transforms the measured force into the equivalent interaction energy per unity area of parallel plates at this same separation. The force-balance technique gives a rough measure of the brush height by measuring the force as a function of the separation between the two solid surfaces. By varying the molecular weight and/or grafting density, force-balance technique would allow for testing of

the scaling laws, although the measurements of the grafting density on mica substrates has proved rater laborious and difficult.

Several groups have measured the forces between polymers end-adsorbed onto mica; the adsorption has been achieved with two different methods. In the first case, the polymers were attached to the substrates with end-functional groups, such as zwitterionic[38,39]. The other more commonly used method is by using block copolymers with one adsorbing and one non-adsorbing block[40,41,42,43,44,45,46]. Recently, atomic force microscopy (AFM) has also been used in to probe the structure of surface-anchored polymers by measuring the force between the polymers and the AFM tip.[47]

The direct force measurements confirmed that under suitable solvent conditions block copolymers adsorb with one block compact and tightly bound and one extended, swollen block stretching away from the surface. These results also agreed quantitatively with the predictions of the scaling models.[l0,11] For terminally anchored block copolymers in a good solvent, the two regimes, "mushroom" and "brush" regimes were also anticipated depending on the grafting density. At high grafting density, force measurements were not sensitive to differences between the parabolic profile predicted by mean field theory and the step function assumed by Alexander and de Gennes.

Some other useful methods could be employed to explore the adsorbed polymers. Cohen Stuart et al[32] and Fleer et al[33] had a valuable review on hydrodynamic methods, electrochemical methods, and disjoining pressure methods.

Spectroscopic and scattering methods

Experiments involving scattering techniques have also been used to investigate the structure of end-grafted polymer systems. These include ellipsometry[48,49,50,51], evanescent-wave fluorescence[52,53], infrared spectroscopy[54], multiple-reflection interferometry[55,56], neutron reflectivity[57], neutron scattering[58], small angle neutron scattering (SANS)[59,60,61], second harmonic generation[62,63], and x-ray fluorescence[64,65] methods. These techniques have been used to determine the extension of the copolymers from the surface and the total number of molecules adsorbed onto the surface (=1/σ).

Optical techniques like IR spectroscopy, evanescent-wave fluorescence, X-ray fluorescence, and second harmonic generation can yield important information about the total amount of polymer adsorbed onto the surface. But these techniques lack the resolution necessary to describe the concentration profile of polymer segments near the surface[66]. Neutron scattering provides more complete data on the polymer density profile within adsorbed layers. Neutron reflectivity (NR) and SANS are typically the techniques of choice. NR experiments provide information on the neutron refractive index profile normal to the reflecting interface and can thus probe the composition of surfaces and interfaces. Some early experiments using NR to investigate the segment density profiles were applied to solid films[67,68], liquid-air interface[69], and liquid-solid interface[70,71]. Because they work in the reciprocal space, both NR and SANS are fraught with complexities in data interpretation[72]. Nevertheless, they can provide information about the structure of the concentration profile of end-anchored polymers.

A part of this thesis will be devoted to testing the scaling laws of mushroom and brushes using a new multivariant methodology. In this technique, we will prepare a molecular gradient of polymerization initiator on the solid substrate. We then carry out the polymerization from the substrate bound initiator centers ("grafting from"). Two neutral polymers, poly(acryl amide) (PAAm) and poly(*tert*-butyl acrylate) (PtBA), will be investigated. With this set up we are able to probe both the "brush regime" (dense polymer layer) as well as the "mushroom regime" (loose polymer layer) and for the first time determine character nature of the "mushroom-to-brush" transition on a single sample.

2.2 Charged surface-anchored polymers

A simple polyelectrolyte may be defined as a homopolymer, whose at least one monomer unit carries an ionizable group.[33] Such a group may be a strong salt, acid or base, so that its charge is virtually independent of pH (strong or "quenched" polyelectrolyte). In contrast to the strong polyelectrolytes, weak or "annealed" polyelectrolytes carry weakly acidic (e.g. carboxylic) or basic (e.g. amino) groups; their solution behaviors depends on pH. In this chapter we will describe the properties of strong and weak polyelectrolyte brushes.

First, why are polyelectrolytes so important? One reason is to understand polyelectrolyte film surfaces; this is important in applied science, where the use of adsorbed polyelectrolytes is ubiquitous. Practical ramifications of these questions have additional obvious implications for numerous industrial processes that rely on the properties of polymer

surfaces. Examples from the chemical biotechnology and food industries include stabilization and rheology of colloidal dispersions (paints), food emulsions (dairy products), coating of fibers in paper industries, wastewater treatment, mineral processing, and chromatographic separations. There are also evident connections to understanding the physics of charged bimolecular, charged proteins, and nucleic acids, cell attachment onto surfaces (cell growth separation), and ramifications in applications such as blood clotting and immunoadsorption. Second, it is important for scientific reasons to understand the formation of polyelectrolyte thin films, their stability, and a response to an outside change of their environments. Intuition concerning uncharged polymers is rather difficult to extend to charged systems. Third, understanding and tailoring the behavior of charged molecules at surfaces and interfaces is important in designing and utilizing novel applications (e.g., pH-controlled flow through polymeric micromembranes), many of which cannot be fabricated using any other set up.

Compared to the behavior of neutral polymer brushes under various conditions, which is rather well understood[73], polyelectrolyte brushes have been investigated to a lesser extent. This is due to the quite complexity of the system, which arises from the appearance of electrostatic interactions in a charged brush, rather only thermodynamic interaction for neutral polymers. Specifically, in addition to the parameters governing the performance of neutral polymer bushes, i.e., polymer molecular weight, N; brush grafting density, σ, and the solvent quality (characterized by the Flory-Huggins interaction parameter, χ), the properties of polyelectrolyte brushes depend strongly on the degree of dissociation of the charge groups

(or degree of dissociation), α; counterion volume fraction in the polyelectrolyte solution, φ_s; counterion valency, q; and in some cases also pH of the solution.

Various theoretical approaches have been utilized to describe the performance of charged macromolecules at interfaces. Scaling theories pioneered by Pincus[74], Zhulina and coworkers[75,76], and the Wageningen group[33,77,78,79] laid the foundation of our current understanding of polyelectrolyte brush behavior. These studies revealed that depending on σ, N, q, pH (if applicable), and φ_s several different regimes of polyelectrolyte brushes can be identified. More detailed information about the structure of the brush has been obtained through more sophisticated methods based on numerical self-consistent field (SCF)[76,77,79,,80,,81] and analytical SCF theories[75,79,82].

2.2.1 Strong polyelectrolytes

Since strong polyelectrolytes have a fixed fraction of charged monomers (quenched), the performance of quenched polyelectrolytes is relatively easy to describe.

We mainly will discuss the behavior of strong polyelectrolytes immersed with monovalent salt ions. In Figure 2.2 we plot the dependence of the polymer height (normalized by N) as a function of the external salt concentration. At high φ_s the salt concentration inside and outside the brush is about the same and the electrostatic interactions are largely screened. Under such conditions the polyelectrolyte brush behaves exactly as a neutral brush (NB), or follows the scaling laws of neutral brushes $H \sim N(v\sigma)^{1/3}$, where v

(=0.5-χ) is the excluded volume parameter. In this NB regime, polyelectrolyte thickness is independent of ion-strength of solution.

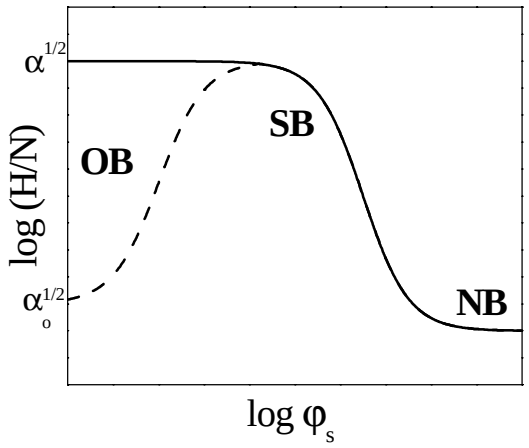

Figure 2.2 Dependence of the brush thickness reduced by the number of polymer repeat units for **monovalent coions**, H/N, on the concentration of the external salt, φ_s, for strong (solid line) and weak (dashed line) polyelectrolyte brushes in neutral brush (NB), salted brush (SB), and osmotic brush (OB) regimes. α and α_o denote the bulk and "internal" (for weak polyelectrolyte brushes only) degree of dissociation, respectively.

When the external salt concentration decreases, there is an unbalance in the ion concentration inside and outside the brush because the polymer charge density inside the brush ($\alpha\varphi$, where φ is the polymer volume fraction) is no longer negligible with respect to φ_s. The system enters the salted brush (SB) regime. In the SB regime, the scaling relationships for the height are:

$$H \sim N(\nu_e \sigma)^{1/3} \tag{2.7}$$

where ν_e ($=\alpha^2/4\varphi_s$) is the electrostatic excluded volume parameter. Due to the electrostatic interactions inside the brush a salted brush is more extended than a neutral one. As schematically shown in Fig. 2.2, the brush expansion increases with decreasing φ_s.

If the external salt concentration is further decreased such that $\varphi_s << \alpha\varphi$ the counter-ions are effectively expelled from the brush and

$$H \sim N\alpha^{1/2} \tag{2.8}$$

In this so-called osmotic brush (OB) regime limiting brush thickness is reached, which is independent of φ_s and σ.

Both negatively charged polyelectrolyte (e.g. polystyrene sulfonate sodium salt PSSNa, polystyrenesulfonic acid PSSH) and positively charged polyelectrolytes (e.g. poly(4-vinyl-N-n-butlypyridinium) bromide BuPVP, poly(N-methyl-4-vinylpyridinium iodide) MePVP have been investigated experimentally. PSSNa and PSSH can be readily prepared by sulfonating originally neutral polystyrenes. BuPVP and MePVP are usually prepared by quanternization of P2VP or P4VP.

Several experimental techniques, which had been used successful to study neutral polymer brushes, are also applied to polyelectrolyte brushes. Among them, direct force measurement[83] was applied to PSSNa brush by atomic force microscopy. Using small angle neutral scattering, Mir et al.[84] obtained segment density profiles of PSSNa of "medium" and "high" grafting densities in pure water as well as salt solutions. X-ray reflectivity measurements[85,86,87,88] were also employed to probe the structure and scaling laws of polystyrene sulfonate brush. Recently, Biesalski and Rühe[89,90,91] in a series of papers

described the preparation of MePVP (or BuPVP) brushes by "grafting from" polymerization and quanternization and their characterization by optical wave guide spectroscopy and ellipsometry.

2.2.2 Weak polyelectrolytes

The behavior of weak polyelectrolyte brushes is different from that of strong polyelectrolytes. Here the number of the backbone charges is not fixed. Specifically, α depends on the proton concentration in the polymer solution, $[H^+]=10^{-pH}$, and is given by:

$$\frac{\alpha}{1-\alpha} = \frac{K}{[H^+]} \tag{2.9}$$

where K is the dissociation constant. When there is an excess of salt ($[S^+]>>[H^+]$), as in the neutral brush (NB) and salted brush (SB) regimes, $[H^+]$ inside and outside the brush is approximately equal and the internal degree of dissociation is the same as that in the bulk solution. That is because the dissociated protons in the brush are exchanged with indifferent salt ions from the bulk while maintaining electroneutrality in the brush. Hence, the scaling for H/N in the NB and SB regimes is the same as in the case of strong polyelectrolyte brushes. Mean-field models predict the scaling relationships of the height to be[75]:

$$H \sim N\sigma^{1/3}\left(\frac{\alpha^2}{[S^+]}\right)^{1/3} \tag{2.10}$$

However, in the limit of zero salt concentration or osmotic brush (OB) regime, a significant electric potential difference develops between the brush and the bulk solution. In addition, $[H^+]$ inside the brush is considerably higher. As a consequence, a portion of the brush charges associate with protons. As a result:

$$\frac{\alpha_0}{1-\alpha_0} = \frac{K}{\sigma\alpha_0^{1/2}} \tag{2.11}$$

where α_o is the "internal" degree of dissociation. This value of α_o may be much smaller than the value in the bulk (α); the weak groups respond to the unfavorable electrostatic condition in OB by discharging themselves. Such a response is, obviously, impossible for strong brushes, which have a fixed α. Figure 2.2 demonstrates the different behavior of weak polyelectrolyte brushes in the OB regime. Because of the discharging process ($\alpha_o<\alpha$), a weak brush in the OB regime is less expanded than the strong brush. The brush height in the OB regime is predicted to scale as[75]:

$$H \sim N\sigma^{-1/3}\left(\frac{\alpha}{1-\alpha}\right)^{1/3}([H^+]+[S^+])^{1/3} \tag{2.12}$$

A simple scaling model predicts that the brush thickness in the OB regime may decrease with increasing grafting density or increase with increasing salt concentration. With increasing salt concentration, however, the brush enters the salted brush regime. In this regime, the rush thickness is predicted to decrease with increasing salt concentration. As a result, H/N passes through a maximum as a function of φ_s, being small for both high and small φ_s, provided the pH and grafting density remain constant.

Despite strong theoretical interest in weak polyelectrolyte, only a few experimental realizations of such systems have been reported in the literature. Two typical experimental probed weak polyelectrolyte function groups are carboxyl group (e.g. poly(acrylic acid) PAA, poly(methacrylic acid) PMAA) and dimethylamino group (poly(2-dimethylamino)ethyl methacrylate PDMAEMA). Using neutron reflectivity, An et al[92,93] studied the properties of PDMAEMA at air/water interface and affects of pH, ionic strength. The brush thickness at fixed grafting density was found to increase with increasing pH. However, the results were not compared with any scaling law for annealed brushes in OB regime. The surface forces between monolayers of anchored PMAA chains were measured by Kurihara and Kunitake.[94] It was observed that the repulsive forces between two grafted polymeric monolayers increased with increasing salt concentration. PAA brushes were investigated experimentally using surface pressure isotherms and ellipsometry.[95,96] Three different grafting density samples were measured at three low pH solutions by changing ion strength of solutions. They found the PAA brush thickness is nonmonotonic as a function of the ionic strength at a given pH and grafting density. The extent of swelling increases with increasing pH and grafting density. Even, the nonmonotonic behavior agrees qualitatively with theoretical predictions, the mean-field power laws for the OB regime at a given pH and σ was not observed. Due to the noncovalent nature of this grafting strategy in their experiments, the PAA chains are (partially) desorbed in a brush-like conformation. The importance of polyeletrolytes in biology has also motivated the studies of protein brush properties, such as those based on poly(L-glutamic acid) (PLGA).[97,98]

Since the lack of experimental studies on weak polyelectrolyte, we are devoted to probe this system more systematically and detailed with the help of our new developed

techniques: First, we are going to form a molecular gradient of polymerization initiator on the solid substrate; Second, polymerization of poly(tert-butyl acrylate) (PtBA) from the substrate bound initiator centers ("graft from "); Third, hydrolysis of PtBA produces poly(acrylic acid) (PAA) brushes with a gradual variation of grafting density. We are going to examine the gradient PAA brushes at three different pH solutions with the change of solution ion strength.

2.3 Neutral and charged polymers investigated with ellipsometry

Ellipsometry method has been applied to study the thickness of polymer layer in both neutral and charged polymer brushes. Since the ellipsometry method is one of our major techniques to characterize our polymer brushes in air ("dry" brush) and in solution ("wet" brush), next section outlines a detail description of ellipsometry and its applications in determining the thickness of surface-grafted polymer layers.

2.3.1 Theory of ellipsometry

In ellipsometry[99], polarized light is impinging on to a sample surface at an oblique angle of incidence. The change in polarization of light reflected parallel (p) and perpendicular (s) to the sample surface is measured. This allows the relative phase change (Δ) and relative amplitude change (ψ) from the reflected surface to be determined.

Ellipsometry can be used to measure film thicknesses; dielectric properties can also be estimated by varying the wavelength of the incident light. A schematic of an ellipsometer is shown in Figure 2.3.

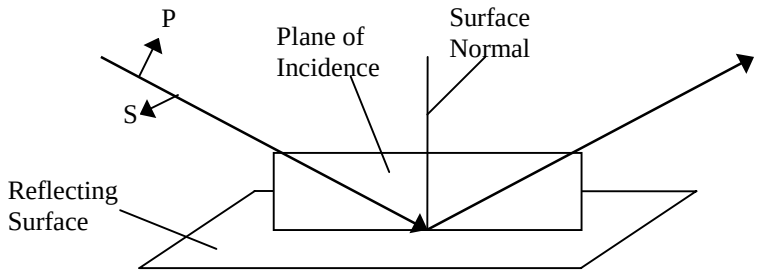

Figure 2.3 Schematic description of ellipsometry.

The phase change Δ can be determined from:

$$\Delta = \delta_p - \delta_s \tag{2.13}$$

where δ_p and δ_s are the phase differences between the parallel and the perpendicular components, respectively, upon reflection.

The amplitude of both the perpendicular and parallel components may change upon reflection. By setting $|R_p|$ and $|R_s|$ as the ratios of the outgoing wave amplitude to the incoming wave amplitude for the parallel and perpendicular components, respectively, we can define Ψ:

$$\tan\Psi = \frac{|R_p|}{|R_s|} \tag{2.14}$$

The fundamental equation for ellipsometry is then:

$$\rho = e^{i\Delta} \tan \Psi = \frac{R_p}{R_s} \tag{2.15}$$

where Δ and Ψ are the quantities measured by an ellipsometer. Because of the nature of the inversion problem, knowledge of Δ and Ψ are is not sufficient for unambiguous determination of the material's index of refraction (n) and film thickness (t). One usually proceeds by assuming certain input values for n and t and uses Fresnel equations to solve for Δ and Ψ. The calculated Δ and Ψ are then compared to the experimental values. This procedure is repeated until a satisfactory agreement between the calculated and the experimental Δ and Ψ is found. The corresponding values n and t used in the final iteration are then proclaimed to be the "true measured" index of refraction ad thickness, respectively.

2.3.2 Instrumentation for ellipsometry

A basic instrument of ellipsometry consists of 1) a monochromatic light source; 2) an optical element to convert unpolarized light to linearly polarized light; 3) an optical element that converts linearly polarized light into elliptically polarized light; 4) a reflection from the sample of interest; 5) an optical element to determine the state of polarization of the resultant light beam; 6) a detector to measure the light intensity (or to determine the presence of a null); 7) Calculation facilities to interpret the results in terms of an assumed model of the sample.

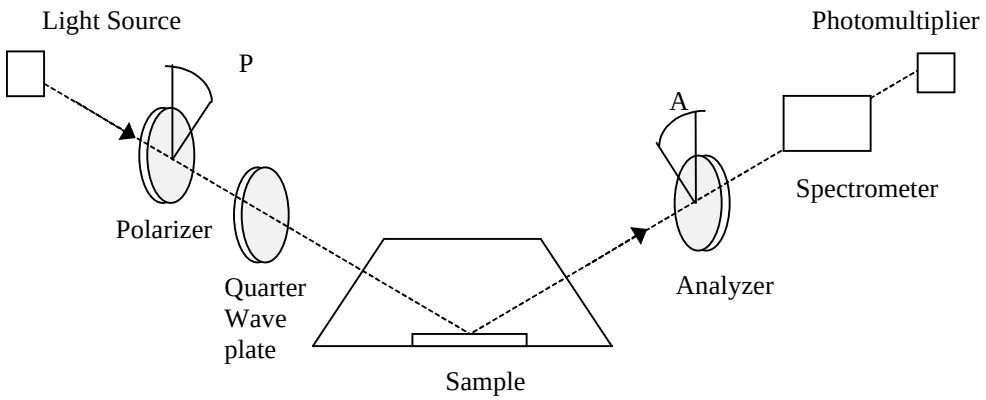

Figure 2.4 Fundamentals of the instrumentation for ellipsometry

The dry polymer thickness could be measured directly with basic ellipsometry set up. In order to measure the wet thickness of polymer brush grafted on solid substrate (polymer brush under solution), the sample is placed into a liquid cell. Two side trapezoidal quartz windows are built at the angle perpendicular to the incidence and reflection light directions. Solution level in the liquid cell must be filled over side windows to eliminate the light refractive affects due to air to liquid phase change.

2.3.3 Thin film measurements with ellipsometer

Ellipsometers can be used to measure film thicknesses ranging from a few molecular layers to up to 20-40 μm with a typical accuracy of $< \pm 5\%$. Evidently the meaning of such measured values depends on the degree to which the real film and substrate correspond to the

assumed model of perfectly flat and parallel films of zero absorption. For non-ideal cases, such as surface roughness and film scattering, models could be applied for the correction.

Modeling the thickness of polymer brushes in air (dry thickness) is relatively straightforward. Because polymers are collapsed on the substrate, only one homogeneous polymer layer is needed in the model, where the structure and refractive index of substrates are predetermined. The refractive index of polymer brush can be assumed to be close to bulk polymer refractive index, which is widely available for most polymers.

Determining the polymer brush thickness in solutions is more complicated. Figure 2.5 shows a multilayer model for a polymer absorbed on silica surface under solution. The (complex) refractive index of silicon under layer, n_3 and dielectric SiO_2 layer, n_2 are known. The thickness of the SiO_2 layer, d_2, is constant and can be readily measured before polymer absorption. The ambient layer or solution layer could be measured directly[100], estimated close to water refractive index n_{water},[101] or estimated as a mixture of all solution components by using following equation[102]:

$$n_0 = n_{water} + \left(\frac{dn}{dc}\right)_s c_s + \left(\frac{dn}{dc}\right)_p c_p \tag{2.16}$$

where n_{water} is the refractive index of pure water, $(dn/dc)_x$ is the refractive index increment of species x in water, and c_x is the concentration of species x. The subscripts s and p in the equation refer to salt and polymer, respectively.

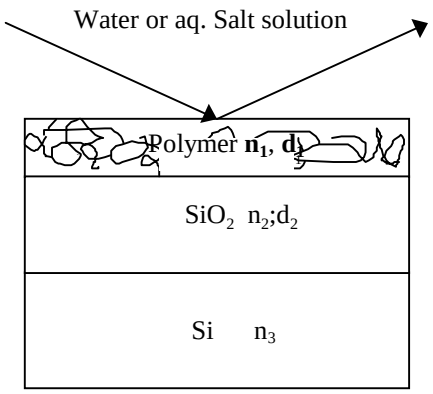

Figure 2.5 Multilayer model of adsorbed homogeneous polymer layer on silica used for data analysis.

The polymer brush layer in this multilayer model is the most complicate and important layer, because it directly reflects on the polymer density profile on substrate surface. From the review above, previous theoretical predications and direct experimental measurements show that the density profiles of polymer brushes under a good solvent could vary from step-like to parabolic-like. Hence, several typical models can be employed in determining the thickness of the grafted polymer layer on the substrate.

I: The box model A simple way to model the polymer brush layer is to assume that it is a homogeneous mixture of polymer and solution, or a layer with refractive index n_1 and thickness d_1. Then Δ and Ψ could be calculated for the multiplayer model depicted in fig. 2.5 using a well-established optical matrix formalism.[103] A reasonable value of n_1 is assumed and a value of d_1 is found that minimized the difference between the calculated and experimental Δ and Ψ. The box model has been used for study neutral brush[100,104,105], strong polyelectrolyte[102], and recently weak polyelectrolyte[95,96].

II: The parabolic model The parabolic profile for polymer layers has been predicted by the polymer brush theories. Biesalski et al[89,90,91] used complementary error functions as a close estimate:

$$\varphi(z) = \frac{1}{2}\left(1 - erf\left(\frac{z-d}{w}\right)\right) \tag{2.17}$$

where φ is the polymer volume fraction, z is spatial coordinate normal to the surface, d is the point of inflection, and w is a measure of the smoothness of the outer edge. For box profiles the parameter w approaches zero.

A comparison of the box and the parabolic models reveals that the box model is simpler and easy to apply and the parabolic model is more complex but closer to real polymer density profile. Extensive testing with different model functions by Biesalski et al[91] shows that the derived thickness of polymer layer does not depend critically on the choice of the model.

III: Graded effective medium approximation model An effective medium approximation (EMA) layer provides a method to mix 2 or 3 sets of optical constants together. The simplest EMA is to simply linearly interpolate between the constituent optical constants, as shown in equation 2.18:

$$n = \varphi_1 n_1 + \varphi_2 n_2 + \varphi_3 n_3 \tag{2.18}$$

where n is the refractive index of the mixture, φ_1, φ_2 and φ_3 are the volume fractions (ranging from zero to one) of each constituent material. And n_1, n_2 and n_3 are the refractive index of the constituent materials. The volume fractions must be total unity. For two constituent

EMA models if φ_3 is fixed at zero. The linear interpolation EMA is not highly accurate, but is often used for graded layers to reduce calculation time. For the above model I and model II, they are essentially using EMA for the fitting. In model I, there is one EMA layer. In model II, there are multiple EMA layers. Except linear interpolation EMA, the Maxwell-Garnett and Bruggemann EMAs are also the most common, and can be used to model a wide range of mixing effects such as surface and interfacial roughness[106].

Graded EMA layer could be used to simulate a layer which is inhomogeneous in the direction perpendicular to the sample surface. The graded layer works by creating a series of homogeneous layers with optical constants that change slightly in each layer. Each of these piecewise constant layers is called a "slice". For each slice, the refractive index is calculated with EMA optical constant model. The layer grading could be discrete or continuous. For continuous grading, a model will be used to define the depth profile of the refractive index.

In this thesis, graded effective medium approximation model will be used for ellipsometry data analysis for the polymer layer. Assume polymer layer are mixture of polymer brush and solution. The model which defines the depth profile is

$$\varphi = (1-d)\times 100 \tag{2.19}$$

where φ is volume fraction of polymer, d is the depth position.

References and notes

[1] Milner S. T. *Science* **251**, 905 (1991).

[2] Napper, D. H. *Steric stabilization of colloidal dispersions*; Academic Press: New York, 1983.

[3] Raphael, E.; de Gennes, P. G. *J. Phys. Chem.* **96**, 4002 (1992).

[4] Klein, J. *Annu. Rev. Mater. Sci.* **26**, 581 (1996).

[5] Klein, J.; Kumacheva, E. *Science* **269**, 816 (1995).

[6] van Zanten, J. H. *Macromolecules* **27**, 6797 (1994).

[7] Parnas, R.S.; Cohen, Y. *Rheol Acta* **33**, 485 (1994).

[8] Gopel, W.; Jones, T. A.; Kleitz, M.; Lundstrom, J.; Seiyama, T. *In: Sensors, A Comprehensive Surey*; Gopel, W., Hesse, J., Zemel, J. N., Eds.; VCH: Weinheim; 1992 Vol. 3.

[9] Ratner, B. D.; Hoffman, A. S.; Schoen, F. J.; Lemons, J. E. *Biomaterials Science, An Introduction to Materials in Medicine*, Academic Press; San Diego, **1996.**

[10] Alexander, S. *J. Phys.* **38**, 983 (1977).

[11] de Gennes, P.-G. *Macromolecules*, **13**, 1068 (1980).

[12] Halperin, A; Tirrell, M. and Lodge, T. P. *Adv. Poly. Sci.* **100**, 31 (1992).

[13] Milner, S. T.; Witten, T. A. and Gates, M. E. *Macromolecules* **21**, 2610 (1988).

[14] Milner, S. T.; Witten, T. A. and Cates, M. E. *Macromolecules* **22**, 853 (1989).

[15] Milner, T. T. *Science* **251**, 905, (1991).

[16] Wijmans, C. M.; Scheutjens, J. M. H. M.; Zhulina, E. B. *Macromolecules* **25**, 2657 (1992).

[17] Carignano, M. A.; Szleifler, I. *Macromolecules* **28**, 3197 (1995).

[18] Martin, J. I. and Wang, Z. G. *J. Phys. Chem.* **99**, 2833 (1995).

[19] Currie, E. P.K.; Wagemaker, M.; Cohen Stuart, M. A. and van Well, A. A. *Macromolecules* **32**, 9041 (1999).

[20] Currie, E. P. K.; Leermakers, F. A. M.; Cohen Stuart M. A.; and Fleer, G. J. *Macromolecules* **32**, 487 (1999).

[21] Murat, M. and Grest G. S. *Macromolecules* **22**, 4054 (1989).

[22] Grest, G. S. *Macromolecules* **27**, 418, (1994).

[23] Chakrabarti, A. and Roral, R. *Macromolecules* **23**, 2016 (1990).

[24] Rex, S.; Zuckermann, M. J.; Lafleur, M. Silvius, J. R. *Biophys. J.* **75**, 2900 (1998).

[25] Kuhl, T. L.; Leckband, D. E.; Lasic, D. D. and Israelachvili, J. N. *Biophys. J.* **66**, 1479 (1994).

[26] Dolan, A. and Edwards, F. *Proc. R. Soc. London, Ser. A* **33**, 509 (1974).

[27] Scheutjens, J. M. J. M. and Fleer, G. J. *J. Phys. Chem.* **83**, 1619 (1979).

[28] Cosgrove, T.; Heath, T.; van Lent, B.; Leermakers, F. A. M. and Scheujens, J. M. H. M. *Macromolecules* **20**, 1692, (1987).

[29] Muthukumar, M. and Ho J. S. *Macromolecules* **22**, 965 (1989).

[30] Milner, S. T. *J. Chem. Soc. Faraday Trans.* **86**, 1349 (1990).

[31] Evers, O. A.; Scheutjens, J. M. H. M. and Fleer, G. J. *J. Chem.. Soc. Faraday Trans.* **23**, 3321 (1990).

[32] Cohen-Stuart, M. A.; Cosgrove, T. and Vincent, B. *Adv. Colloid Interface Sci.* **24**, 143 (1986).

[33] Fleer, G.J.; Cohen-Stuart, M. A.; Scheutjens, J. M. H. M.; Cosgrove, T.; Vincent, B., *Polymers at Interfaces*, Chapman & Hall: London, (1993).

[34] Stouffer, J. M. and McCarthy. T. J. *Macromolecules* **21**, 1204 (1988).

[35] Netzer, L. and Sagiv, J. *J. Am. Chem. Soc.* **85**, 674 (1983).

[36] Israelachvili, J. N. and Adams, G. E. *J. Chem. Soc. Faraday Trans.* 1 **74**, 975 (1978).

[37] Derjaguin, B. V.; Churaev, N. V.; Muller, V. M. *Surface Forces*; Kisin, V. I., translator; Consultants Bureau: New York, (1987).

[38] Taunton, H. J.; Toprakcioglu, C.; Fetters, L. and Klein, J. *Nature* **332**, 712 (1988).

[39] Taunton, H. J.; Toprakcioglu, C.; Fetters, L. and Klein, J. *Macromolecules* **23**, 571 (1990).

[40] Hadziioannou, G.; Patel, S.; Granick, S. and Tirrell, M. *J. Am. Chem. Soc.* **108**, 2869 (1986)

[41] Patel, S. S. and Tirrell, M. *Annu. Rev. Phys. Chem.* **40**,597 (1989).

[42] Marra, J. and Hair, M. L. C*olloids Surf.* **34**, 215 (1989).

[43] Klein, J. *J. Chem. Soc., Faraday Trans.* **79**, 99 (1983).

[44] Kuhl, T. L.; Leckband, D. E.; Lasic, D. D. and Israelachvili, J. N. *Biophys. J*. **66**, 1479 (1994).

[45] Belder, G.F., Brinke, G. ten, and Hadziioannou, G. *Langmuir* **13**, 4102 (1997).

[46] Parsonage, E., Tirrell, M.; Watanabe, H. and Nuzzo, R. *Macromolecules* **24**, 1987 (1991).

[47] Kelley, T. W.; Schorr, P. A.; Johnson, K. D.; Tirrell, M. and Frisbie, C. D. *Macromolecules* **31**, 4297 (1998).

[48] Kawaguchi, M.; Takahashi, A. *J. Polym. Sci., Polym. Phys. Ed.* **18**, 2069 (1980).

[49] Sauer, B. B., Yu, H. and Kim, M. W. *Langmuir* **5**, 278 (1989).

[50] Baekmark, T. R.; Elender, G.; Lasic D. D. and Sackmann, E. *Langmuir* **11**, 3975 (1995).

[51] Biesalski, M. and Rühe J. *Macromolecules* **35**, 499 (2002).

[52] Allain, C.; Ausserre, D. and Rondelez, F. *Phys. Rev. Lett.* **49**, 1694 (1982).

[53] Ausserré, D.; Hervet, H. and Rondelez, F. *Macromolecules* **19**, 85 (1986).

[54] Kawaguchi, M.; Kawarabayashi, M.; Nagata, N.; Kato, T.; Yoshioka, A. and Takahashi, A. *Macromolecules* **21**, 1059 (1988).

[55] Munch, M. R. and Gast A. P. *Macromolecules* **23**, 2313 (1990).

[56] Munch, M. R. and Gast, A. P. *J. Chem. Soc. Faraday Trans.* **86**, 1341 (1990).

[57] Since neutron reflectivity method has been widely used, some selected references will be listed during following separated review.

[58] Cosgrove, T.; Heath, T. G.; Ryan, K. and Crowley, T. L. *Macromolecules* **20**, 2879 (1987).

[59] Auroy, P.; Auvray, L. and Léger, L. *Phys. Rev. Lett.* **66**, 719 (1991).

[60] Auroy, P. and Auvray, L. *Macromolecules* **25**, 4134 (1992).

[61] Auroy, P.; Mir, Y. and Auvray, L. *Phys. Rev. Lett.* **69**, 93 (1992).

[62] Kim, M. W.; Liu, S.-N. and Chung, T. C. *Phys. Rev. Lett.* **60**, 2745 (1988).

[63] Grubb, S. G.; Kim, M. W.; Rasing, Th. and Shen, Y. R. *Langmuir* **4**, 452 (1988).

[64] Bloch, J. M.; Sansone, M.; Rondelez, F.; Peiffer, D. G.; Pincus, P.; Kim, M. W. and Eisenberger, P. M. *Phys. Rev. Lett.* **54**, 1039 (1985).

[65] Majewski, J.; Kuhl. T. L.; Kjaer, K.; Gerstenberg, M. C.; Als-Nielsen, J.; Israelachvili, J. N.; Smith, G. S. *J. Am. Chem. Soc.* **120**, 1469 (1998).

[66] Satija, S. K.; Majkrzak, C. F.; Russell, T. P.; Sinha, S. K.; Sirota, E. B. and Hughes, G. J. *Macromolecules* **23**, 3860 (1990).

[67] Russell, T. P.; Karim, A. Mansour, A.; Felcher, G. P. *Macromolecules* **21**, 1890 (1988).

[68] Anastasiadis, S. H.; Russell, T. P.; Satija, S. K.; Majkrzak, C. F. *Phys. Rev. Lett.* **21**, 1890 (1989).

[69] Rennie, A. R.; Crawford, R. J.; Lee, E. M.; Thomas, R. K.; Crowley, T. L.; Roberts, S.; Qureshi, M. S. and Richards, R. W. *Macromolecules* **22**, 3466 (1989).

[70] Cosgrove, T.; Heath, T. G.; Phipps, J. S.; Richardson, R. M. *Macromolecules* **24**, 94 (1991).

[71] Satija, S. K.; Majkrzak, C. F.; Russell, T. P.; Sinha, S. K.; Sirota, E. B. and Hughes, G. J. *Macromolecules* **23**, 3860 (1990).

[72] Auvray, L.; de Gennes, P. G. *Europhys. Lett.* **2**, 647 1986.

[73] Halperin, A.; Tirrell, M. and Lodge, T. P. *Adv. Polym. Sci.* **100**, 31 (1991).

[74] Pincus, P. *Macromolecules* **24**, 2912 (1991).

[75] Zhulina, E. B.; Birshtein, T. M. and Borisov. O. V. *Macromolecules* **28**, 1491 (1995).

[76] Zhulina, E. B. and Borisov, O. V. *J. Chem. Phys.* **107**, 5952 (1997).

[77] Israëls, R.; Scheutjens, J. M. H. M. and Fleer, G. J. *Macromolecules* **27**, 3087 (1994).

[78] Israëls, R.; Leermakers, F. A. M., Fleer, G. J., and Zhulina, E. B. *Macromolecules* **27**, 3249 (1994).

[79] Fleer, G. J. Ber. Bunsenges, *Phys. Chem.* **100**, 936 (1996).

[80] Israëls, R.; Leermakers, F. A. M., and Fleer, G. J. *Macromolecules* **27**, 3087 (1994).

[81] Israëls, R.; Leermakers, F. A. M., and Fleer, G. J. *Macromolecules* **28**, 1626 (1994).

[82] Lyatskays, Yu. V.; Leemakers, F. A. M.; Fleer, G. J.; Zhulina, E. B. and Birshtein, T. M. *Macromolecules* **28**, 3562 (1995).

[83] Kelly, T. W.; Schorr, P. A.; Johnson, K. D.; Tirrell, M. and Frisbie, C. D. *Macromolecules* **31**, 4297 (1998).

[84] Mir, Y.; Auroy, P. and Auvray, L. *Phys. Rev. Lett.* **75**, 2863 (1995).

[85] Ahrens, H.; Förster, S. and Helm, C. A. *Macromolecules* **30**, 8447 (1997).

[86] Ahrens, H.; Förster, S. and Helm, C. A. *Phys. Rev. Lett.* **81**, 4172 (1998).

[87] Guenoun, P.; Schlachli, A.; Sentenac, D.; Mays, J. W. and Benattar, J. J. *Phys. Rev. Lett.* **74**, 3628 (1995).

[88] Guenoun, P.; Muller, F.; et al *Phys. Rev. Lett.* **81**, 3872 (1998).

[89] Biesalski, M. and Rühe J. *Macromolecules* **32**, 2309 (1999).

[90] Biesalski, M. and Rühe J. *Langmuir* **16**, 1943 (2000).

[91] Biesalski, M. and Rühe J. *Macromolecules* **35**, 499 (2002).

[92] An, S. W.; Thirtle, P. N.; Thomas, R. K.; Baines, f. L.; Billingham, N. C.; Armes, S. P. and Penfold, J. *J. Phys. Chem. B* **102**, 387 (1998).

[93] An, S. W.; Thirtle, P. N.; Thomas, R. K.; Baines, f. L.; Billingham, N. C.; Armes, S. P. and Penfold, J. *J. Phys. Chem. B* **102**, 5120 (1998).

[94] Kurihara, K.; Kunitake, T.; Higashi, N. and Niwa, M. *Langmuir* **8**, 2087 (1992).

[95] Currie, E. P. K.; Sieval, A. B.; Fleer, G. J. and Cohen Stuart, M. A. *Langmuir* **15**, 7116 (1999).

[96] Currie, E. P. K.; Sieval, A. B.; Fleer, G. J. and Cohen Stuart, M. A. *Langmuir* **16**, 8324 (2000).

[97] Abe, T.; Higashi, N.; Niwa, M. and Kurihara, K. *Langmuir* **15**, 7725 (1999).

[98] Hayashi, S.; Abe, T.; Higashi, N.; Niwa, M. and Kurihara, K. *Langmuir* **18**, 3932 (2002).

[99] Tompkins, H. G. *A user's guide to ellipsometry*, Boston : Academic Press, 1993.

[100] Minko, S.; et al. *Macromolecules*, 32, **4532** (1999).

[101] Currie, E. P. K.; et al. *Langmuir* **16**, 8324 2000.

[102] Amiel, C.; Sikka, M.; Schneider Jr., J. W.; Tsao, Y.; Tirrell, M. and Mays, J. W. *Macromolecules* **28**, 3125 (1995).

[103] Azzam, R. M. A. and Bashara, N. M. *Ellipsometry and Polarized Light*; North-Holland: Amsterdam, 1977.

[104] Motschmann, H.; Stamm, M. and Toprakcioglu, Ch. *Macromolecules* **24**, 3681 (1991).

[105] Siqueira, D. F.; Breiner, U.; Stadler, R. and Stamm, M. *Langmuir* **11**, 1680 (1995).

[106] *Guide to Using WVASE32TM*, J.A. Woollam Co., Inc 1998.

Chapter 3

Preparation of surface-anchored polymers

3.1 Adsorption of polymers on solid substrates

The control of surface properties is central to many areas of research and in numerous commercially important technologies ranging from biotechnology to advanced microelectronics[1,2]. One of several methods of adjusting the surface properties of materials is based on anchoring polymers to these surfaces, or termed as "polymer brushes".

Traditionally, polymeric brushes have been prepared through the physisorption of either homopolymers or block copolymers where one block is strongly adsorbed to the surface and the other block forming the brush layer[2,3,4,5]. One common example involves polymer brushes prepared by adsorption of PS-*b*-PVP block copolymers onto silica or mica surfaces using toluene as a selective solvent, where the PVP block forms an anchor layer on the surface while the PS block forms a brush. The noncovalent nature of this grafting strategy is a weakness, however, since desorption of the brush can subsequently occur upon exposure to a good solvent for the surface-anchored layer or the polymer can be displaced by other polymers or low molecular weight compounds, which compete for adsorption sites at the surface. In addition, the demanding block copolymer synthesis limits the choice of functional groups for the block copolymer structure. Finally, the obtained films are often thermally unstable due to the rather weak interactions between the polymer and the solid substrate.[6,7]

To circumvent these deficiencies, an increasing amount of interest has been devoted to the covalent attachment of polymer chains to surfaces[8], which makes the polymer brushes robust and resistant to common chemical environmental conditions. In order to establish a

chemical bond between the polymer molecules and the surfaces, end-functionalized polymers are often synthesized and reacted with appropriate surfaces sites ("grafting onto" technique) on carbon black,[9] silica,[10] and gold substrates.[11,12,13] Through the "grafting onto" route, the molecular weight and the molecular dispersity of the surface-grafted polymers can be controlled before the surface reaction is conducted. Due to the advantages, "grafting onto" is a very common approach to immobilized polymer films. A review of recent applications of this technique is given by Zhao and Brittain.[14] In general, only a small amount of polymer can be immobilized onto the surface by the "grafting to" approach. That is due to the inherent limitation by the crowding of chains at the surface, which hinders the diffusion of chain ends to the surface for further attachment. Therefore, the formation of surface-bound polymer monolayers by such a "grafting onto" methodology is intrinsically restricted to low graft densities and small film thickness.

In addition to the physisorption and "grafting onto" techniques described above, grafted polymer layers can also be prepared by so-called "grafting from" techniques, in which the macromolecule is generated from polymerization initiators residing directly at the surface[14]. The main advantage of this "grafting from" methodology is that the entropic constraints associated with confining the molecules to the solid surface are greatly minimized for the monomers as compared to macromolecules. The accessibility of a monomer to the surface-reactive groups is larger than that of a polymer; therefore, the reactivity in the "grafting from" approach should be much greater than in the "grafting onto" experiment. Also, the "grafting from" technique is convenient where the polymers do not dissolve in most typical organic solvents, whereas their monomers do. A detailed review of experiments

using the “grafting from” technique will be given in the rest of the chapter, since this approach is also used in our experiments.

3.2 Principles of “grafting from” polymerizations

“Grafting from” techniques have been employed for a variety of monomers and different polymerization types. The first type is by using *layer-by-layer self-assembly* of small molecules that have functional groups at both ends.[15] The first layer is self-assembled on the substrate, and the second layer is then deposited on top of the first layer. A multiplayer structure is built by repeating this process. The limitation of this method is the difficulty of achieving 100% efficiency of reacting each terminal group. This happens because the density of the layers decreases as layers get farther away from the substrate. The second type of grafting, called *multiple-step surface grafting*, is utilized to construct hyperbranched and amorphous polymer films.[16] In this method, macromolecules instead of small molecules are used for the assembly, and the anchoring groups for film growth lie everywhere within the film layer instead of only at the ends. This method is not broadly applicable in chemical separations because the anchoring groups are usually carboxylic acids or amines, which introduce new charges in the film. While generally successful, the first two multistep approaches bear the complication of possible side reactions and ambiguities in the composition of the initiator layer.

These limitations can be removed (or at least minimized to some extent) by using alternative chemical routes. One of such methodologies is based on ring-opening polymerization of N-carboxyanhydride derivatives, initiated by amine groups self-assembled on substrates.[17] With this method, oriented peptide layers up to 100 nm can be built. This reaction needs a specific structure for monomers, N-carboxyanhydride, whereas chemical separations require a great diversity of functional groups, including nonadsorbing surfaces.

The fourth, and perhaps the best approach, is based on forming linear polymer chains directly from the surface to give the covalently attached polymer brushes with moderate graft densities and high molecular weights, or so called "graft from" technique. Based on different polymerization types, this method could be categorized into following subgroups: conventional radical polymerization, controlled radical polymerization, and other polymerization methods.

Before going into some examples of different polymerization, we will review the common methods to immobilize the initiator, because it is also very crucial for the polymer brush preparation. There are two typical methods.

Method I: An anchor molecule is immobilized on the solid substrate surface and then the initiating species are linked to the anchor molecules in one or more additional steps. For example, Boven et al[18] treated glass beads with 3-aminopropytriethoxysilane (γ-APS) to obtain amino functional groups on the surface. The azo initiators are then immobilized onto the surface through the formation of amide bonds between the γ-APS modified surface and an acid chloride functionalized azo initiator. Subsequent surface initiated radical polymerization produced tethered poly(methyl methacrylate) PMMA chains. Recently,

Kong et al[19] use this method to immobilize initiators as shown in figure 3.1 and graft poly(methyl methacrylate) PMMA and poly(acryl amide) (PAAm) with atom transfer radical polymerization (ATRP).

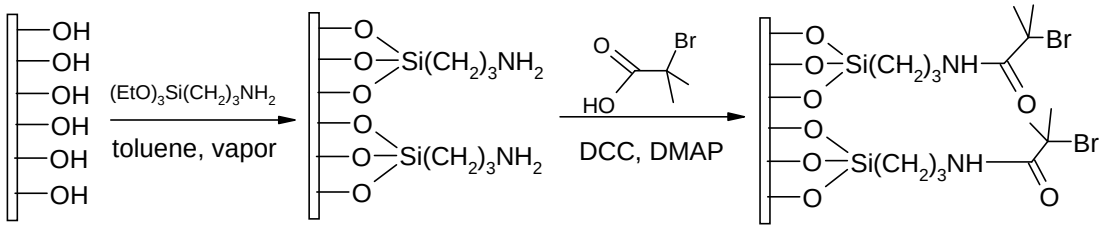

Figure 3.1 Initiator immobilization with linker molecular (γ-APS)[19]

Although this method is successfully used in a large amount of studies to prepare polymer brushes, there are several disadvantages. The immobilization of the initiator on the surface involves several steps, which may lead to low graft densities of the initiators and the tethered polymers if the reactions are not quantitative. Secondly, side reactions, which possibly exist in the initiator immobilization reaction, may introduce some undesired structures on the surface. Accurate characterization of the initiator layer is nontrivial. This lack of knowledge about the exact composition of the initiator layer makes the understanding of polymerization mechanism difficult in some cases. In the above case, it has been show that the γ-APS layer is a very complex structure, sometimes multiplayer structures may result.

Method II: The initiator itself is able to chemically attach to the substrate in one step by self-assembly method (SAM) techniques. The complete initiator molecular is synthesized

in the way, where one end is able to react with substrate surface and the other end function group initializes the polymerization. One example is done by using 1-trichlorosily-2-(m-p-chloromethylphenyl)ethane (CMPE) as initiator.[20] The trichlorosilane ends readily bond to silicon substrate surface, as shown in figure 3.2.

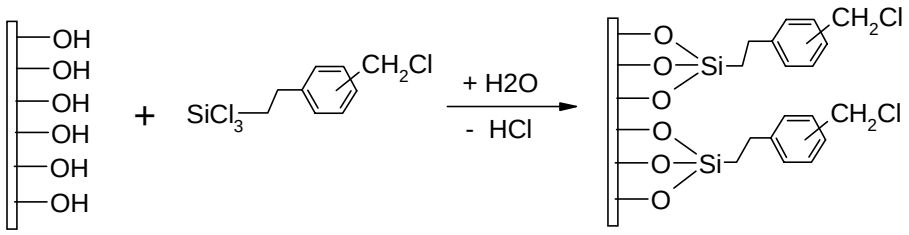

Figure 3.2 Initiator immobilization by SAM technique[20]

The chloromethylphenyl ends are the initiators for the polymerization, where poly(acryl amide) is synthesized from the surface. One difficulty for this method is the characterization of polymers, due to the surface confinement. One way to circumvent this problem is to cleave the polymers off from silica surface by using hydrofluoric acid (HF) solution.[21] Another way is to synthesize one initiator, which contains a cleavable group,[22] so polymers could be cleaved off at this point after polymerizations.

With the initiator on the substrate surface, different polymerization could be applied. Here we present only some representative examples of each type of polymerization. A more detailed review was provided by Zhao and Britain[14].

3.2.1 Conventional radical polymerization

Conventional radical polymerization or free radical polymerization is the most widely used method for the production of polymers in industry. By using the first method to immobilize initiator, Boven et al[23] performed surface initiated radical polymerization of poly(methyl methacrylate) on microparticulate silica. Photoemulsion polymerization was applied by Ballauff and coworkers[24] to prepare spherical poly(acrylic acid) PAA brushes. Rühe and coworkers reported a series of surface free radical polymerization method leading to the formation of neutral polystyrene PS[25], PMMA[26] brushes, and polyelectrolytes MePVP[27] and BuPVP[28]. Free radical polymerization has been very successful because the density of the initiators at the surface can be easily varied, and the functionalized polymer chains can be readily prepared. However, cross-linking, competitive side-, and termination reactions are augmented for this kind of polymerization. Also, the use of traditional free radical polymerization precludes the formation of block copolymer brushes or accurate control of polymer structure.

3.2.2 Controlled radical polymerization

Controlled radical polymerization or living radical polymerization reactions represent one of the most promising (and in some cases preferred) alternatives to the traditional radical polymerization, because it could achieve a better control of the molecular weight and the molecular weight distribution and synthesize novel polymer brushes like block copolymer

brushes. Controlled radical polymerizations include iniferter, TEMPO-mediated radical polymerizations, ATRP and reverse ATRP.

The iniferter radical polymerization was explored by Otsu el al[29] in the early 1980s. The concept of this polymerization is to prepare a non-conventional initiators, which could produce a reactive *ini*tial radical and a relatively stable counter radical, where the latter does not participate in the initiation, but merely acts as a trans*fer* agent and *ter*minating species (*iniferter*). One such application of grafting polymerization involves the preparation of N,N-(diethyamino)dithiocarbamoylbenzyl(trimethoxy)silane (SBDC) as surface anchored initiator[30], shown in figure 3.3.

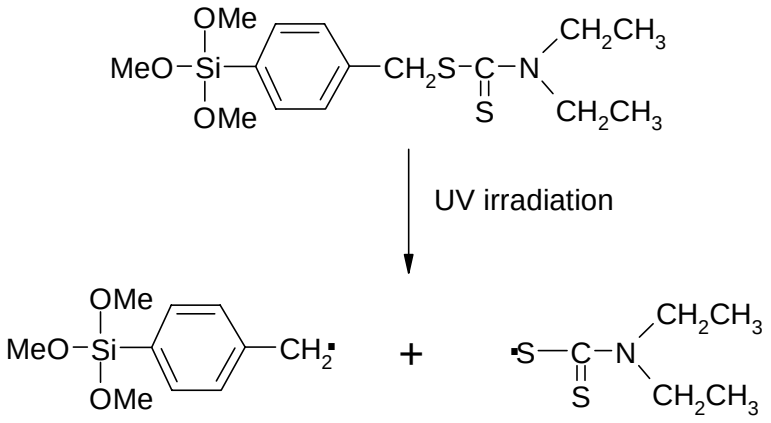

Figure 3.3 Radicals formation from SBDC[30]

TEMPO-mediated radical polymerizations are also called nitroxide-mediated free radical polymerization because of alkoxyamine structure in the initiator. The synthesis of polystyrene brushes by this method onto silicate surface is accomplished successfully by

adding some free alkoxyamine initiator (so-called sacrificed initiator) in the polymerization solution[31], because surface initiator concentration only is too low for the polymerization control. The following scheme figure 3.4 shows this application.

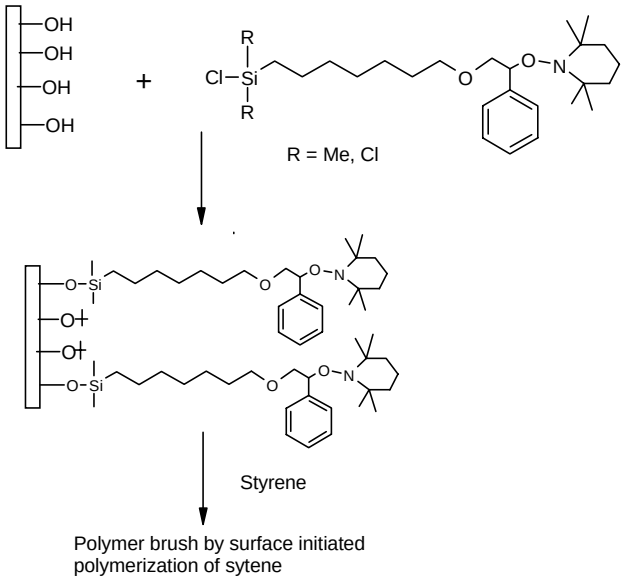

Figure 3.4 Synthesis of polystyrene brushes by TEMPO-mediated radical polymerization[31]

ATRP is a newly developed controlled radically polymerization[32]. Due to its simplicity, robustness and the ability to synthesize polymer brushes with narrow molecular weight distributions, ATRP has been one of choices for most surface-initiated "living" radical polymerization processes. Also because ATRP is the polymerization method in our research, a detailed introduction about ATRP will be provided in chapter 3.3.

3.2.3 Other polymerization methods

There are some other important methods employed in the synthesis of tethered polymer brushes. Even though they are used as wide as radical polymerization, they are needed in some specific circumstances.

It is known that living anionic polymerization could produce strictly linear vinyl polymers with the lowest polydisperisties, due to the highly living nature of the propagating species and total absent of side reactions.[33] Jordan et al[34] used anionic polymerization to synthesize polystyrene brushes on gold substrates with initiators immobilized by SAMs. Using similar strategy, Ingall et al[35] synthesized a tethered poly(acrylonitrile) film with a thickness up to 245 nm. In spite of its ability to generate polymers with very well defined molecular characteristics and narrow molecular weight distributions, the applicability of living anionic polymerization is limited because it is also sensitive to impurities.

Carbocationic polymerization also is a good technique to prepare tethered polymer brushes. As early as 1980s, Vial et al.[36,37] use this method to graft polyisobutylene on a silica surface. Recently, several other groups[38,39] also reported on surface initiated polymerizations via carbocationic polymerization.

Other polymerization methods, such as ring-opening metathesis polymerization[40], group transfer polymerization[41], also are used in surface initiated polymerization.

3.3 Atom transfer radical polymerization (ATRP)

The development of controlled/living radical polymerization (CRP) methods have been a long-standing goal in polymer chemistry, as a radical process in more tolerant of functional groups and impurities, comparing to anionic, cationic, coordination, and ring-opening polymerization.[42] Also radical polymerization is industrially the most widespread method to produce polymers. Due to the major drawbacks of conventional radical polymerizations, such as high polydispersities and lack of control over the polymer structure, wide interests focus on the development and understanding of new CRP methods.[43,44]

New CRP methods include iniferter radical polymerization, nitroxide mediated polymerization (NMP) or TEMPO-mediated polymerization, atom transfer radical polymer (direct ATRP and reverse ATRP), reversible addition fragmentation chain transfer processes (RAFT), and stable free radical polymerization (SFRP). As mentioned above, this introduction will focus on the mechanism of ATRP and polymers synthesized via ATRP.

An ATRP system consists of an initiator, a metal halide complexed with some ligand(s), and a monomer.[45] A general mechanism of ATRP is shown in Figure 3.5.

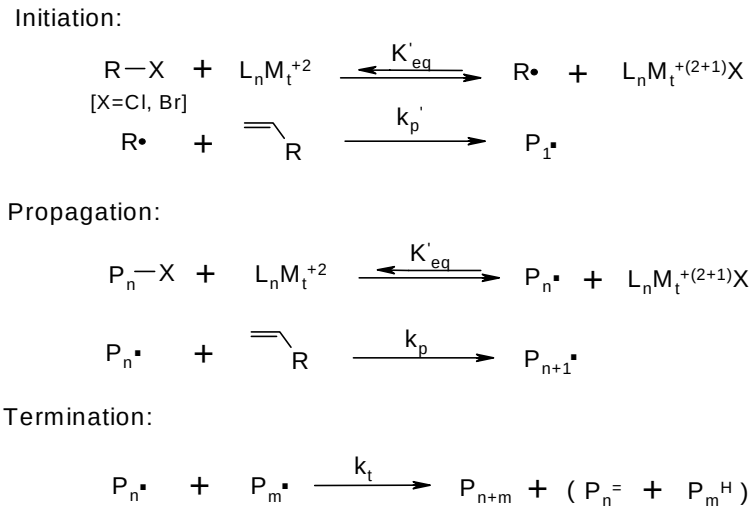

Figure 3.5 A general mechanism of ATRP

The mechanism consists of initiation and propagation processes that are phenomenologically related. These sequences consist of an atom transfer equilibrium and an addition of the intermediate radical to a monomer. Termination by radical coupling and disproportionation is included in the mechanistic scheme because of the magnitude of the associated rate constant, but it becomes insignificant due to the persistent radical effect. A successful ATRP will have not only a small contribution of terminated chains, but also a uniform growth of al the chains, which is accomplished through fast initiation and rapid reversible deactivation.

With recent advances in the field, the popularity of ATRP system has increased rapidly. Wide range of polymers has been synthesized via ATRP. For example, the copper-based ATRP system has been adapted successfully for the polymerization of styrenes, acrylates, methacrylates, acrylonitrile, and other monomers[46]. The ruthenium/aluminum alkoxide-based ATRP system has been demonstrated to work with methacrylatexin[47,48], acrylates and styrene[49]. The iron-based ATRP system has been demonstrated to work with

styrenes and methacrylates[50,51], while the nickel-based ATRP systems have been shown to work for methacrylates[52,53].

A variety of initiators, typically alkyl halides, have been used successfully in ATRP. Also the low termination rate (<5%) of ATRP maintains the halogen at the polymer chain ends, which allows block copolymers synthesis and other end group transformations.[54]

By combining the ATRP with Langmuir-Blodgett (LB) technique[55] or self-assembly method (SAM)[20], a variety of polymers and copolymers brush can be prepared by the "grafting from" methodology. The LB or SAM techniques provide a well-organized set of initiating sites on the substrate that serve as starting points for growing relatively monodisperse polymer brushes. In this thesis, initiators will be chemically immobilized with SAMs technique. Following that, ATRP will be applied for polymerization.

References and notes

[1] Halperin, A.; Tirrell, M.; Lodge, T.P. *Adv. Polym. Sci.* **100**, 31 (1991).

[2] Fleer, G.J.; Cohen-Stuart, M.A.; Scheutjens, J.M.H.M.; Cosgrove, T.; Vincent, B., *Polymers at Interfaces*, Chapman & Hall: London, 1993.

[3] Hadziioannou, G.; Patel, S.; Granick, S.; Tirrell, M. *J. Am. Chem. Soc.* **108**, 2869 (1986).

[4] Dan, N.; Tirrell, M. *Macromolecules* **26**, 4310 (1993).

[5] Belder, G.F.; ten Brinke, G.; Hadziioannou, G. *Langmuir* **13**, 4102 (1997).

[6] Yerushalmi-Royen, R., Klein, J., Fetters, L. *Science* **263**, 793 (1994).

[7] Reiter, G. *Europhys. Lett.* **33**, 29 (1996).

[8] Jordan, R., Graf, K., Riegler, H., Unger, K.K. *J. Chem. Soc. Chem. Commun.* **9**, 1025 (1996).

[9] Tsubokawa, N.; Hosoya, M.; Yanadori, K.; Sone, Y. *J., Macromol. Sci. Chem.* **A27**, 445 (1990).

[10] Ben Ouada, H.; Hommel, H.; Legrand, A.P.; Balard, H.; Papirer, E. *J. Colloid Interface Sci.* **122**, 441 (1988).

[11] Sun, F., Grainger, D. W., Castner, D. G., and Leach-Scampavia, D. K. *Macromolecules* **27**, 3053 (1994).

[12] Stouffer, J. M., McCarthy. T. J. *Macromolecules* **21**, 1204 (1988).

[13] Lenk, T. J., Hallmark, V. M., Rabolt, J. F., Haussling, L., and Ringsdorf, H. Macromolecules **26**, 1230 (1993).

[14] Zhao, B. and Brittain, W. *J. Prog. Polym. Sci.* **25**, 677 (2000).

[15] Netzer, L., Sagiv, J., *J. Am. Chem. Soc.* **85**, 1059 (1983); Maos, R., Matis, S., Dimasi, E., Ocko, B.M., Sagiv, J., *Nature* **384**, 150 (1996); Tillman, N., Ulman, A., Penner, T.L., *Langmuir* **5**, 101 (1989); Collins, R. J., Bae, I. T., Scherson, D. A., Sukenik, C.

N., *Langmuir* **12**, 5509 (1996); Heid, S., Effenberger, F. *Langmuir* **12**, 2118 (1996); Li, D. Q., Ratner, M. A., Marks, T. J., Zhang, C. H., Yang, J., Wong, J. K., *J. Am. Chem. Soc.* **112**, 7389 (1990); Roscoe, S. B., Ytzchaik, S., Kakkar, A. K., Marks, T. J., Lin, W., Wong, G. K. *Langmuir* **10**, 1337 (1994); Liu, Y., Zhao, M., Bergbreiter, D. E., Crooks, R. M., Wells, M. *J. Am. Chem. Soc.* **119**, 8720 (1997).

[16] Zhou, Y., Bruening, M.L., Bergbreiter, D. E., Crooks, R. M., Wells, M. *J. Am. Chem. Soc.* **118**, 3773 (1996); Zhou, Y., Bruening, M. L., Liu, Y., Crooks, R.M., and Bergbreiter D. E. *Langmuir* **12**, 5519 (1996); Beyer, D., Bohanon, T. M., Knoll, W., and Ringsdorf, H. *Langmuir* **12**, 2514 (1996).

[17] Chang, Y-C, and Frank, C. W. *Langmuir* **12**, 5823 (1996); Whitesell, J. K., Chang, H. K., *Science* **261**, 73 (1993); Wieringa, R.H., Schouten, A.J. *Macromolecules* **29**, 3032 (1996).

[18] Boven G.; Folkersma R.; Challa, G. and Schouten A. *J. Polym Commun* **32**, 50 (1991).

[19] Kong, X.; Kawai, T.; Abe, J. and Iyoda, T. *Macromolecules* **34**, 1837 (2001).

[20] Huang, X. and Wirth, M. *J. Anal. Chem.* **69**, 4577 (1997).

[21] Huang, X. and Wirth, M. J. *Macromolecules* **32**, 1694 (1999).

[22] Prucker O, Rühe J. *Macromolecules* **31**, 592 (1998).

[23] Boven, G., Oosterling, M. L. C. M., Challa, G., and Schouten, A. *Polymer* **31**, 2377 (1991).

[24] Guo, X.; Weiss, A. and Ballauff, M. *Macromolecules* **32**, 6043 (1999).

[25] Prucker, O.; Rühe, J. *Macromolecules* **31**, 592 (1998).

[26] Prucker, O.; Ruhe, J. *Macromolecules* **31**, 602 (1998).

[27] Biesalski, M. and Rühe J. *Macromolecules* **35**, 499 (2002).

[28] Biesalski, M. and Rühe J. *Macromolecules* **32**, 2309 (1999).

[29] a) Otsu, T.; Yoshida, M. *Makromol. Chem., Rapid Commun.* **3**, 127 (1982). b) Otsu. T.; Yoshida, M.; Tazaki, T. *Makromol. Chem., Rapid Commun.* **3**, 133 (1982).

[30] De Boer, B.; Simon, H. K.; Werts, M. P. L.; van der Vegte, E. W. and Hadziioannou, G. *Macromolecules* **33**, 349 (2000).

[31] Husseman, M., Malmstrom, E.E., McNamara, M., Mate, M., Mecerreyes, D., Benoit, D.G., Hedrick, J.L., Mansky, P., Huang, E. Russell, T.P., and Hawker, C.J. *Macromolecules* **32**, 1424 (1999).

[32] Patter, T. E.; Xia, J.; Abernathy, T. and Matyjaszewski, K. *Science* **272**, 866 (1996).

[33] Szwarc, M. *Nature* **178**, 1168 (1956).

[34] Jordan, R.; Ulman, A.; Kang, J. F.; Rafailovich, M. H. and Sokolov, J. *J. Am Chem. Soc.* **121**, 1016 (1999).

[35] Ingall, M. D. K.; Honeyman, C. H.; Mercure, J. V.; Bianconi, P. A. and Kunz, R. R. *J. Am. Chem. Soc.* **121**, 1016 (1999).

[36] Vidal, A.; Guyot, A. and Kennedy, J. P. *Polym. Bull.* **2**, 315 (1980).

[37] Vidal, A.; Guyot, A. and Kennedy, J. P. *Polym. Bull.* **6**, 401 (1982).

[38] Jordan, R. and Ulman, A. *J. Am. Chem. Soc*. **120**, 243 (1998).

[39] Zhao, B. and Brittain, W. J. *Macromolecules* **33**, 342 (2000).

[40] Weck, M.; Jackiw, J. J.; Rossi, R. R.; Weiss, P. S. and Grubbs, R. H. *J. Am. Chem. Soc*. **121**, 4088 (1999).

[41] Hertler, W. R.; Sogah, D. Y. and Boettcher, F. P. Macromolecules **23**, 1264 (1990).

[42] Matyjaszewski, K.; Gaynor, S. G. In *Applied Polymer Science*: Craver, C. D., Carraher, C. E. Jr., Eds.; Pergamon Press: Oxford, UK. 2000.

[43] Matyjaszewski, K., *Controlled Radical Polymerization*; American Chemical Society: Washington, DC, 1998, vol. 685.

[44] *Controlled/Living Radical polymerization: Progress in ATRP, NMP, and RAFT*; Matyjaszewski, K., Ed.; American Chemical Society: Washington, DC, 2000, Vol. 768.

[45] Pattern, T. E. and Matyjaszewski, K. *Adv. Mater.* **10**, 901 (1998).

[46] Coessens, V.; Pintauer, T. and Matyjaszewski, K. *Prog. Polym. Sci.* **26**, 337 (2001).

[47] Kato, M., Kamigaito, Sawamoto, M., Higashimura, T. *Macromolecules* **28**, 1721 (1995).

[48] Ando, T., Kato, M., Kamigaito, M., Sawamoto, M. *Macromolecules* **30**, 2249 (1997).

[49] Sawamoto, M., Kamigaito, M., *Polym. Prepr.* (Am. Chem. Soc., Div. Polym. Chem.), **38**, 740 (1997).

[50] Ando, T., Kato, M., Kamigaito, M., Sawamoto, M. *Macromolecules*, **30**, 4507 (1997).

[51] Matyjaszewski, K., Wei, M., Xia, J., McDermott, N.E. *Macromolecules* **30**, 8161 (1997).

[52] Granel, C., Dubois, P., Jerome, R., Teyssie, P. *Macromolecules* **29**, 8576 (1996).

[53] Uegaki, H., Kotani, Y., Kamigaito, M., Sawamoto, M. *Macromolecules* **30**, 2249 (1997).

[54] Matyjaszewski, K. and Xia, *J. Chem. Rev.* **101**, 292 (2001).

[55] Ejaz, M., Yamamoto, S., Ohno, K., Tsujii, Y., and Fukuda, T. *Macromolecules* **31**, 5934 (1998).

Chapter 4

Surface bound molecular gradients

4.1 Self-assembled monolayers

Self-assembled monolayers (SAMs) are molecular assemblies that form spontaneously by the immersion of an appropriate substrate into a solution of an active surfactant or by exposure to vapor of reactants[1,2]. From the energetic point of view, a self-assembling molecule can be divided into three parts (Fig. 4.1). The first part is the head group. During the self-assembly this group is chemisorbed on the substrate surface. The very strong molecular-substrate interactions result in an apparent pinning of the head group to a specific site on the surface through a chemical bond. The second molecular part is the alkyl chain, and the energies associated with its inter-chain interactions are due to van der Waals forces. The third molecular part of a self-assembling molecule is its terminal functionality, which, in the case of a simple alkyl chain, is a methyl ($-CH_3$) group. By substituting various chemical groups into this terminal moiety the surface properties of the SAMs can be tuned.

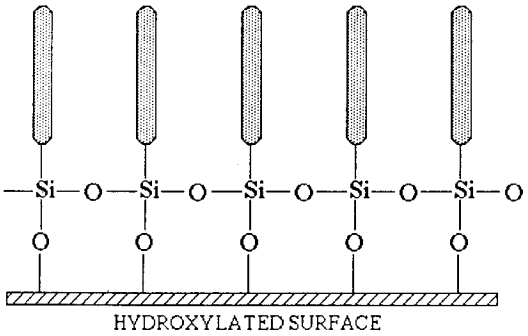

Figure 4.1 A SAM of alkyltrichlorosilane on a hydroxylated surface [taken from Ref. 3].

Deposition of self-assembled monolayers represents one of the highest quality methods of modifying systematically the chemical properties of solid surfaces[3]. Traditionally, inorganic or metal surfaces have been used as supports for SAMs. Systematic studies of modification of surfaces with organic polymers by SAMs have recently also emerged[4,5]. SAMs on organic polymers may be useful in cases where the deformability of the support is needed, such as the case with implantable biomaterials that require a certain degree of mechanical flexibility.

Recent advances in the field of self-assembly combined with new deposition technologies, such as soft lithography techniques[6], have enabled alternative means of fabricating two- and three-dimensional surface structures. However, most soft-lithography techniques are based on selective and controlled deposition of self-assembled monolayers (SAMs) on material surfaces[3]. Various structural patterns with lateral dimensions ranging from hundreds of nanometers to several micrometers are created on the material surface using an elastomeric "pattern-transfer element" (or stamp) that has a three-dimensional structure molded onto its surface. Because of the molecular nature of the SAMs, the surface patterns generated via "soft lithography" are rather thin (thicknesses range from several Angstroms to several nanometers). Some applications, particularly those involving subsequent microfabrication steps, such as etching, require that thicker layers of the surface coating be formed. Hence, techniques involving the patterning of thicker polymer layers grafted to the substrate have been developed[7,8,9,10,11,12,13]. The latter group of technologies is based on selectively decorating the material surfaces with polymerization initiators and then growing the macromolecules directly from the surface (so-called "grafting from"). Using

this method, the thickness of the overcoat film can be adjusted by simply varying the polymerization conditions (time, monomer concentration, temperature).

The soft-lithography technologies always produce sharp boundaries between the distinct chemical regions on the substrate. This feature makes soft-lithography useful for decorating substrates with well-defined chemical patterns of various shapes and dimensions. However, for some applications, it is desirable that the physico-chemical characteristics, such as wetting of the substrate, change gradually. This can be accomplished by producing surfaces with a position dependent and gradually varying chemistry. In these so-called "gradient surfaces", the gradient in surface energy is responsible for a position-bound variation in physical properties, most notably the wettability[4]. Recent studies have reported on the preparation of molecular gradients on length scales ranging from nanometers to centimeters[14,15] thus offering the prospect of meeting the demands of a variety of novel applications. For example, such gradient substrates can useful in high-throughput studies of the interfacial behavior of molecules and macromolecules[16] (the entire behavioral spectrum can be accessed in a single experiment), they can serve as templates for further processing, or be used as active elements in controlled surface transport of materials.

The aim of this chapter is to introduce the surface bound molecular preparation, characterization and their applications. Several examples will be referenced documenting utility of the wettability gradients in combinatorial studies of adsorption, phase behavior in thin liquid and polymer films, templating, and material transport on surfaces. The dual nature of molecular gradients (discrete on molecular scales, continuous on meso scales) endows them with unique properties that can be exploited to generate combinatorial libraries, which in turn will find use in the discovery of new materials and phenomena. Moreover,

utilizing molecular gradients will provide simple means of mimicking molecular and biomolecular transport.

4.2 Methods of preparing gradients

Over the past 40 years, several strategies for making molecular gradients have been conceived and developed. Each has its advantages and disadvantages and each is best applied on one length scale (*cf.* Table 4.1). These methods are briefly described below and discussed in a recent review[17].

Table 4.1 Comparison of various methods used to produce chemical gradients

	Spatial range			
Gradient preparation method	**nm**	**μm**	**mm**	**cm**
Shadowing evaporation[18]			◄·····►	
Liquid diffusion[19]			◄·····►	
Density gradient solution[20]			◄·····►	
Hydrolysis of poly(vinylene carbonate)[21]			◄·····►	
Radio frequency plasma discharge[22]			◄····►	
Corona discharge[23]			◄·····►	
Gradient UVO treatment of hydrophobic SAMs[24]			◄····►	
Vapor evaporation[4]			◄·····►	
Vapor evaporation on flexible substrates[14]			◄·····►	
Diffusion of alkanethiols in polysaccharide[25,26]			◄····►	
Electrochemical desorption of alkanethiols[27]			◄····►	
Replacement lithography[15]		◄·····►		
Polyatomic deposition[28]			◄·····►	
Heterobifunctional photolinkers[29,30]			◄·····►	
Microfluidic networks[31,32,33,34]			◄·····►	

The first report describing formation of wettability gradients dates back to the mid 1960s. Carter described a technique based on evaporating palladium metal on cellulose acetate-covered glass[18]. A short length of stainless steel rod was first placed in contact with the cellulose acetate film and a small amount (≈2 mg) of fine palladium wire, positioned at a distance of ≈10 cm from the rod, was evaporated under vacuum. This set up produced a relatively heavy deposition of palladium, which clearly outlined the intervening rod. However, owing to the scattering of metal particles a much finer deposit of palladium extended beyond the visibly shadowed area and tapered in the narrowing angle under the curved surface of the rod. The technique is very simple but does not offer much control over the gradient properties.

In the mid 1980s, Elwing proposed a new method of preparing molecular gradients[19]. In his technique (*cf.* Figure 4.2a), the wettability gradient on the solid silicon-oxide covered substrate was produced by diffusion of dichlorodimethyl silane (DDS) between two organic solvents that have different densities but are mutually soluble. In a typical experiment, a silica-covered substrate was placed vertically into a container that was filled with xylene (XYL). Trichloroethylene (TCE) was mixed with a small amount of DDS and was delivered under the XYL phase in the container. During the incubation the two solvents interdiffused, the DDS diffused to the XYL region and was simultaneously attached to the silica surface. The technique is relatively simple but it offers limited control over the gradient properties – except the length that can be controlled by varying the diffusion time. The main limitation of the liquid diffusion technique – namely that the shape of the diffusion profile was always

Fickian– was removed in the density gradient solution method developed by Gõlander and coworkers[20]. In their technique (*cf*. Figure 4.2b), a solution of TCE was mixed continuously

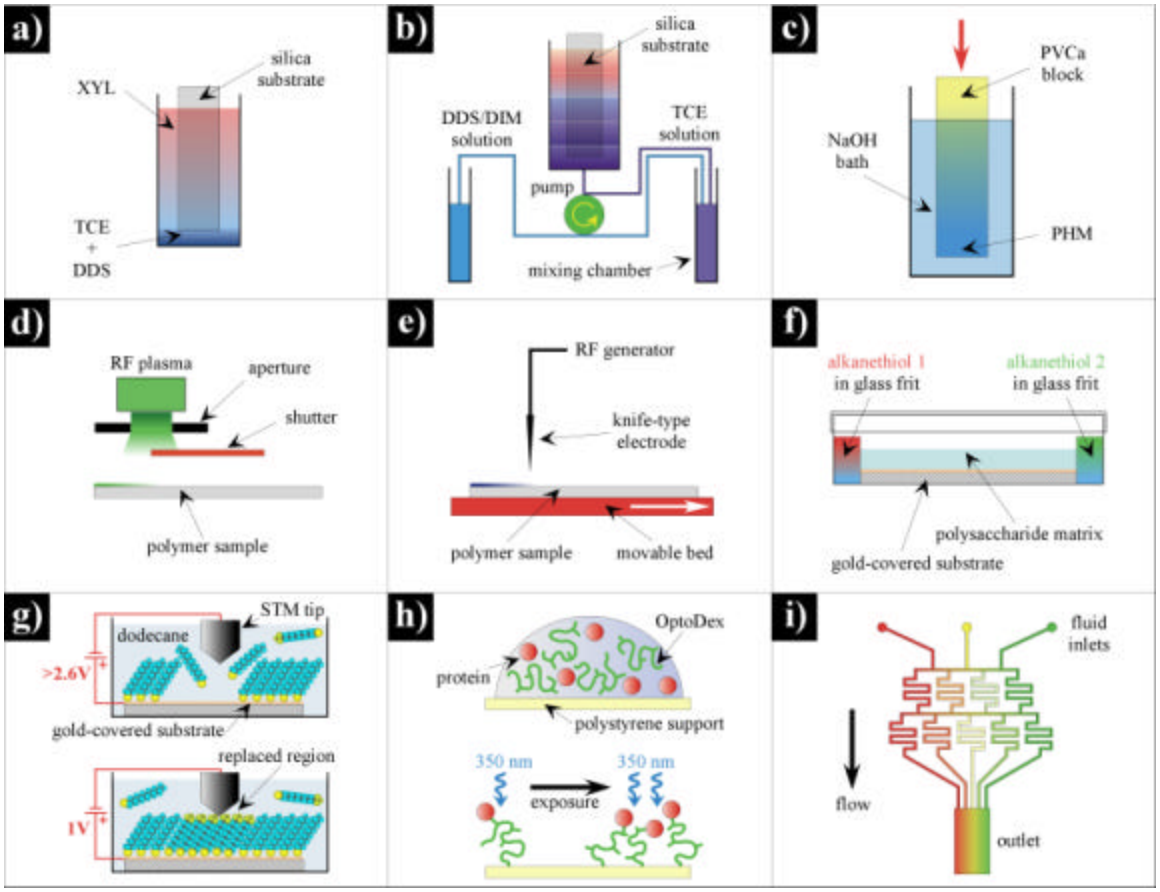

Figure 4.2 Schematic illustrating the formation of wettability gradient using: a) liquid diffusion technique; b) density gradient solution method; c) hydrolysis of poly(vinylene carbonate); d) radio frequency plasma discharge; e) plasma discharge; f) diffusion of alkanethiols in polysaccharide matrix; g) molecular gradients via replacement lithography; h) gradients of proteins by means of heterobifunctional photolinkers; and i) solution and surface gradient using microfluidics [taken from Ref. 17].

and pumped from a mixing chamber into the bottom of a container containing vertically positioned silica-covered substrates. Simultaneously, the TCE solution was replenished in the mixing chamber with a solution from a second flask that contained DDS dissolved in diiodomethane (DIM). The concentration of DDS in the mixing chamber increased with time and as a result a vertical density gradient containing a DDS concentration gradient built up in the container containing the substrates (with increasing concentration from the bottom). The wettability gradient was formed upon chemisorption of DDS to the silica substrate. While it allows for multiple gradient profiles, this technique is rather laborious.

Ueda-Yukoshi and Matsuda showed that poly(vinylene carbonate) (PVCa) can be hydrolyzed to produce poly(hydroxyl methylene) (PHM) in an alkaline solution (*cf.* Figure 4.2c). The researchers utilized this chemical conversion method to produce a wettability gradient on a PVCa surface[21]. A glass slide was first covered with a thin layer of PVCa, dried, and gradually immersed into an alkaline solution of NaOH. This process produced a surface, whose position-dependent wettability changed from hydrophobic (PVCa) to hydrophilic (PHM). By controlling the immersion speed, the gradient steepness was allowed to vary from several millimeters to several centimeters.

A versatile method for decorating polymer surfaces with chemical gradients is based on moving a shutter over the polymer surface during exposure of the surface to a radio frequency plasma discharge[22](*cf.* Figure 4.2d). This technique is capable of producing various gradient shapes on a variety of polymers under various gas conditions. However, the chemical nature of the plasma-modified surfaces is not well defined – the surface consists of a mixture of various hydrophilic groups and radicals. Moreover, some materials have a

tendency to roughen when exposed to a radio frequency plasma discharge. Lee and coworkers produced wettability gradient on low-density polyethylene surface by treating the polymer sheets in air with corona from a knife-type electrode whose power gradually increased along the sample length[23](*cf.* Figure 4.2e). While this method has the same characteristics as that based on a radio frequency plasma discharge, it is easier to accomplish and the treatment can be done under ambient conditions.

Roberson and coworkers developed a simple method of preparing surfaces with gradually varying wetting properties on a millimeter scale[24]. They first deposited SAMs made of n-octyl trichorosilane (OTS) on flat silica surfaces and exposed such surfaces to a gradient UV/ozone (UVO) radiation. In order to produce the gradient of UVO, Roberson and coworkers used variable density filter made of fused silica that was modified with inconel (a Ni, Cr, Fe alloy). The optical density varied from 0.04 to 1.0 (measured at λ=330 nm) across the fused silica optical filter in 11 equidistant steps (4 mm each) giving a linear transmission gradient in the intensity of the UV radiation. The filter was placed close to the SAM-covered surface. Atomic oxygen, generated from molecular oxygen in the proximity of the surface by the UV radiation, converted a fraction of the $-CH_2-$ and $-CH_3$ groups in the hydrophobic OTS moieties into hydrophilic functional groups (*e.g.*, -COOH). The molar concentration of the atomic oxygen (and thus the density of the hydrophilic groups on the surface) was directly proportional to the incident UV intensity. Measurements using contact angle and time-of-flight secondary ion mass spectrometry confirmed the existence of linear wettability gradients; the surface energy was shown to increase from 26 mJ/m^2, on the untreated side, to 72 mJ/m^2, close to the UVO-modified side of the substrate.

Liedberg and Tengvall prepared molecular gradients by cross-diffusion of two different ω-substituted alkanethiols from opposite ends of a polysaccharide matrix deposited on top of a gold-covered planar substrate[25](*cf.* Figure 4.2f). As the two alkanethiols interdiffused, they bonded to the underlying gold substrate and formed a self-assembled monolayer, whose composition changed along the diffusion path. Liedberg and coworkers demonstrated that this methodology can be used to prepare one-dimensional molecular gradients with hydrophilic/hydrophobic variation as well as ordered/disordered structures[26].

The ability to control electrochemically the adsorption/desorption of alkanethiol molecular assemblies on/from a noble metal surface and its utilization in preparing structures with spatiotemporal characteristics has been exploited by Bohn and coworkers[27]. They first formed a self-assembled monolayer of n-octanethiol (OT) on a gold-coated substrate. OT gradients were formed by applying a 15 nV/mm in-plane potential gradient, which selectively removed the OT molecules from the regions exposed to a higher potential. After washing with pure solvent, the sample was re-immersed into another solution containing a hydrophilic mercapto propionic acid (MPA), whose molecules filled the bare areas on the gold substrate. A two-component linear gradient in composition (and hence wettability) was thus generated.

Gorman and coworkers recently developed a novel technique for preparing molecular gradients, whose dimensions can be controlled on the nanometer scale[15] (*cf.* Figure 4.2g). In their methodology, an organized SAM of an ω-substituted alkanethiol was formed on an atomically flat gold substrate. Such a substrate was then immersed into a dodecane solution containing another ω-substituted alkanethiol. The substrate bound SAM was be repeatedly

imaged with scanning tunneling microscopy without apparent change in their appearance under conditions of setpoint bias of +1 V (positive substrate bias) and setpoint current of ≈6-8 pA. Upon changing the bias to +3.0 V or slightly higher (up to +4.0 V), replacement of the thiolate on the surface by the different thiol in solution occurred. This replacement was observed by scanning the tip in one area at the higher voltage, reducing the setpoint voltage back to 1V and scanning the tip across a larger area. By rastering the tip in a defined pattern above the substrate, features with ≈10-15 nm resolution and a variety of pattern shapes were generated.

Wijesundara and coworkers showed that surfaces with gradient wettabilities can be obtained by hyperthermal polyatomic ion deposition[28]. A poly(methyl methacrylate) (PMMA)/fluorocarbon gradient was produced by exposure of PMMA surface to $C_3F_5^+$ ions. A linear variation in wettability was achieved by linearly increasing the fluency of the $C_3F_5^+$ ions while allowing the ion source to scan across the PMMA substrate. The researchers also established that polyatomic deposition method can be used to form wettability gradients on other materials, including polymers (polystyrene, PS), semiconductors (H-terminated silicon), and oxides (Al_2O_3). In each case, the parameters of the gradients can be tuned by varying the ion type, fluency, and the scanning speed.

Hypolite and coworkers proposed a method for creating microscale gradients using photoreactive cross-linking agents[29](*cf.* Figure 4.2h). In their methodology, a conjugation reagent containing a photoactivable benzophenone (BP), a water-soluble tetraethylene glycol (TEG) spacer, and an amine reactive N-hydroxysuccinimide (NHS) ester was prepared and used to derivatize a protein, R-phycoerythrin (PE). A surface with a PE concentration

gradient was created by scanning Cd/He laser beam across the surface in a raster pattern but with increasing scanning speed in consecutive lines. Exposure to the laser beam activated BP, which set on a reaction scheme that resulted in protein immobilization on the substrate. Increasing the exposure time of the surface to the laser beam increased the amount of BP-TEG-PE immobilized on the surface. Higher scanning velocities (shorter exposure times) resulted in lower concentrations of immobilized protein relative to the slower velocities.

Caelen and coworkers utilized similar technology to form discrete gradients of immobilized proteins on surfaces[30]. They mixed protein probes with the photolinker polymer OptoDex (a polysaccharide-based polymer substituted with aryldiazirines). The solution was deposited on the surface in a gradient fashion via ink-jet printing. After drying, the surface was irradiated with light of 350 nm wavelength. Photoactivation of the aryldiazirine molecules led to the formation of reactive carbenes. Some carbenes underwent insertion reactions with covalent bonds of probe proteins, others bound to the underlying polystyrene surface. A discrete protein gradient on the surface was formed by removing non-covalently attached protein by washing.

Caelen and coworkers proposed that gradients of immobilized proteins on surfaces can be prepared by utilizing microfluidic networks[31]. In this methodology, a poly(dimethyl siloxane) (PDMS) substrate was placed across the channels of a microfluidic network made on micromachined silicon to pattern lines of proteins onto the PDMS substrate. Capillary forces between a solution containing proteins and the hydrophilized walls of the microfluidic network induced filling of the channels and the protein was gradually depleted by fast

adsorption of the proteins to the hydrophobic regions of the PDMS substrate exposed to the filled channels. After separating the PDMS from the microfluidic network, the underivatized areas of PDMS were blocked with bovine serum albumin. In the final step, fluorescently labeled immobilized antigens with antibodies were attached to the protein gradient areas to visualize the gradient. Whitesides and coworkers utilized a network of multi-inlet microfluidic channels to fabricate gradients in composition in solution and gradients in topography on the surface[32,33,34](*cf.* Figure 4.2i).

A microfluidic gradient generator comprising multiple generation branches in poly(dimethyl siloxane) network was fabricated by rapid prototyping[34] and soft lithography. Multiple solutions were simultaneously infused into the network through the inlets. As the fluid streams traveled down the network, they were repeatedly split, mixed, and recombined. After several generations of branched systems, each branch contained different proportions of the infused solutions. A gradient was established – perpendicular to the flow - in a single large channel that combined all branches. Various gradient shapes and profiles were generated, including periodic gradients, asymmetric gradients, superposed gradients, and dynamic gradients. By flowing hydrofluoric acid through the microfluidic network a gradient in surface topography was also generated on silica.

In this thesis, we will use several strategies of producing gradient-based surfaces. All methodologies are based on generating the wettability gradient using the vapor deposition technique suggested more than 10 years ago by Chaudhury and Whitesides[4]. In this method, shown schematically in Figure 4.3, an organosilane (either chloro- or alkoxy- based) is mixed

with paraffin oil (PO) and the mixture is placed in an open container that is positioned close to an edge of a silicon wafer.

Figure 4.3 Schematic picture of gradient preparation using vapor deposition

As the silane evaporates, it diffuses in the vapor phase and generates a concentration gradient along the hydrophilic substrate. Upon impinging on the substrate, the silane molecules react with the substrate -OH functionalities and form an organized SAM. The breadth and position of the silane molecular gradient can be tuned by varying the silane diffusion time and the flux of the silane molecules. The latter can be conveniently adjusted by varying the silane:PO ratio and/or the temperature of the silane:PO mixture. After the gradient SAM deposition, any physisorbed silane molecules are removed by thoroughly washing the substrates with warm deionized water (75°C, resistivity >16 MΩ·m) for several minutes. In some instances, the molecular gradients serve as precursors for further processing. Specifically, we document later in chapter 5 and 6 that molecular gradients can be used as templates for the formation of 3D structures by allowing polymer chains to grow from the molecules within the gradient (so called "grafting from" technology).

4.3 Characterization of gradient properties

Several surface analytical techniques can be applied to study the properties of the gradient substrates. Perhaps the easiest and most widely available method is based on measuring the wettability using either static or dynamic contact angles. In static contact angle experiments, one measures the wetting angle of a small volume of probing liquid on the surface. While in some instances, contact angles are reported for cases where the droplet is separated from the needle, most measurements are performed under the conditions where the needle and the probing liquid are not separated. The latter set of measurements allows for determining so-called advancing and receding contact angles. Contact angle measurements on wettability gradients are usually performed such that the needle is in contact with the probing liquid. Separating the needle from the liquid would allow the liquid to move on the surface (see ref. 4), particularly in gradients with steep boundaries between the hydrophobic/hydrophilic regions. The dynamic contact angle (DCA) measurements are usually performed using the Wilhelmy plate techniques. Examples of the DCA measurements on gradient substrates can be found elsewhere[35].

While useful in providing macroscopic level information about the chemistry on the gradient surfaces, contact angle methods are not capable of delivering information about the structural properties of the gradients on a molecular level (such as concentration of a particular chemical group, orientation of molecules, etc). For information regarding the above one has to turn to more sophisticated techniques. Ruardy and coworkers discuss several examples describing the utilization of x-ray photoelectron spectroscopy (XPS) and infrared spectroscopy (IR)[35]. Recently, near-edge x-ray absorption fine structure

spectroscopy (NEXAFS) spectroscopy has been applied to study the physico-chemical characteristics of gradient surfaces. NEXAFS turned out to be very beneficial because it allowed for simultaneous investigation of both the surface chemistry and the molecular orientation.

In the following section we provide some details pertaining to the contact angle, IR, and NEXAFS methods, which we used in our experiments.

4.3.1 Contact angle measurements

Contact angle measurements represent a simple and yet a very reliable method of characterizing the surface character of a material. The fundamental equation for determining the surface tension of a solid by contact angle measurements is described by the relationship first proposed by Young:

$$\gamma_{sv} - \gamma_{sl} = \gamma_{lv} \cos\theta_e \tag{4.1}$$

where γ_{sv}, γ_{sl}, and γ_{lv} are the interfacial tensions between solid/vapor, solid/liquid, and liquid/vapor respectively, and θ_e is the equilibrium contact angle (defined in Figure 4.4). Depending on the value of θ_e surfaces are either hydrophobic (θ_e >90°) or hydrophilic (θ_e <90°).

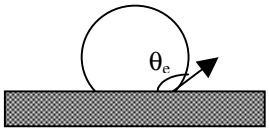

Figure 4.4 Contact angle measurement

The most commonly used method for contact angle measurements of solids is the sessile drop technique. In this technique, a droplet of a purified liquid is placed on a surface using a syringe. The wetting angle, defined as the tangent to the drop at the three-line interface, is measured using a goniometer or a charge coupled device (CCD) camera fitted onto a microscope. The angle formed by adding liquid to the droplet, causing it to advance over the surface is termed the advancing contact angle (θ_a). The angle formed by removing liquid from the droplet, causing it to recede over the surface is named the receding contact angle (θ_r).

The difference between the advancing and the receding contact angle is referred to as the hysteresis, $\Delta\theta = \theta_a - \theta_r$. While for an "ideal" surface $\Delta\theta=0$, for "real" surfaces $\Delta\theta>0$. The extent of the contact angle hysteresis depends on the surface roughness, the surface chemical heterogeneity, and also on the contact time of the contact time of the droplet and the surface. The advancing contact angle tends to reflect the hydrophobic (lower surface energy) regions whereas the receding contact angle reflects the hydrophilic (higher surface energy) region. For static contact angle measurement, the angle is obtained simply by putting a drop of liquid on the surface. Such values are frequently reported, but this method provides no information about the hysteresis.

4.3.2 FTIR-ATR spectroscopy

A commonly used method to characterize the chemical structure on the surface is infrared (IR) spectroscopy using the attenuated total reflection (ATR) technique. The ATR technique enables identification of specific molecules and groups located in the surface layer, typically 1 to 10 μm. The arrangement of the specimen in ATR-IR spectroscopy is shown schematically in Fig. 4.5.

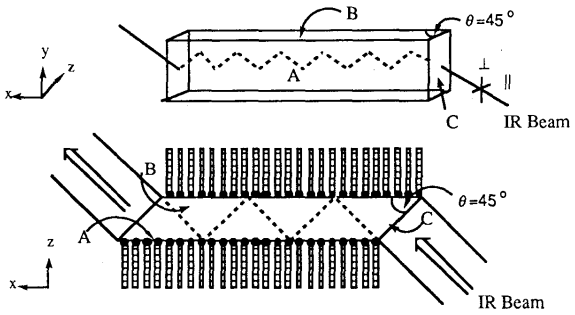

Figure 4.5 A schematic description of an optical setup for ATR measurement [taken from Ref. 3].

Since it is nondestructive and highly sensitive to various chemical functionalities, Fourier transform infrared (FTIR) spectroscopy is an excellent tool for studying the chemistry and orientation of thin organic films at the molecular level. For molecular orientation determination, various modes of IR have been used, such as reflection-absorption (RA), transmission, attenuated total reflection (ATR), with either unpolarized or polarized infrared beams. Frequently, combinations of results of several modes have been used.

The combination of RA and transmission modes of IR spectroscopy has been frequently employed because these two modes are effective in differentiating transition moments lying parallel (or close to parallel) to the film surface from those normal (or close to normal) to that surface. It should be noted, however, that sample films must be prepared on a specular metallic surface for the IR-RA mode and on another nonabsorbing substrate for the IR transmission mode. Previous studies have ignored the effect of the substrate surface on the molecular orientation or assumed that it is the same. Furthermore, for monomolecular films the signal-to-noise (S/N) ratios of the RA and transmission modes are often too low to allow precise determination of orientation. FTIR-ATR has much higher S/N ratios than the above modes.

4.3.3 Near-edge absorption fine structure (NEXAFS) spectroscopy

NEXAFS involves the resonant soft X-ray excitation of a K or L shell electron to an unoccupied low-lying antibonding molecular orbital of σ or π symmetry, σ^* and π^*, respectively[36]. The initial state K or L shell excitation gives NEXAFS its element specificity, while the final-state unoccupied molecular orbitals provide NEXAFS with its bonding or chemical selectivity. A measurement of the intensity of NEXAFS spectral features enables the identification of chemical bonds and determination of their relative population density within the sample. Because of the fixed geometry between the sample and the X-ray beam and the fact that the $1s \rightarrow \sigma^*$ and $1s \rightarrow \pi^*$ excitations are governed by dipole selection rules, the resonance intensities vary as a function of the direction of the electric vector **E** of the

incident polarized X-ray relative to the axis of the σ* and π* orbital. This, coupled with the fact that sharp core level excitations for elements C, N, O, and F occur in the soft X-ray spectral region, makes NEXAFS an ideal technique for probing molecular orientations of organic molecules. Since its first introduction as a routine analytical technique, NEXAFS has proven advantageous in determining the orientation of both small molecules, as well as large macromolecular systems. Recently, we have demonstrated that NEXAFS can be used to sense the chemistry and determine molecular orientation on gradient materials surfaces[37,38]. In order to measure the spatial distribution of a given molecule, the sample is mounted onto a goniometer, which controls the orientation of the sample with respect to the polarization vector of the X-rays and enables horizontal and vertical sample motion. After tuning the monochromator energy to that corresponding to a given characteristic 1s → σ* (or 1s → π*) transition, the sample is moved with small increments (usually between 0.5-1 mm) and after each step a new NEXAFS data set is recorded. In order to determine the concentration of a given chemical moiety, the angle between the sample normal and the electric vector **E** of the polarized X-ray beam, θ, is set at θ ≈ 50-55°. At this angle – so-called "magic angle" - the NEXAFS intensity is independent of the molecular orientation on the substrate. If orientation information is required, the above procedure is repeated for at least three different angles θ (usually 20°, 50°, and 90°) and the molecular orientation is evaluated using standard techniques (for details see [ref. 36,37]).

4.4 Applications of gradients on substrates

Continuous or discrete molecular gradients represent a chief tool for combinatorial chemistry and materials science[39],[40]. The combinatorial approach leads to rapid technological development with improved efficiency and lower research cost[41]. In addition, as documented below, the unique properties of gradient substrates can be also utilized to study transport phenomena on surfaces.

4.4.1 Combinatorial studies of cell/substrate interactions

Successful application of a biomaterial inside the body necessitates that it mimics the function of the body part where it will be implanted. This requires that the implant responds to protein adsorption, cellular adhesion, and inflammatory reactions in the same way as the body part does. Most of the above mentioned functions are influenced by wettability of the biomaterial surface. Traditional experiments designed to study the effect of wettability suffered from different surface chemistry of various biomaterials used to achieve a wide behavioral spectrum. For example, it was often difficult to segregate the effect of wettability on the studied phenomenon from that of surface chemistry of the surface. This incertitude is minimized to a great extent by studying protein and cell adsorption on a molecular gradient surface, where the observed response can be attributed primarily to variation in wettability along the surface. In addition, it has been recognized that immobilization of proteins and peptides on the surface of a material offers a powerful method for probing cell response and

migration, biodetection, and activity control. The need for such well-defined surfaces as well as the requirement of reducing the number of specimens necessary for these studies has stimulated the development of methodologies providing gradients of biological macromolecules. Several techniques listed in the previous part of this chapter have been utilized in these studies. A recent review summarizes the progress in the application of gradient substrate in studies of cellular interaction phenomena up until 1997.[35]

4.4.2 Thin film behavior on gradient substrates

There is a considerable need for understanding the structure, stability and phase behavior of thin liquid and polymer films. Several studies have appeared that reported on utilizing combinatorial approaches to study the coalescence of droplets on chemically heterogeneous gradient substrates[42], order-disorder transition in grafted oligoalkanes on surfaces[26], and phase separation in immiscible polymer blends[43]. For example, Genzer and Kramer studied the phase separation in thin films of poly(ethylene propylene) (PEP) and its deuterated analog (dPEP) deposited on wettability gradient substrates prepared using the diffusion of alkanethiols in polysaccharide matrix[25]. By adjusting the composition of the alkanethiol solutions used to produce the wettability gradient, the surface energy (γ_{SAM}) was allowed to vary over a narrow window (from 30 to 21 mJ/m^2). Elastic recoil detection was used to measure the volume fraction profiles of dPEP and PEP in the samples. Figure 4.6 shows a series of such volume fraction *vs.* depth profiles of dPEP for various positions along the gradient substrate (open circles). It is evident that the air/mixture interface is always wet

by the dPEP-rich phase. The situation at the mixture/SAM interface is more complex. For γ_{SAM}<25 mJ/m^2 the mixture/substrate interface is wet by a dPEP-rich phase. However, the thickness of this layer depends strongly on γ_{SAM} and decreases with increasing γ_{SAM}. At γ_{SAM}=25.6 mJ/m^2 the mixture/SAM interface is wet by the PEP-rich phase. The results in Figure 4.6 also show that as the thickness of the dPEP phase at the mixture/substrate interface decreases, the thickness of the dPEP-rich phase at the air/mixture interface increases. This observation indicates that as γ_{SAM} increases there is a redistribution of dPEP material from the mixture/SAM interface to the air/mixture interface. This pretransitional behavior was shown to originate from the long-range nature of the van der Waals interaction between layers and was predicted by a simple model that considered the dependence of the free energies of the two dPEP-rich layers at the surface and substrate interfaces on their thicknesses.

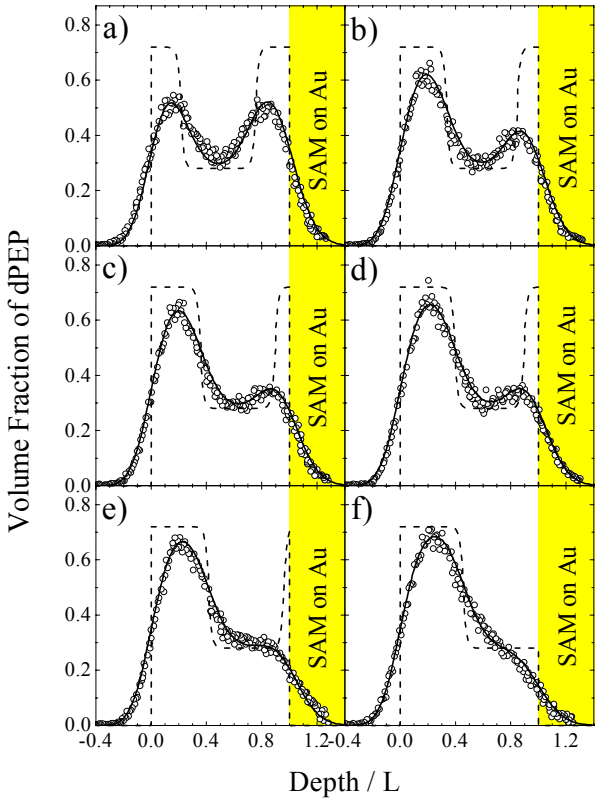

Fig. 4.6 Series of volume fraction *vs.* depth profiles of dPEP for various positions along the gradient substrate (open circles). [taken from Ref. 43]

4.4.3 Motion of liquids on gradient substrates

Chemical gradients are capable of transporting materials in a directional manner and are responsible for driving many important biological and physical processes[35]. Initial empirical observations have evolved into deliberate efforts to direct liquid motion along chemical gradients[44]. It has long been known that a continuous liquid film can spontaneously break into droplets that move freely over surfaces without application of an obvious external force. For example, the formation of wine drops from a continuous liquid film spreading over the wineglass surface is driven by the change in surface tension caused by the evaporation of alcohol. Variations in surface tension and the resulting changes in wetting behavior of the liquid by composition or temperature gradients were studied and explained over 100 years ago and are associated with the name of the Italian physicist Carlo Marangoni[45]. Motion due to chemical gradients on the substrate was demonstrated by Chaudhury and Whitesides[4] with droplets of water moving on a surface of varying hydrophobicity created by coating a silicon wafer partially with n-decyl trichlorosilane (DTS). A drop of water moved from the hydrophobic end to the hydrophilic end of the wafer, but only very slowly and only over a distance of the order of 1 mm. Very recently much higher drop speeds have been observed for small water droplets formed by condensation of steam onto a gradient surface[46] and droplets on vibrating gradient surfaces[47].

4.4.4 Molecular gradients as 2D templates

Gradient substrates have also been utilized as molecular templates for controlling the spatial distribution of non-polymeric objects. Plummer and Bohn reported on electrochemically generating a gradient of amino-terminated thiol-based self-assembled monolayer on a gold-covered substrate[48]. In order to produce particle gradients, Plummer and Bohn attached carboxylic acid-modified, fluorescently doped polystyrene nanospheres (diameter of 200 nm) to the amio-termini of the gradient SAM. Bhat and coworkers prepared assemblies of 17 nm gold nanoparticles with continuous gradients in number density on flat silica-covered substrates[49](*cf.* Figure 4.7). Their methodology consisted of first forming a one dimensional molecular gradient of amino groups ($-NH_2$) on the substrate by vapor diffusion of amine-terminated silane molecules, followed by attachment of gold nanoparticles to the $-NH_2$ functional groups by immersing the substrate in a colloidal gold solution. Experiments using scanning force microscopy revealed that the number density of nanoparticles on the substrate varied continuously as a function of the position on the substrate. NEXAFS studies confirmed that the nanoparticle number density gradient was closely correlated with the concentration gradient of $-NH_2$ groups anchored to the substrate. Bhat and coworkers demonstrated that the number density of nanoparticles within the gradient and the length of the gradient can be tuned by controlling the vapor diffusion of silane molecules. The adhesive molecular template can be modified to attract different kinds of particles for different applications, all of them arranged in gradient pattern. The ability to vary and control the concentration of captured particles allows one to devise sensors, filters, *etc*. Some components of fluids, for example, could pass through the gaps in the less-

concentrated part of the particle gradient, but be blocked by the thicker concentration. Such filters could also be tailored to detect or capture harmful viruses or toxins.

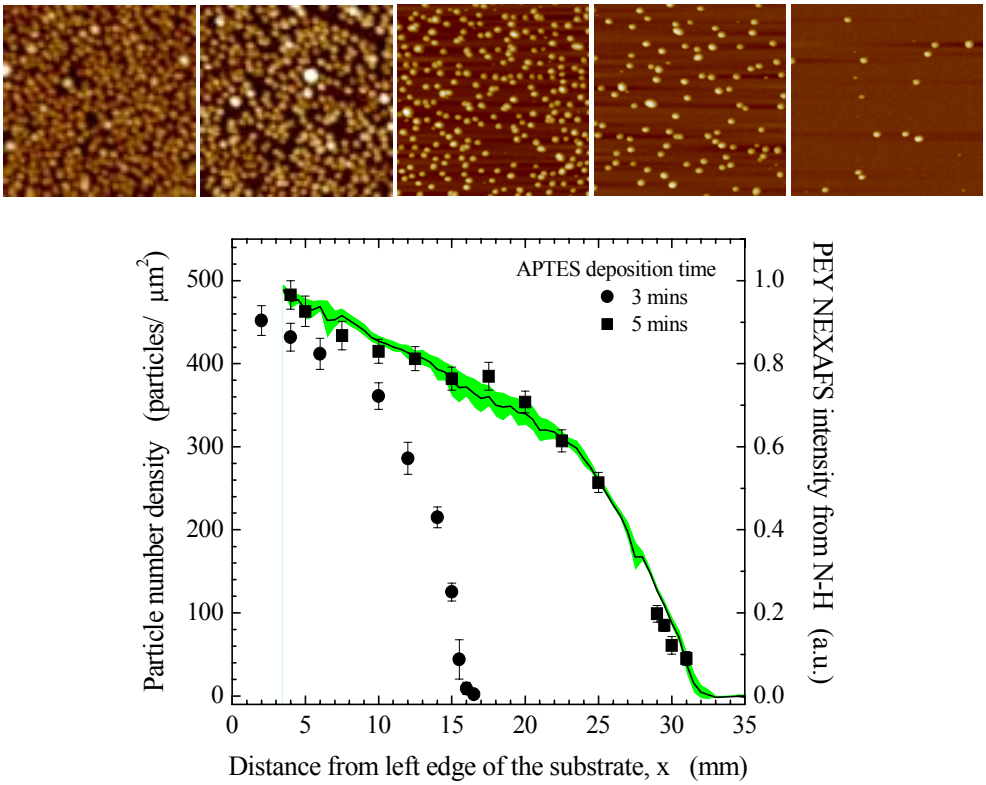

Figure 4.7 (Upper panel) Scanning force microscopy images of gold nanoparticles (diameter ≈17 nm) adsorbed along a substrate prepared by evaporating an (3-aminopropyl) triethoxysilane (APTES)/paraffin oil (PO) mixture (50/50 w/w) for 5 min followed by immersion in colloidal gold solution (pH≈6.5) for 24 hrs (Edge of each image = 1 μm). (Lower panel) Particle number density profile (left) for two gradients prepared by evaporating APTES/PO mixtures for 3 (●) and 5 (■) mins. The line represents the partial electron yield (PEY) near-edge x-ray absorption fine structure (NEXAFS) profile (right) of N-H bonds from an ATEPS gradient prepared by evaporating APTES/PO mixture for 5 minutes. The area around the PEY NEXAFS line denotes the measurement uncertainty [taken from Ref. 49].

All gradient techniques presented to date let to the formation of two-dimensional gradient patters. Recently it has been recognized that molecular gradients can serve as useful templates for creating 3-dimensional structures. In this thesis, methods will be developed for fabricating anchored polymers o solid substrate with a gradual variation of the grafting density. And these 3-dimensional structures will be applied to investigate polymer and polyelectrolyte brush properties.

References and notes

[1] Bigelow, W.C.; Pickett, D.L.; Zisman, W.A. *J. Colloid Interface Sci.* **1**, 513 (1946).

[2] Zisman, W.A. *Adv. Chem. Ser.* **43**, 1 (1964).

[3] Ulman, A., *An introduction to ultrathin organic films from Langmuir-Blodgett to self-assembly*, Academic press: New York, 1991

[4] Chaudhury, M. K. and Whitesides, G. M. *Science* **255**, 1230 (1992).

[5] Chaudhury, M. K. *Biosensors & Bioelectronics* **10**, 785 (1995).

[6] Xia, Y.; Whitesides, G. M.; *Angew. Chem. Int. Ed. Engl.* **37**, 550 (1998); Xia, Y.; Rogers, J. A.; Paul, K. E.; Whitesides, G. M. *Chem. Rev.* **99**, 1823 (1999).

[7] Husseman, M.; Mecerreyes, D.; Hawker, C. J.; Hedrick, J. L.; Shah, R.; Abbott, N. L. Angew. *Chem. Int. Ed. Engl.* **38**, 647 (1999).

[8] Shah, R.; Mecerreyes, D.; Husemann, M.; Rees, I.; Abbott, N. L.; Hawker, C. J.; Hedrick, J. L. *Macromolecules* **33**, 597 (2000).

[9] Jeon, N. L.; Choi, I. S.; Whitesides, G. M.; Kim, N. Y.; Laibinis, P. E.; Harada, Y.; Finnie, K. R.; Girolami, G. S.; Nuzzo, R. G. *Appl. Phys. Lett.* **75**, 4201 (1999); Kim, N.; Jeon, N. L.; Choi, I. S.; Takami, S.; Harada, Y.; Finnie, K. R.; Girolami, G. S.; Nuzzo, R. G.; Whitesides, G. M.; Laibinis, P. E. *Macromolecules* **33**, 2793 (2000).

[10] de Boer, B.; Simon, H. K.; Werts, M. P. L.; van der Vegte, E. W.; Hadziioannou, G. *Macromolecules* **33**, 349 (2000).

[11] Ghosh, P.; Lackowski, W. M.; Crooks, R. M. *Macromolecules* **34**, 1230 (2001).

[12] Jones, D. M.; Huck, W. T. S. *Adv. Mater.* **13**, 1256 (2001).

[13] Hyun, J.; Chilkoti, A. *Macromolecules* **34**, 5644 (2001).

[14] Efimenko, K.; Genzer, J. *Adv. Mater.* **13**, 1560 (2001).

[15] Fuierer, R. R.; Carroll, R. L.; Feldheim, D. L.; Gorman, C. B. *Adv. Mater.* **14**, 154 (2002).

[16] Meredith, J. C. Karim, A.; Amis, E. J. *MRS Bulletin* **27**, 330 (2002).

[17] Genzer, J. "*Molecular gradients: Formation and applications in soft condensed matter science*", Encyclopedia of Materials Science, (K.H.J. Buschow, R.W. Cahn, M.C. Flemings, B. Ilschner, E.J. Kramer, S. Mahajan, Eds.), Elsevier, Oxford, 2002.

[18] Carter, S. B. *Nature* **208**, 1183 (1965).

[19] Elwing, H; Welin, S.; Askendal, A.; Nilsson, U.; Lundstrőm, I. *J. Colloid Interface Sci.* **119**, 203 (1987).

[20] Gőlander, C. G.; Caldwell, K.; Lin, Y.-S. *Coll. Surf.* **42**, 165 (1989).

[21] Ueda-Yukoshi, T.; Matsuda, T. *Langmuir* **11**, 4135 (1995).

[22] Pitt, W. G. *J. Colloid Interface Sci.* **133**, 223 (1989).

[23] Lee, J. H.; Kim, H. G.; Khang, G. S.; Lee, H. B.; Jhon, M. S. *J. Colloid Interface Sci.* **151**, 563 (1992).

[24] Roberson, S. V.; Fahey, A. J.; Sehgal, A.; Karim, A. *Appl. Surf. Sci.* **9427**, 1 (2002).

[25] Liedberg, B. and Tengvall, P. *Langmuir* **11**, 3921 (1995).

[26] Lestelius, M.; Enquist, I.; Tengvall, P.; Chaudhury, M. K.; Liedberg, B. *Coll. Surf. B: Biointerfaces* **15**, 57 (1999).

[27] Terrill, R. H.; Balss, K. M.; Zhang, Y.; Bohn, P. W. *J. Am. Chem. Soc.* **122**, 988 (2000).

[28] Wijesundara, M. B.; Fuoco, E.; Hanley, L. *Langmuir* **17**, 5721 (2001).

[29] Hypolite, C. L.; McLernon, T. L.; Adams, D. N.; Chapman, K. E.; Herbert, C. B.; Hunag, C. C.; Distefano, M. D.; Hu, W.-S. *Bioconjug. Chem.* **8**, 658 (1997).

[30] Caelen, I.; Gao, H.; Sigrist, H. *Langmuir* **18**, 2463 (2002).

[31] Caelen, I.; Bernard, A.; Juncker, D.; Michel, B.; Heinzelmann, H.; Delamarche, E. *Langmuir* **16**, 9125 (2000).

[32] N. L. Jeon, S. K. W. Dertinger, D. T. Chiu, I. S. Choi, A. Stroock, G. M. Whitesides, *Langmuir* **16**, 8311 (2000).

[33] Dertinger, S. K. W.; Chiu, D. T.; Jeon, N. L.; Whitesides, G. M. *Anal. Chem.* **73**, 1240 (2001).

[34] Duffy, D. C.; McDonald, J. C.; Schueller, O. J. A.; Whitesides, G. M. *Anal. Chem.* **70**, 4974 (1998).

[35] Ruardy, T. G.; Schakenraad, J. M.; van der Mei, H. C.; Busscher, H. J. *Surf. Sci. Rep.* **29**, 1 (1997).

[36] Stöhr, J. *NEXAFS Spectroscopy*, Springer-Verlag, Berlin (1992).

[37] Genzer, J.; Fischer, D. A.; Efimenko, K. *Appl. Phys. Lett.* **82**, 266 (2003).

[38] The NEXAFS experiments were carried out at the NIST/Dow soft X-ray materials characterization facility at the National Synchrotron Light Source at Brookhaven National Laboratory. For detailed information about the NIST/Dow Soft X-ray Materials Characterization Facility at NSLS BNL see: http://nslsweb.nsls.bnl.gov/nsls/pubs/newsletters/96-nov.pdf

[39] van Dover, R. B.; Scheemeyer, L. F.; Fleming, R. M. *Nature* **392**, 162 (1998).

[40] Jandeleit, B.; Schaefer, D. J.; Powers, T. S.; Turner, H. W.; Weinberg, W. H. *Angew. Chem. Int.* Ed. **38**, 2494 (1999).

[41] Amis, E. J.; Xiang, X.-D.; Zhao, J.-C. *MRS Bulletin, special issue on combinatorial materials science* **27**, 295 (2002).

[42] Zhao, H.; Beysens, D. *Langmuir* **11**, 627 (1995).

[43] Genzer, J.; Kramer, E. J. *Europhys. Lett.* **44**, 180 (1998).

[44] Bain, C. D. *Chemphyschem* **2**, 580 (2001).

[45] Scriven, L. E.; Sternling, C. V. *Nature* **187**, 186 (1960).

[46] Daniel, S.; Chaudhury, M. K.; Chen, J. C. *Science* **291**, 633 (2001).

[47] Daniel, S.; Chaudhury, M. K. *Langmuir* **18**, 3404 (2002).

[48] Plummer, S. T.; Bohn, P. W. *Langmuir* **18**, 4142 (2002).

[49] Bhat, R. R.; Fischer, D. A.; Genzer, J. *Langmuir* **18**, 5640 (2002).

Chapter 5

Multivariant investigation of the mushroom-to-brush crossover in surface anchored poly(acryl amide)

5.1 Abstract

This chapter presents a method for generating assemblies comprising anchored polymers with a gradual variation of grafting densities on solid substrates. These structures can be generated by first covering the substrate with a molecular gradient of the polymerization initiator, followed by polymerization from these substrate-bound initiator centers ("grafting from"). We apply this technique to prepare grafting density gradients of poly(acryl amide) (PAAm) on silica-covered substrates. We show that using the grafting density gradient geometry, the mushroom-to-brush transition can be accessed conveniently on a single sample. This transition is detected by monitoring the dependence of the thickness of the grafted PAAm in a good solvent using ellipsometry. Wettability experiments performed on the gradient PAAm substrate provide complementary information about the nature of the mushroom-to-brush transition.

5.2 Motivation

Recent advances in the field of self-assembly have led to the development of a plethora of new technologies based on soft lithography[1], that enable alternative ways of fabricating two and three dimensional patterns on material surfaces. Most of the soft lithography techniques are based on selective deposition of self-assembled monolayers (SAMs)[2]. Various structural patterns with dimensions ranging from hundreds of nanometers to several micrometers are created on the material surface using a "pattern-transfer element" or stamp that has a three-dimensional structure moulded onto its surface. Because of the

molecular nature of the SAMs, the surface patterns generated via "soft lithography" are rather thin (several Angstroms to several nanometers). Some applications, particularly those involving subsequent microfabrication steps, such as etching, require that thicker layers of the surface coating be formed. Hence techniques, involving the patterning of thicker polymer layers grafted to the substrate have been developed[3,4,5,6,7,8,9]. The latter group of technologies is based on selectively decorating the material surfaces with polymerization initiators and then performing the polymerization directly on the surface ("grafting from"). Using this methodology, the thickness of the overcoat film can be adjusted by simply varying the polymerization conditions (*i.e.*, time, monomer concentration, temperature).

The soft-lithography techniques always produce sharp boundaries between the distinct chemical regions on the substrate. This feature is useful for creating substrates with well-defined chemical patterns of various shapes and dimensions. However, for some applications, it is desirable that the physico-chemical characteristics, such as wetting of the substrate, change gradually. This can be accomplished by producing surfaces with a position-dependent and gradually varying chemistry. In these so-called "gradient surfaces", the gradient in surface energy is responsible for a position-bound variation in physical properties, most notably the wettability[10]. Recent studies have reported on the preparation of molecular gradients on length scales ranging from nanometers to centimeters[11,12].

All gradient techniques presented to date led to the formation of two-dimensional gradient patterns. As mentioned earlier, manufacture of miniature devices and applications in lithography often requires the formation of three-dimensional structures. This part of work will present a method of preparing surface anchored polymers with gradually varying grafting densities by combining the technique of preparing molecular gradients on solid flat

substrates with the surface-initiated polymerization. Surface initiated polymerization (or "grafting from") will be used to prepare surface-anchored polymers. It has been appreciated that relative to the "grafting onto" methodology, in which the surface anchored polymers are prepared y simply adsorbing the chains from solution onto the surface, the "grafting from" method produces polymers higher grafting densities[13]. The grafting densities are not limited severely by sterical barriers imposed by the already bonded chains, since the smaller monomer can readily access the initiator site or the propagating chain end. Taking full advantages of living polymerization reaction mechanism, atom transfer radical polymerization (ATRP), a newly developed controlled radically polymerization[14], will be used for the polymer synthesis on forming linear polymer chains with narrow molecular weight distribution.

We wish to demonstrate the versatility of this novel assembling technique by using it to study the mushroom-to-brush transition.

5.3 Experimental approach

5.3.1 Preparation of poly(acryl amide) gradients on silica substrate

As mentioned earlier, the preparation of PAAm brushes with a gradual variation of grafting density on silica substrate consists of two steps: i) deposition of molecular gradient of polymerization initiator on the solid substrate, and ii) polymerization from the substrate bound initiator centers with ATRP surface "graft from" technique.

i) Initiator gradient deposition

Silicon wafers, which have a ≈19 Å thick silicon oxide layer, are used as the substrate. The silica substrates are first exposed to ultraviolet/ozone (UVO) in a commercial UVO chamber (Jelight Company, Inc., Model 42). After 30 minutes, the UVO treatment produces a hydrophilic surface with mainly hydroxide functionality groups (-OH)[15].

Figure 5.1 Schematic illustrating the formation of the CMPE gradient on a flat silica-covered substrate.

We formed gradients of the polymerization initiator on silica substrates using the methodology proposed by Chaudhury and Whitesides[10]. Specifically, as shown in Fig. 5.1, 1-trichlorosilyl-2-(m/p-chloromethylphenyl)ethane (CMPE) (United Chemical Technologies, Inc.) was mixed with paraffin oil (PO) and the mixture was placed in an open container that was positioned close to an edge of a silicon wafer. As CMPE evaporated, it diffused in the vapor phase and generated a concentration gradient along the silica substrate. Upon impinging on the substrate, the CMPE molecules reacted with the substrate -OH functionalities and formed an organized self-assembled monolayer (SAM). The breadth and position of the CMPE molecular gradient can be tuned by varying the CMPE diffusion time

and the flux of the CMPE molecules. The latter can be conveniently adjusted by varying the chlorosilane:PO ratio and/or the temperature of the CMPE:PO mixture. In order to minimize any physisorption of monomer and/or the polymer formed in solution on the parts of the substrate that do not contain the CMPE-SAM, we backfilled the unexposed regions on the substrate (containing unreacted –OH functionalities) with n-octyl trichlorosilane, (OTS) (Gelest, Inc.). After the OTS-SAM deposition, any physisorbed CMPE and OTS molecules were removed by thoroughly washing the substrates with warm deionized water (75°C, resistivity > 16 MΩ·m) for several minutes.

ii) Polymerization of poly(acryl amide)

The polymerization of PAAm is performed by atom transfer radial polymerization (ATRP), as described earlier[16,17,18], by placing the samples into 100 mL of N,N'-dimethylformamide and by adding 0.3 g of CuCl, 1.0 g of bipyridine, and 24.0 g of acrylamide (all obtained from Aldrich and used as received). Purged with nitrogen for 5 min, the flask was then sealed under N_2, placed into an oil bath, and the reaction was performed at 130°C for 48 hrs to form PAAm brushes on silica substrates. After the reaction, any physisorbed monomeric and polymeric acrylamide was removed by soxhlet extraction with deionized water for 48 hrs and dried with nitrogen.

5.3.2 Procedure of poly(acryl amide) synthesis on silica gel

Since it is difficult to collect enough polymer grown from flat surface to measure its molecular weight, PAAm brushes were grown on small silica gel particles (Davisil^{TM}, grade 645, surface area ≈300 m^2/g), cleaved off and the resulting free polymer was analyzed with size exclusion chromatography.

i) Initiator (CMPE) deposition

Solution deposition method is used to form initiator SAMs on the silica gel surface. First, 2.5g silica gel particles were cleaned in HNO_3/H_2O (50:50) for 4 hrs, then rinsed with a large volume of distilled water, and dried under N_2 at 110ºC for 3 hrs. This treatment resulted in hydrophilic silica surface with predominantly hydroxyl groups.

Next, the silica gels were humidified at 55% relative humidity for 4 hr and removed into a 250 mL flask. 50 mL anhydrous toluene was added into the flask, followed by 0.45 mL of the initiator. Nitrogen gas was flowed over the mixture for the first 10 min to remove the produced HCl gas. Then, the reaction was allowed to proceed overnight under continuous stirring.

After the reaction, the subsequent silica gel particles were filtered and rinsed with toluene, MeOH, CH_2Cl_2, and acetone. Modest vacuum could be applied for the filtration if necessary. Finally, the silica gels were dried in an oven at 110ºC for 1 hr.

ii) Surface polymerization on silica gel

In order to perform the ATRP reaction, 2.0 g of modified silica gels were added into 50 mL of N,N'-dimethylformamide, followed by adding 0.15 g of CuCl, 0.5 g of bipyridine, and 12.0 g of acrylamide. The mixture was purged with nitrogen for 5 min and then left under nitrogen seal. The polymerization was performed at 130ºC in oil bath for 48 hrs. After the reaction, the solution was cooled down and filtered. The silica gel particles were had a dark yellow color due to the copper complexes. The silica particles were thoroughly washed with DI water until silica gel turned white.

To cleave the polymer chains, the PAAm-coated porous silica gels were removed into 125 mL flask, and then 50 mL HF solution (10% w/w) was added. After 2 hrs under constant stirring, the solution was neutralized by slowly adding sodium carbonate until no CO_2 was produced. Then silica gels were separated by filtration and the polymers were precipitated into acetone. After decanting, the polymers were dried and left under mild vacuum overnight.

5.3.3 Size exclusion chromatography (SEC) measurement

The molecular weight of PAAm was determined by size exclusion chromatography (SEC) on Superose^{TM} 12 column (Äkta Explorer, Amersham Bioscience) equipped with differential refractometer and multiangle light scattering detector DAWN DSP-F (Wyatt Technology Corp.). 0.3 M sodium acetate buffer (pH≈6.5) was used as the mobile phase. The flow rate was 0.5ml/min. The molecular weight of the PAAm macromolecules cleaved

from the silica gels was (M_w=17kDa, polydispersity index=1.7). We note that Huang and Wirth reported a value of M_w=15.6kDa for the concentration of monomer, polymerization temperature and time that were the same as in our experiments [17]. The molecular weight of the solution-polymerized PAAm polymers was found to be consistently 3-5 times that of the cleaved PAAm. Presumably, the purification procedure could not completely remove the initiating system and; PAAm formed complexes with the bipyridine/copper salts mixtures. In our analysis we only use the molecular weight determined on the cleaved PAAm.

5.3.4 Ellipsometry measurement

The thickness of the SAM and the polymer layer was measured using a single-wavelength fixed geometry ellipsometer (AutoEL II, Rudolph Technologies) and a variable angle spectroscopic ellipsometry (J.A. Woollam, Inc.). The thickness was evaluated from the experimentally measured ellipsometric angles Ψ and Δ using the supplied software (DafIMB and WVASE32). The indices of refraction of the SAMs and PAAm were taken to be equal to 1.45[2] and 1.54[19], respectively. The wet thickness of the PAAm in aqueous solutions was measured by placing the samples in a custom-designed solution cell, incubating them for a desired period of time and performing the experiments with VASE at ϕ=70°, where ϕ is the angle between the incoming beam and the sample normal. The ellipsometric angles Ψ and Δ were collected for a series of wavelengths ranging from 240 to 1000 nm. The wet PAAm thickness was evaluated using a graded effective medium approximation model based on linear combination of the optical constants of the deionized water and PAAm.

5.3.5 Contact angle measurement

The wetting experiments were performed using a Ramé-Hart contact angle goniometer (model 100-00) equipped with a CCD camera, and analyzed with the Ramé-Hart software. The advancing contact angles were read by injecting 6 μL of probing liquid. Each data represents an average over five measurements on the same sample. The data points have an error better than ±1.5°.

5.3.6 NEXAFS measurement

Near edge x-ray absorption fine structure (NEXAFS) was used to study the chemistry and molecular orientation of the SAMs surfaces [20]. The NEXAFS experiments were carried out on the U7A NIST/Dow Materials Soft X-ray Materials Characterization Facility at the National Synchrotron Light Source at Brookhaven National Laboratory (NSLS BNL). The NEXAFS spectra were collected in the partial electron yield (PEY) at the normal (θ=90°), grazing (θ=20°), and so-called "magic" angle (θ=55°) incidence geometries, where θ is the angle between the sample normal and the polarization vector of the x-ray beam.

5.4 Experimental results

In Figure 5.2 we plot the variation of the contact angle of deionized (DI) water, θ_{DIW}, as a function of the position on the sample measured on the CMPE-SAM covered substrate

(closed circles) and the substrate that is backfilled with the OTS-SAM (open circles). The CMPE source (CMPE:OTS ratio=1:1 (w/w/)) is allowed to diffuse for 2 minutes at 88°C, the OTS was deposited for 15 minutes at room temperature. The data in Figure 5.2 illustrates that the contact angle of CMPE decreases gradually from ≈77° down to ≈0° as one moves across the substrate starting at the CMPE side. After the OTS deposition, the regions on the substrate far from the diffusing source are covered with a complete monolayer of OTS (contact angle ≈100°). As one traverses across the CMPE gradient, the contact angle decreases from ≈100° (OTS side) down to ≈88° (CMPE side). The minute increase of the contact angle within the CMPE-SAM is likely a result of small interpenetration of OTS into the CMPE SAM.

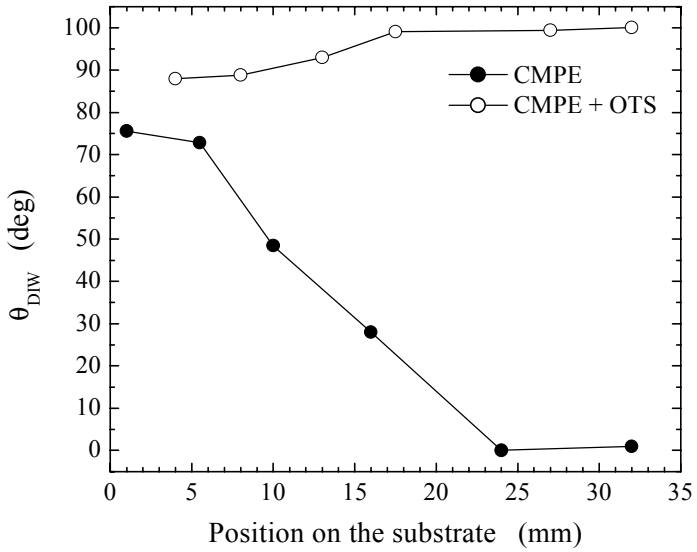

Figure 5.2 Dependence of the DI water contact angles, θ_{DIW}, on the position along the gradient substrate measured after the CMPE-SAM formation (solid circles) and after backfilling with the OTS-SAM (open circles). The lines are mean to guide the eye.

NEXAFS spectroscopy is used to provide detailed chemical and structural information about the SAMs on the substrate. In Figure 5.3 we plot the carbon edge K-edge NEXAFS spectra taken from CMPE-SAM (top) and OTS-SAM (bottom) samples.

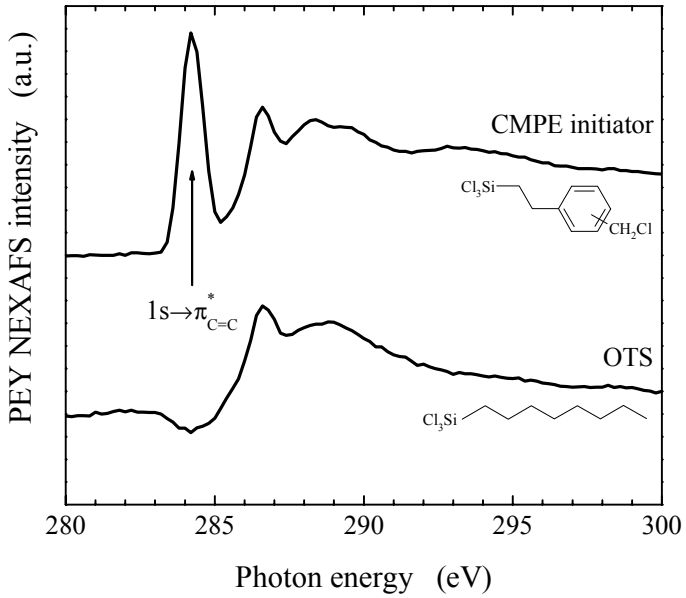

Figure 5.3 Carbon K-edge PEY NEXAFS spectra collected from the CMPE-SAM (top) and OTS-SAM (bottom). The arrow marks the position of the $1s\rightarrow\pi^*$ transition for phenyl C=C, present only in the CMEP-SAM sample.

The NEXAFS spectra collected at the "magic" angle are indistinguishable from those recorded at the normal and grazing incidence geometries. This reveals that the CMPE-SAMs are not oriented, rather they form a "liquid-like" structure. This observation is in accord with recent studies from Chaudhury and Allara groups that reported that the borderline between the "liquid-like" and "semi-crystalline-like" structures in hydrocarbon SAMs exists at $-(CH_2)_{12}-$ [21]. The NEXAFS spectra in Figure 5.3 both contain peaks at 286.0 and 288.5 eV that correspond to the $1s\rightarrow\sigma^*$ transition for the C-H and C-C bonds, respectively. In

addition, the spectrum of CMPE also exhibits a very strong signal at 284.2 eV, which can be attributed to the 1s→π* transition for phenyl C=C [20]. The latter signal can thus be used as an unambiguous signature of the CMPE in the sample.

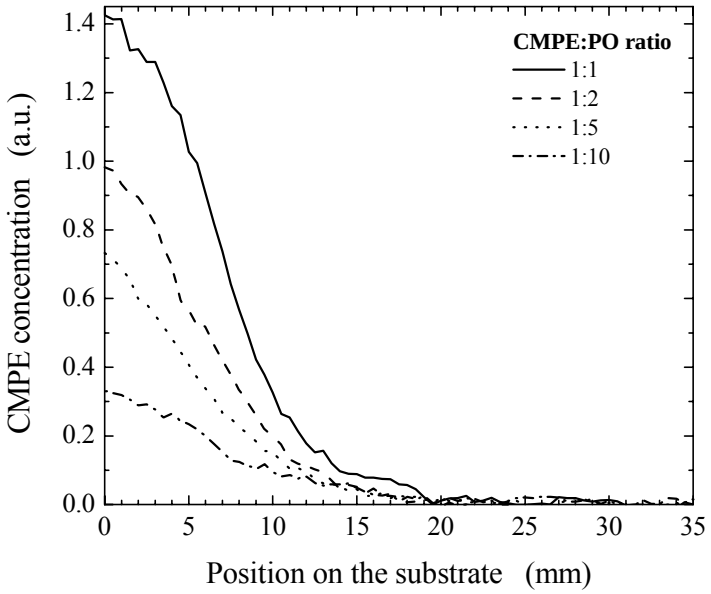

Figure 5.4 PEY NEXAFS intensity measured at E=284.2 eV as a function of the position the substrates containing the initiator gradients made of CMPE:OTS mixtures (w/w) 1:1 (solid line), 1:2 (dashed line), 1:5 (dotted line), and 1:10 (dash-dotted line).

With the x-ray monochromator set to 284.2 eV, we collected the PEY NEXAFS signal by scanning the x-ray beam across the gradient. The lines in Figure 5.4 show the variation of the PEY NEXAFS intensity measured at 284.2 eV across the gradient samples prepared by diffusing CMPE for 2 minutes from mixtures with various CMPE:PO ratios equal to 1:1 (solid line), 1:2 (dashed line), 1:5 (dotted line), and 1:10 (dash-dotted line). In the reminder of the paper, we refer to such substrates as S1, S2, S5, and S10, respectively. The data in Figure 5.3 reveal that the NEXAFS intensity from the C=C phenyl bond and thus

the concentration of CMPE in the sample decreases as one moves from the CMPE side of the sample towards the OTS-SAM; the functional form closely resembles that of a diffusion-like profile. Moreover, the concentration within each gradient can be fine-tuned by varying the CMPE:PO ratio. Experiments using VASE confirm that only a single monolayer was formed along the CMPE gradient substrate.

After the preparation of the CMPE-gradient substrate, the ATRP polymerization of PAAm is performed as described previously. Ellipsometry is used to measure the thickness of the dry polymer film, h, as a function of the position on the substrate. In Figure 5.5 we plot the values of h for samples prepared on the a) S1 (open squares), b) S2 (open circles), and c) S5 (open triangles) substrates.

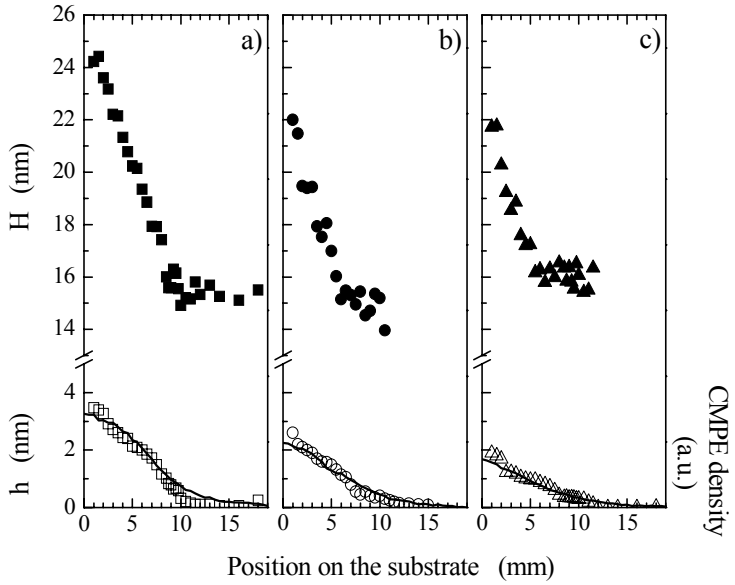

Figure 5.5 Dry thickness, h, (open symbols) and wet thickness, H, (closed symbols) of PAAm and the CMPE concentration (solid line) as a function of the position on the substrate for samples prepared on substrates containing the initiator gradients made of CMPE:OTS mixtures (w/w) 1:1 (squares), 1:2 (circles), 1:5 (triangles).

From Figure 5.5, h decreases gradually as one moves across the substrate starting at the CMPE edge. Note the agreement between the variation of h and the concentration profiles of the CMPE initiator (solid lines). Because the polymers grafted on the substrate have all roughly the same number of segments (see discussion below), the variation of the polymer film thickness can be attributed to the difference in the density, σ, of the CMPE grafting points on the substrate. The grafting density can be calculated from

$$\sigma = \frac{h\rho N_A}{M_w} \tag{5.1}$$

where ρ is the density of PAAm (=1.302 g/cm^3), N_A is the Avogadro's number, and M_w is the polymer molecular weight.

The substrates with the grafted PAAm are placed into a solution cell that was filled with DI water (pH ≈ 7), a good solvent for PAAm, and incubated for at least 5 hours. The wet thickness of PAAm grafted polymer in DI water, H, was measured using VASE. The top parts of Figure 5.5 shows the values of H for samples prepared on the a) S1 (closed squares), b) S2 (closed circles), and c) S5 (closed triangles) substrates. The data show that in all cases H decreases as one traverses across the substrate stating at the CMPE side. The maximum brush height at the CMPE edge of the sample decreases with decreasing CMPE concentration on the substrate (S1 > S2 > S5).

5.5 Discussion

We have established that the grafting density of end-anchored polymers on surfaces can be conveniently adjusted by first creating a gradient density of the surface-bound initiator followed by "grafting-from" polymerization. Our analysis presented in the previous section shows that the concentration of the CMPE polymerization initiator varies gradually across the substrate. The gradient profile width measured by NEXAFS is in accord with that obtained from the position-dependent contact angle data (*cf.* Fig. 5.2). We have also shown that the concentration of the CMPE molecules within the gradient can be fine tuned by varying the CMPE:PO ratio. We note that the width of the gradient (and its position on the substrate) can also be adjusted by varying the diffusion time or/and the temperature of the CMPE:PO diffusing source. For each sample studied, the dry PAAm thickness profile as a function of the position on the substrate coincides with the concentration profile of the CMPE initiator (*cf.* Figure 5.4). This agreement demonstrates that the initiator molecules are firmly bonded to the substrate and that they do not desorb from the substrate during the polymerization.

In Figure 5.6 we plot the wet polymer thickness as a function of the PAAm grafting density on the S1 (squares), S2 (circles), S5 (triangles) substrates. The results in Figure 5.6 reveal that at low σ, H is independent of the grafting density. Hence, the surface anchored PAAm chains are in the mushroom regime. At high polymer grafting densities, H increases with increasing σ, which is a signature of the brush behavior. The cross-over between the two regimes occurs at $\sigma \approx 0.065$ nm^{-2}. We note that recent publications reported that the crossover region is rather broad [22,23]. We will return to this point later in the reminder of

discussion. By fitting the data in the brush regime to $H \sim N\sigma^n$ we obtain n equal to 0.37±0.04 (S1 substrate), 0.39±0.05 (S2 substrate), and 0.40±0.06 (S5 substrate). We note that n obtained by fitting the experimental data is slightly higher that the predicted value of n=1/3; this observation is in agreement with recent reports [24].

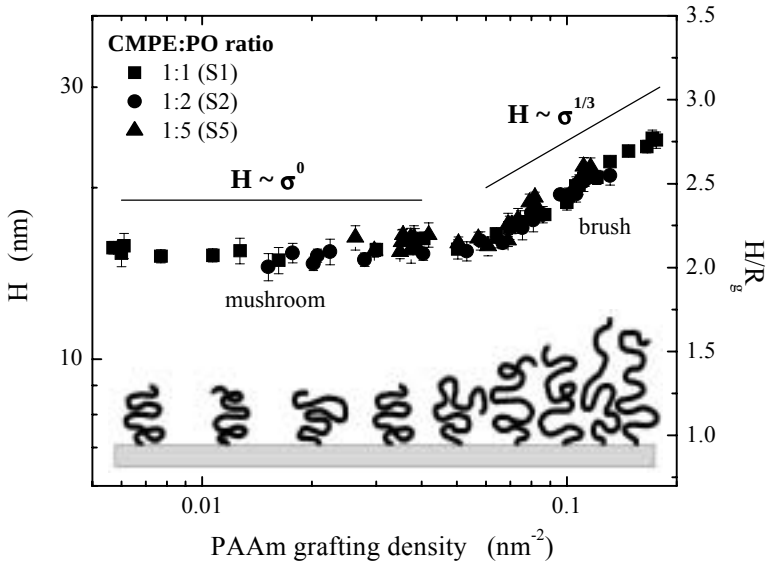

Figure 5.6 Wet thickness of PAAm as a function of the PAAm grafting density for samples prepared on substrates containing the initiator gradients made of CMPE:OTS mixtures (w/w) 1:1 (squares), 1:2 (circles), 1:5 (triangles). The inset shows a cartoon illustrating the polymer behavior.

A remark has to be made about the possible variation of the chain length with grafting density. Jones and coworkers recently reported on studies of grafting from polymerization of poly(methyl methacrylate) using ATRP from substrates having various surface densities of the polymerization initiator, ω-mercaptoundecyl bromoisobutyrate [25]. Their study revealed that the grafting density of the polymer depends on the grafting density of the initiator. However, based on the data presented in Ref. 25 it is uneasy to discern whether the kinetics of the polymerization also depends on the grafting density of the initiator. Currently we have

no means of measuring the molecular weight of the grafted brushes directly on the gradient substrate. While we cannot exclude the possibility that the length PAAm chains polymerized on the various parts of the molecular gradient substrate varies with σ, we note that the fact that the curves in Figure 5.6 superimpose on a single master curve indicates that the polymers have likely very similar lengths, which is not surprising for the rather short anchored polymers synthesized in this work.

In addition to the measurement of the wet brush thickness, we have also performed wettability experiments as a function of the PAAm grafting density on the substrate. Our aim is to corroborate the ellipsometric data and provides more insight into the polymer packing in the surface grafting density gradient.

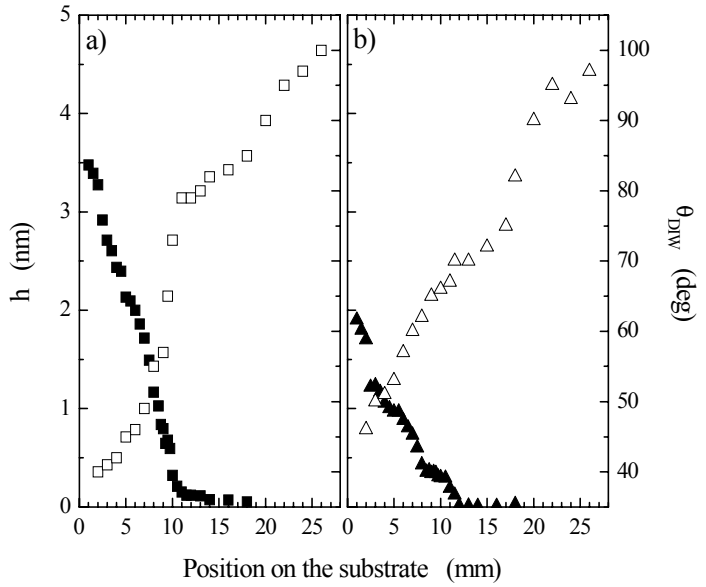

Figure 5.7 Dry thickness of PAAm, h, (closed symbols) and contact angle of DI water, θ_{DIW}, (open symbols) as a function of the position on the substrate for samples prepared on substrates containing the initiator gradients made of CMPE:OTS mixtures (w/w) 1:1 (squares) and 1:5 (triangles).

In Figure 5.7 we plot the dry PAAm thickness, h, (closed symbols) and the contact angles of DI water, θ_{DIW}, (open symbols) as a function of the position on the substrate for samples prepared on the S1 (squares) and S5 (triangles) substrates. In both samples, the dry thickness of PAAm decreases gradually as one moves across the substrate starting at the CMPE edge. The θ_{DIW} values increase as one traverses across the substrate stating at the CMPE side. The increase in θ_{DIW} is not monotonous, it follows a "double S"-type shape. While the "double S"-type dependence of θ_{DIW} on the position on the sample is detected in both S1 and S5 samples, there are differences in the plateau values. Specifically, while for the S1 sample, the three plateaus are located at $\theta_{DIW} \approx 40°$, $\approx 83°$, and $\approx 100°$ the corresponding values for the S2 sample are $\theta_{DIW} \approx 47°$, $\approx 70°$, and $\approx 97°$. Based on the dry thickness data and our previous discussion, the three plateaus in the contact angle behavior can be attributed to the wetting characteristics inside the brush, mushroom, and OTS (no PAAm) regions. At distances far away from the CMPE edge, where the θ_{DIW} values are high, there is no grafted PAAm on the sample. The contact angle experiments detect the presence of the OTS monolayer. By moving closer towards the CMPE edge, the contact angles decrease by $\approx$ 20-30° indicating that some polymers are present on the substrate. However, their grafting densities are low so that the probing liquid can penetrate between the grafted chains; the measured contact angle represents a weighted average between the PAAm and OTS. Upon approaching the mushroom-to-brush transition region, the contact angle further decreases. The decrease is steeper for PAAm on the S1 substrate and more gradual for the S2 sample, indicating that the density of PAAm increases more rapidly in the former case. The contact angles in the lowest plateau are $\theta_{DIW} \approx 40°$ and $\approx 47°$ for samples S1 and

S5, respectively. In independent experiments we have established that the θ_{DIW} of a pure PAAm is ≈35-38° [26]. Because in both cases the PAAm polymers grafted on the substrate have roughly the same degree of polymerization, the variation of the polymer film thickness can be attributed to the difference in the density of the CMPE grafting points on the substrate. Specifically, close to the CMPE edge, the PAAm macromolecules form a dense brush on the S1 substrate and a "semi-dense" brush on the S5 substrate.

The previous discussion revealed that the θ_{DIW} depends on the grafting density of the PAAm chains on the substrate. Earlier we have shown that the wet thickness of PAAm prepared on substrates with various CMPE concentrations can be collapsed on a single master curve when plotted as H vs. σ. One would thus expect that also the wettabilities of the substrates plotted versus the PAAm grafting density should exhibit similar universal behavior.

In Figure 5.8 we plot the negative cosine of θ_{DIW} as a function of the grafting density of PAAm on substrates S1 (squares) and S5 (triangles). As anticipated, the data collapse on a single master curve. A close inspection of the results present in Figure 5.8 shows that the data can be divided into three distinct regions. For σ>0.1 nm^{-2}, the chains are expected to be in a brush regime – the wettabilities are close to the pure PAAm ($-\cos(\theta_{DIW}) \approx -0.79$). For $\sigma < 0.011$ nm^{-2} the PAAm chains form mushroom conformations on the substrate. In this regime, the wettabilities change slightly because the distance between the chains also changes, although they are already loosely separated on the substrate. At grafting densities $0.011 \text{ nm}^{-2} < \sigma < 0.1 \text{ nm}^{-2}$, the slope of $-\cos(\theta_{DIW})$ changes rather rapidly. The data in Figure 7 show that the position of the mushroom-to-brush crossover determined using the

wettability approach is in accord with the ellipsometric measurements (the transition location was established to be at $\sigma \approx 0.065$ nm^{-2}). However, in the former case, the transition region extends over almost one order of magnitude in σ, which is broader that the transition region predicted by the H vs. σ data. We speculate that the small difference between the widths of the mushroom-to-brush region inferred from both types of experiments is likely associated with the inaccuracy in H, which was obtained indirectly by the model fitting of the VASE data.

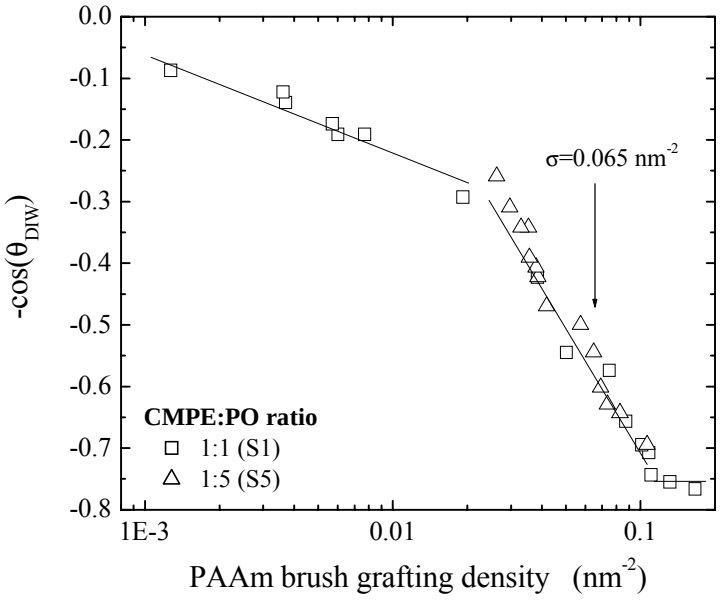

Figure 5.8 Negative cosine of the contact angle of DI water as a function of the PAAm grafting density on the substrate for samples prepared on substrates containing the initiator gradients made of CMPE:OTS mixtures (w/w) 1:1 (squares) and 1:5 (triangles). The lines are meant to guide the eyes.

5.6 Summary

This chapter described a method leading to the preparation of surface-anchored polymer assemblies, whose grafting density varies gradually as a function of the position on the substrate. Specifically, we have shown that such structures can be fabricated by first generating a molecular gradient of polymerization initiator on the solid substrate, and subsequently carrying out "grafting from" polymerization from the substrate bound initiator centers. In this work we used the above technology to prepare gradient polymer brushes of poly(acryl amide) on silica-covered substrates. We have measured the wet thickness (H) of PAAm in a good solvent as a function of the PAAm grafting density on the substrate (σ). Our measurements revealed that at low grafting densities, the PAAm chains were in the mushroom regime, the values of H were independent of σ. At high grafting densities, H was found to scale as σ^n, where n ranged from 0.37 to 0.40. This exponent was just slightly higher than the value predicted by mean-field theories of polymer brushes (n = 1/3). Complementary wetting experiments on the same samples were performed that confirmed the results of the ellipsometry measurements. Moreover, the wettability experiments revealed that the mushroom-to-brush transition spans a broad range of grafting density (about an order of magnitude in σ).

Acknowledgements. This work is supported by the National Science Foundation, Grant No. CTS 0209403, The Camille Dreyfus Teacher-Scholar award, and The 3M Non-Tenured Faculty award. The NEXAFS experiments are carried out at the National Synchrotron Light Source, Brookhaven National Laboratory, which is supported by the U.S.

Department of Energy, Division of Materials Sciences and Division of Chemical Sciences. The authors thank Dr. Daniel Fischer (NIST) for his assistance during the course of the NEXAFS experiments and Dr. Vladimír Šubr (Institute of Macromolecular Chemistry in Prague) for his assistance with the size exclusion chromatography measurements.

References and notes

[1] Xia, Y.; Whitesides, G. M. *Angew. Chem. Int. Ed. Engl.* **37**, 550 (1998); Y. Xia, et al. *Chem. Rev.* **99**, 1823 (1999).

[2] Ulman, A. *An Introduction to Ultrathin Organic Films from Langmuir-Blodgett to Self Assembly*, (Academic Press: New York, 1991).

[3] Husseman, M. et al. Angew. Chem. *Int. Ed. Engl.* **38**, 647 (1999).

[4] Shah, R. et al. *Macromolecules* **33**, 597 (2000).

[5] Jeon, N. L. et al. *Appl. Phys. Lett.* **75**, 4201 (1999); Kim, N. et al. *Macromolecules* **33**, 3793 (2000).

[6] Boer, B. de et al. *Macromolecules* **33**, 349 (2000).

[7] Ghosh, P. et al. *Macromolecules* **34**, 1230 (2001).

[8] Jones, D. M. and Huck, W. T. S. *Adv. Mater.* **13**, 1256 (2001).

[9] Hyun, J. and Chilkoti, A. *Macromolecules* **34**, 5644 (2001).

[10] Chaudhury, M. K. and Whitesides, G. M. *Science* **256**, 1539 (1992).

[11] Efimenko, K. and Genzer, J. *Adv. Mater.* **13**, 1560 (2001).

[12] Fuierer, R. R. et al. *Adv. Mater.* **14**, 154 (2002).

[13] For detail review, see chapter 3 of this Thesis.

[14] Patter, T. E.; Xia, J.; Abernathy, T. and Matyjaszewski, K. *Science* **272**, 866 (1996).

[15] Efimenko, K.; Wallace, W. E. and Genzer, J. *J. Colloid Interface Sci.* **254,** 306 (2002).

[16] Huang, X.; Doneski, L. J.; Wirth, M. J. *Chemtech* **19**, Dec (1998); Huang, X.; Doneski, L. J.; Wirth, M. J. *Chemtech* **19**, (Dec 1998); *Anal. Chem.* **70**, 4023 (1998).

[17] Huang, X.; Wirth, M. J. *Macromolecules* **32**, 1694 (1999).

[18] Wu, T.; Efimenko, K.; Genzer, J. *Macromolecules* **34**, 684 (2001).

[19] Brandrup, J.; Immergut, E. H. and Grulke, E. A. (Editors): *Polymer handbook* (Wiley, New York, 1999).

[20] Stöhr, J. *NEXAFS Spectroscopy* (Springer-Verlag, Berlin, 1992).

[21] Chaudhury, M. K. Owen, M. J. J. Phys. Chem., **97**, 5722; (1993); Allara, D. L. Parikh, A. N. Judge, E. *J. Chem. Phys.*, **100**, 1761 (1994).

[22] For a recent review see Kent, M. S. *Macromol. Rapid Commun.*, **21**, 243 (2000) and references therein.

[23] Douglas, J. F. et al., Polymer Brushes: Structure and Dynamics", *Encyclopedia of Materials: Science and Technology* (Elsevier, 2001, pp. 7218-7223).

[24] Wamamoto, S. et al., *Macromolecules*, **33**, 5608 (2000).

[25] Jones, D. M. Brown, A. A. Huck, W. T. S. *Langmuir*, **18**, 1265 (2002).

[26] In order to measure the contact angle of DI water on a pure PAAm, we have first grown PAAm from a substrate covered homogeneously with the CMPE initiator. The polymerization conditions were the same as for the sample described in the text. The contact angle was determined suing the technique described in the text.

Chapter 6

Behavior of surface-anchored weak polyelectrolytes with grafting density gradients on solid substrates

6.1 Abstract

In this chapter we will describe experiments on surface-anchored poly(acylic acid) (PAA) with a gradual variation of the grafting densities on flat surfaces and provide detailed analysis of their properties. The PAA gradients are generated by first covering the substrate with a molecular gradient of the polymerization initiator, followed by the "grafting from" polymerization of poly(*tert*-butyl acrylate) (PtBA) from these substrate-bound initiator centers, and finally converting the PtBA into PAA. We use spectroscopic ellipsometry to measure the wet thickness of the grafted PAA chains with two different molecular weights in aqueous solutions at three different pH values (4, 5.8, and 10) and a series of ionic strengths (IS). Our measurements reveal that at low grafting densities, σ, the wet thickness of the PAA (H) remains relatively constant, the polymers are in the mushroom regime. Beyond a certain value of σ, the macromolecules enter the brush regime. Here H increases with increasing σ. For a given σ, H exhibits a non-monotonous behavior as a function of the IS. At large IS, the H is small because the charges along PAA are completely screened by the excess of the external salt. As IS decreases, H also increases, reaches a maximum at a certain IS and then decreases again. This behavior is consistent with that predicted by the theories of the weak electrolyte brushes. We provide detailed discussion of the behavior of the grafted PAA chains in the so-called salted and osmotic regimes. Finally, we show that data from PAA with two different molecular weights can be collapsed on a single master curve by plotting H/R_g versus σ, where R_g is the radius of gyration of the PAA.

6.2 Motivation

The properties of neutral polymer brushes under various conditions have been studied rather extensively over the past two decades and their behavior is relatively well understood.[1] Both the scaling dependences for the average brush characteristics and the fine details of the intrinsic brush structure predicted theoretically are in reasonable agreement with experimental observations[2,3]. Much less work has been done on charged brushes[4], *i.e.*, polymer assemblies comprising macromolecules containing ionizable groups. This is due to the complexity of the system, which is associated with the presence of electrostatic interactions. Specifically, in addition to the parameters governing the performance of neutral polymer bushes, *i.e.*, the degree of polymerization, N; brush grafting density, σ, and the solvent quality (characterized by the Flory-Huggins interaction parameter, χ), the properties of polyelectrolyte brushes depend strongly on the degree of dissociation of the charge groups (or degree of dissociation), α; concentration of the external salt in the polyelectrolyte solution, φ_s; counterion valency, q, and in some cases also the pH of the solution. Depending on the nature of the electrostatic charges along the polymer backbone, one can distinguish between two types of polyelectrolytes: strong and weak. While strong ("quenched") polyelectrolytes have a fixed α, their properties thus do not depend on the pH of the solution, in weak ("annealed") polyelectrolytes α depends on pH.

Various theoretical approaches have been utilized to describe the performance of charged macromolecules at interfaces. In particular, scaling theories pioneered by Pincus[4], Zhulina and coworkers[5,6], and the Wageningen group[1,7,8,9] laid the foundation of our current understanding of polyelectrolyte brush behavior. These studies revealed that several

different regimes of polyelectrolyte brushes could be identified depending on the concentration of the external salt in solution. More detailed information about the structure of the brush has been obtained through more sophisticated methods based on numerical self-consistent field (SCF)[7,8,9,,10,11] and analytical SCF theories[5,9,12].

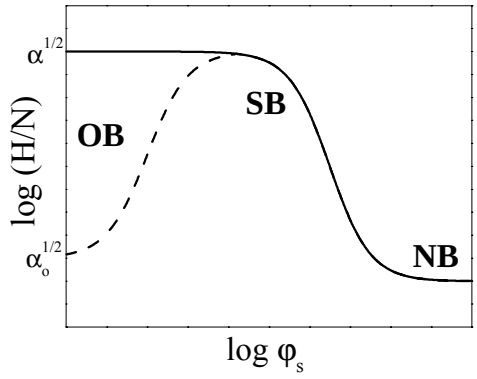

Figure 6.1 Dependence of the brush thickness reduced by the number of polymer repeat units for **monovalent co-ions**, H/N, on the concentration of the external salt, φ_s, for strong (solid line) and weak (dashed line) polyelectrolyte brushes in neutral brush (NB), salted brush (SB), and osmotic brush (OB) regimes. α and α_o denote the bulk and "internal" (for weak polyelectrolyte brushes only) degree of dissociation, respectively.

We start by briefly describing the behavior of quenched polyelectrolytes immersed in solutions of monovalent salt ions. At high φ_s the salt concentration inside and outside the brush is about the same and the electrostatic interactions are largely screened. Under such conditions the polyelectrolyte brush behaves exactly as a neutral brush (NB) and $H/N \approx (\nu\sigma)^{1/3}$, where ν (=0.5-χ) is the excluded volume parameter. When the external salt concentration decreases, there is an unbalance in the ion concentration inside and outside the brush because the polymer charge density inside the brush ($\alpha\varphi$, where φ is the polymer

volume fraction) is no longer negligible with respect to φ_s. The system enters the salted brush (SB) regime. In the SB regime, H/N scales as $H/N \approx (\nu_e \sigma)^{1/3}$, where ν_e ($=\alpha^2/\varphi_s$) is the electrostatic excluded volume parameter. Due to the electrostatic interactions inside the brush, a salted brush is more extended than a neutral one. As shown schematically in Figure 6.1, the brush expansion increases with decreasing φ_s. If the external salt concentration is further decreased such that $\varphi_s << \alpha\varphi$ the co-ions are effectively expelled from the brush and $H/N \approx \alpha^{1/2}$. In this so-called osmotic brush (OB) regime limiting brush thickness is reached, which is independent of φ_s and σ. Several experimental studies have appeared recently that reported on the interfacial properties of surface-grafted strong polyelectrolytes. Most experiments have focused on sodium polystyrene-sulfonate (PSSNa)[13,14,15], and recently poly(N-methyl-4-vinylpyridinium iodide) (MePVP) [16,17,18] brushes.

The behavior of weak polyelectrolyte brushes is different from that of strong polyelectrolytes. Here the number of the backbone charges is not fixed. Specifically, α depends on the proton concentration in the polymer solution, $[H^+]=10^{-pH}$, and is given by $\alpha/(1-\alpha)=K/[H^+]$, where K is the dissociation constant. When there is an excess of salt, as in the NB and SB regimes, $[H^+]$ inside and outside the brush is approximately equal and the internal degree of dissociation is the same as that in the bulk solution. Hence, the scaling for H/N in the NB and SB regimes is the same as in the case of strong polyelectrolyte brushes:

$$H \sim N\sigma^{1/3}\left(\frac{\alpha^2}{\varphi_S}\right)^{1/3} \tag{6.1}$$

When the system enters the OB regime, a significant electric potential difference develops between the brush and the bulk solution. In addition, $[H^+]$ inside the brush is considerably higher. As a consequence, a portion of the brush charges associate with protons and $\alpha_o/(1-\alpha_o)=K/(\sigma\alpha_o^{1/2})$, where α_o is the "internal" degree of dissociation. This value of α_o may be much smaller than the value in the bulk (α); the weak groups respond to the unfavorable electrostatic condition in OB by discharging themselves. The brush height in the OB regime is predicted to scale as:[5]

$$H \sim N\sigma^{-1/3}\left(\frac{\alpha}{1-\alpha}\right)^{1/3}([H^+]+\varphi_S)^{1/3} \tag{6.2}$$

Such a response is impossible for strong brushes, which have a fixed α. Figure 6.1 illustrates the different behavior of weak polyelectrolyte brushes in the OB regime. Because of the discharging process ($\alpha_o<\alpha$), a weak brush in the OB regime is less expanded than the strong brush. As a result, H/N passes through a maximum as a function of φ_s, being small for both high and small φ_s. The unusual feature that at low φ_s the brush contracts with decreasing φ_s is a typical property of weak groups, which can respond to a change in the local environment. As Israëls suggested[10], by equating the expressions for H given in Equation 6.1 and 6.2, the value of φ_S at the transition between the OB and SB regimes scales as:

$$\varphi_s^{max} \sim \sigma(\alpha^b)^{1/2} \tag{6.3}$$

Several groups investigated the behavior of weak polyelectrolytes anchored at surfaces. For example, Kurihara and Kunitake measured the surface forces between

monolayers of anchored poly(acrylic acide) (PAA).[19] Kurihara and Kunitake observed that the repulsive forces between two grafted polymeric monolayers increased with increasing salt concentration. Properties of PAA brushes were also studied using surface pressure isotherms and ellipsometry.[20,21] Samples with three different grafting densities were measured at three low pH solutions as a function of the solution ionic strength. Currie and coworkers found that the PAA wet brush thickness is a non-monotonous function of the ionic strength at a given pH and grafting density. The extent of swelling of the brush increased with increasing pH and grafting density. Although the non-monotonous behavior agreed qualitatively with theoretical predictions, the mean-field power law for the OB regime at a given pH and σ, *cf.* Eq. (6.2.), was not observed. Moreover, because of the non-covalent nature of the PAA grafting to the substrate used in Refs. 20 and 21, which investigated polyelectrolyte brushes comprising polystyrene-poly(acrylic acid) (PS-PAA) diblock copolymers, the copolymer chains partially desorbed from the surface when the copolymer compositional asymmetry increased and the length of the anchoring PS block decreased below a certain critical number of segments.

The goal of this work is to extend the previous work on PAA by characterizing the interfacial properties of surface-grafted PAA as a function of its molecular weight, σ, pH, and IS. Due to its simplicity, robustness and the ability to synthesize polymer brushes with narrow molecular weight distributions, ATRP will be used to perform the surface-initiated polymerization.[22] Previous studies have revealed that acrylic-based polymers are difficult to polymerize by ATRP because of the interaction of the carboxylic acid functionalities with the ATRP catalyst[23]. Hence, in order to form a surface-anchored PAA with a grafting density

gradient, we first used the previously developed method[24] to synthesize a gradient of poly(t-butyl acrylate) (PtBA) and then converted the PtBA into PAA by acid wash poly(acrylic acid) [25,26]. We will use spectroscopic ellipsometry to measure the thickness of both dry PAA and PAA exposed to aqueous solution of various pH and ionic strengths.

6.3 Experimental approach

6.3.1 Initiator synthesis

The ATRP initiator used in this study is (11-(2-Bromo-2-methyl)propionyloxy)-undecyl-trichlorosilane, $Br(CH_3)_2CCOO(CH_2)_{11}SiCl_3$ (BMPUS). The initiator was synthesized following a two-step procedure[27] shown in Figure 6.1. All reagents used in synthesis were obtained from Aldrich. Toluene and tetrahydrofuran are dried with sodium sulfate and filtered. Other chemicals are used without further purification.

Step I: Synthesis of 10-Undecen-1-yl 2-Bromo-2-methylpropionate

First, 2.1 mL of pyridine (26.5 mmol) was added to a solution of 4.257 g (25 mmol) of ω-undecylenyl alcohol in 25 mL of dry tetrahydrofuran. Under stirring, 3.10 mL of 2-bromoisobutyryl bromide (25 mmol) was added drop wise using a syringe. The originally clear solution turned milky. The reaction mixture was stirred at room temperature in dark overnight and then diluted with hexane (50 mL) and washed with the same amount of 2 N HCl, and twice with deionized (DI) water. Only the top organic phase was taken and dried over sodium sulfate. After filtering, the solvent was removed from the filtrate under reduced pressure, and the colorless oily residue (≈6.33 g) used without further purification.

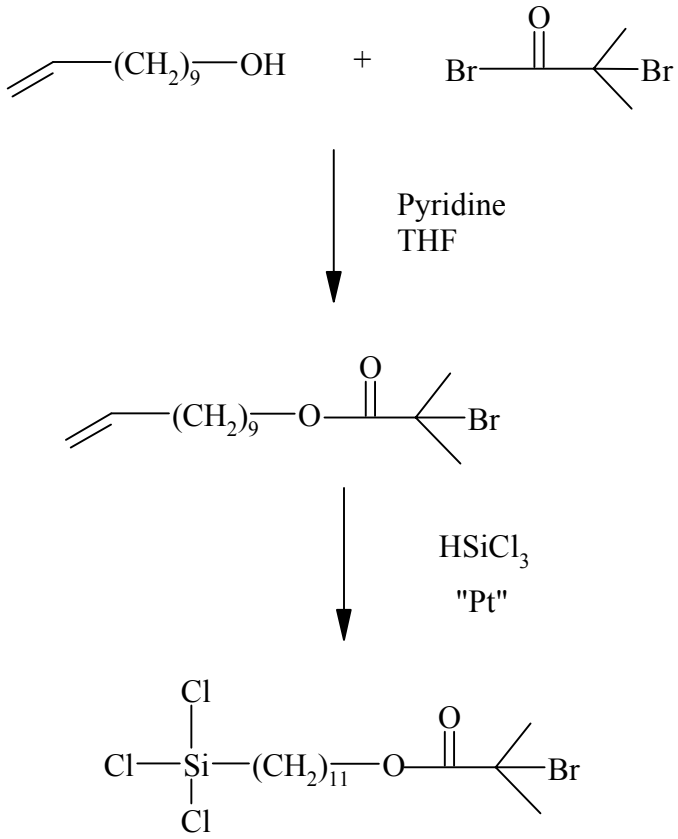

Figure 6.2 Schematic of the synthesis of 11-(2-Bromo-2-methyl)propionyloxy) undecyltrichlorosilane.

Step II: Synthesis of (11-(2-Bromo-2-methyl)propionyloxy)undecyltrichlorosilane

First, 1.35 g of 10-Undecen-1-yl 2-Bromo-2-methylpropionate was added into a 20 mL vial, followed by quickly adding 5.635 g of trichlorosilane. Then, 10 μL Platinum(0)-1,3-divinyl-1,1,3,3-tetramethyldisiloxane complex solution were added with a micropipette. The mixture was sealed and stirred at room temperature. After 5 hrs, the solution was quickly filtered through a plug of silica gel to remove the catalyst. Anhydrous toluene was

used to flux through the column. The excess reagent was then removed under reduced pressure. The structure of the synthesized initiator was confirmed by NMR experiments.

6.3.2 Formation of the gradient of the polymerization initiator

Silicon wafers covered with a native silicon oxide (thickness ≈1.9 nm) were used as substrates. The silicon wafers were first exposed to an ultraviolet/ozone (UVO) treatment in a commercial UVO chamber (Jelight Company, Inc., Model 42) for 30 minutes in order to generate surface-bound hydrophilic surfaces comprising predominantly the hydroxide functionalities (-OH).[28]

A molecular gradient of n-octyltrichlorosilane (OTS) (Gelest, Inc) was formed following the vapor diffusion technique developed by Chaudhury and Whitesides.[29] Specifically, as shown in Figure 6.3, a mixture of OTS and paraffin oil (PO) was placed into an open container that was positioned close to an edge of the silicon wafer. As the OTS evaporated, it diffused in the vapor phase and generated a concentration gradient along the silica substrate. Upon impinging on the substrate, the OTS molecules reacted with the substrate -OH functionalities and formed a self-assembled monolayer (SAM). The breadth and position of the OTS molecular gradient can be tuned by varying the OTS diffusion time and the flux of the OTS molecules. In this work, the OTS:PO ratio was kept 1:2 and the diffusion time was 2 minutes. The concentration of the substrate regions unmasked by the OTS molecules increased gradually as one traversed from the OTS-side of the substrate

towards the OTS-unexposed edge. These were to be filled by the (11-(2-Bromo-2-methyl)propionyloxy) undecyltrichlorosilane (BMPUS).

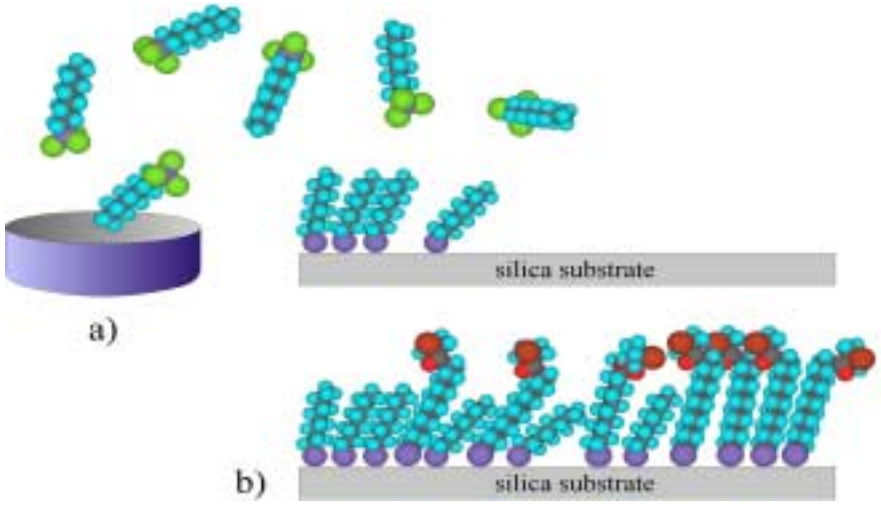

Figure 6.3 Schematic illustrating the preparation of the ATRP initiator gradient. In the first step, a molecular gradient of OTS is prepared on the flat silica-covered substrate (a). In the second step, the substrate is immersed in a solution of (11-(2-Bromo-2-methyl)propionyloxy)undecyltrichlorosilane (b).

In a vial, 20 μL of the initiator was added into 20 mL anhydrous toluene and mixed thoroughly. The OTS gradient-covered silicon wafers were placed into this solution for 18 hrs without stirring. After the initiator deposition, the samples were removed from the solution, thoroughly washed with toluene, acetone, and ethanol, and finally dried with nitrogen. Ellipsometry measurements confirmed that only a single self-assembled monolayer of both OTS and BMPUS formed on the Si substrates.

6.3.3 Polymerization of poly(*tert*-butyl acrylate)

The polymerization of poly(*tert*-butyl acrylate) (PtBA) was performed by atom transfer radial polymerization (ATRP), as described earlier. [30] Copper(I) Bromide (CuBr) (0.1564 g, 1.1×10^{-3} mol) and Copper(II) Bromide ($CuBr_2$) (0.012 g, 4.2×10^{-5} mol) were added to a dry Teflon-capped vial, followed by adding deoxygenated acetone (1.6 g) and *tert*-butyl acrylate (tBA) (14.0 g, 1.08×10^{-1} mol). After purging the solution with nitrogen for 5 minutes, 240 μL N,N,N,N',N'-Pentamethyldiethylenetriamine (PMDETA) was added. The solution was stirred until the Cu complex formed. After the complex formation, the gradient-covered Si wafers were placed into the solution. The solution was purged with nitrogen for 2 mins and then the vial was sealed and placed in a temperature controlled oil bath set at 60°C. After a predetermined reaction time, the samples were removed and washed thoroughly with acetone, methanol and dried with nitrogen.

6.3.4 Hydrolysis of surface grafted PtBA

The silica substrates covered with a PtBA gradient were placed into a flask, which contained a mixture of 20 mL 1,4-dioxane and 3 mL concentrated HCl (37%). The flask was connected to a condenser, and the solution was heated to reflux. The samples were removed after 2-5 hrs (see discussion below) and thoroughly washed with the DI water and methanol.

6.3.5 Solution polymerization and hydrolysis of PtBA

In addition to the surface polymerization, we have also prepared a small amount of PtBA in solution. For the solution polymerization of PtBA, the procedure described earlier was duplicated with the exception that after all reagents had been combined and homogeneity reached, methyl 2-bromopropionate (240 μL, 2.2×10^{-3} mol) was added as a solution initiator instead of BMPUS. The polymerization time of the solution-polymerized polymers was identical to the PtBA formed on the silicon wafer. After the polymerization, the solutions were precipitated into a 15-fold excess of a 50:50 water:MeOH (v/v) bath. After decanting off the solvent, the polymer was re-dissolved in diethyl ether; the solution turned deep blue. Several drops of water were added to extract the copper complexes out of the solution. After separation, the polymer solution was re-precipitated until the polymer remained white. The final polymer was dissolved in acetone and dried under vacuum overnight. The PtBA polymerized in free solution was used to determine the corresponding molecular weigh. We note the polymerization rate in the solution is likely faster than as that on the flat substrate. Nevertheless, the molecular weight of the solution-based polymer provided a useful estimate for further analysis.

In order to convert solution polymerized PtBA into PAA, PtBA (2.5 g) was added to a solution of 20 mL dioxane and 3 mL of concentrated HCl (37%). The solution was heated over a reflux. After 2-5 hrs reaction, the solution was cooled and a part of the excess reagents (≈10 mL) were removed by evaporation under vacuum. Subsequently, the PAA solution was precipitated into 200 mL methyl ethyl ketone (MEK). After decanting off the solvent, the polymers were dried under high vacuum overnight.

6.3.6 SEC measurement

Molecular weights of PtBA and PAA were measured by size exclusion chromatography (SEC) by our collaborators, Dr. Petr Vlček and Dr. Vladimír Šubr, at the Institute of Macromolecular Chemistry in Prague, Czech Republic. The PtBA SEC experiments were conducted at 20°C using a Labora set apparatus (Czech Republic) with a two-column separation system (Polymer Standards Service GmbH, Germany, porosities 10^5 and 10^3 angstroms). THF was used as the mobile phase. The flow rate was 1 ml/min and the concentration of samples for injection was approx. 1% (w/w). The system was calibrated with PMMA standards (PSS GmbH, Germany). Eluograms were analyzed using a software Caliber (Polymer Laboratories) and the Mark-Houwink-Sakurada equation with $K=3.3 \times 10^{-5}$ and $a=0.80$.[31] The system is equipped with two detectors of the Czech provenience: differential refractometer RIDK-102 and UV detector LCD-2040 with adjustable wavelength. The polymer weights were calculated from the RI traces. The molecular weight of the PtBA synthesized in solution for 6 hrs was M_n=5.94 kDa with M_w/M_n=1.07. These values are comparable to those reported previously (M_n=6.0 kDa for PtBA) for polymers prepared under the identical reaction conditions.[30] PtBa polymerized for 10 hrs in solution had M_n=8.56 kDa with M_w/M_n=1.15.

After the conversion of PtBA to PAA, the molecular weight of PAA was also determined by SEC by using Superose^{TM} 12 column (Äkta Explorer, Amersham Bioscience) equipped with differential refractometer and multiangle light scattering detector DAWN DSP-F (Wyatt Technology Corp.). 0.3 M sodium acetate buffer (pH≈6.5) was used as the

mobile phase. The flow rate was 0.5ml/min. The molecular weight of PAA for 6 hrs was M_n=3.56 kDa with M_w/M_n=1.32, and for 10 hrs was M_w=4.1 kDa with M_w/M_n=1.29.

In Table 6.1, we list the average molecular weights (M_n) and polydispersity indices (M_w/M_n) of PtBA and PAA obtained using the SEC measurements. The molecular weights of PAA calculated from the PtBA SEC measurements are in a good agreement with the direct PAA measurements (the accuracy of ±15% is well within the acceptable limit). In the data analysis that follows, we are going to use the degree of polymerization of PAA that was calculated from the PtBA SEC measurements. We justify our choice by the fact that in contrast to PAA, PtBA is a neutral polymer, which is insensitive to the pH and ionic strength of the mobile phase. We thus believe that the PtBA SEC measurements are more accurate. Moreover, as indicated by the relatively narrow molecular weight distribution, $M_{n,PtBA}$ values should be more reliable.

Table 6.1 Comparison of SEC experiment results for PtBA and PAA

	Polymerization time (hrs)	
	6	10
Experimental $M_{n,PtBA}$ (kDa)	5.94	8.56
M_w/M_n	1.07	1.15
N_{PtBA} calculated from $M_{n,PtBA}$	≈46	≈67
$M_{n,PAA}$ calculated from $M_{n,PtBA}$ (kDa)	3.34	4.81
$M_{n,PAA}$ calculated from $M_{n,PtBA}$ (kDa)	3.34	4.81
Experimental $M_{n,PAA}$ (kDa)	3.56	4.10
M_w/M_n	1.32	1.29
N_{PAA} calculated from $M_{n,PAA}$	≈49	≈57

6.3.7 Ellipsometry measurement

The thickness of the SAM and the polymer film was measured using a single-wavelength fixed geometry ellipsometer (AutoEL II, Rudolph Technologies) and a variable angle spectroscopic ellipsometry (J.A. Woollam, Inc.). The thickness was evaluated from the experimentally measured ellipsometric angles Ψ and Δ using the supplied software (DafIMB and WVASE32). The following refractive indices were used for various material: 1.45 for SAMs,[2] 1.466 for poly(*tert*-butyl acrylate),[32] 1.527 for poly(acrylic acid).[33] The wet thickness of the PAA in aqueous solutions was measured by placing the samples in a custom-designed solution cell, incubating them for a desired period of time (typically >5 hrs) and performing the experiments with VASE at ϕ=70°, where ϕ is the angle between the incoming beam and the sample normal. The ellipsometric angles Ψ and Δ were collected for a series of wavelengths ranging from 240 to 1000 nm. The wet PAA thickness was evaluated using a graded effective medium approximation model based on linear combination of the optical constants of the DI water and PAA.

The pH and the ionic strength of the aqueous solution were adjusted as follows. A desired amount of aqueous solution was removed and a replaced with corresponding amount of concentrated NaCl, HCl, or NaOH solutions. In the following we illustrate the procedure used to prepare a solution with the pH=4 and various ionic strengths. First, the ellipsometric cell was filled with 75 mL of aqueous solution, followed by adding 75 μL of 0.1 M HCl in order to obtain solution with pH=4. We also prepared a stack NaCl solution (concentration=2M and pH=4). The right column in Table 6.2 lists the corresponding

amounts of the aqueous solution that was replaced with the NaCl in order to prepare the ionic strength listed in the left column of Table 6.2.

Table 6.2 An example of adjusting the ionic strength of pH=4 solution

75mL cell solution ionic strength	Amount of aqueous solution (mL) replaced by the NaCl solution (concentration=2M, pH=4)
1.00E-04	-
1.00E-03	0.034
5.00E-03	0.150
1.00E-02	0.188
1.00E-01	3.392
5.00E-01	15.789
7.50E-01	12.500
1.00E+00	15.000

6.3.8 NEXAFS measurements

Near-edge x-ray absorption fine structure (NEXAFS) was used to study the spatial concentration of PAA on the sample substrates[34]. The NEXAFS experiments were carried out on the U7A NIST/Dow Materials Soft X-ray Materials Characterization Facility at the National Synchrotron Light Source at Brookhaven National Laboratory (NSLS BNL). The NEXAFS spectra were collected in the partial electron yield (PEY) at the so-called "magic" angle (θ=55°) incidence geometries, where θ is the angle between the sample normal and the polarization vector of the x-ray beam.

6.3.9 FTIR spectroscopy measurements

Fourier transform infrared (FTIR) spectroscopy was collected in the transmission mode with Nicolet 750. A total of 1024 scans were made with resolution 8 cm^{-1} for each measurements, which required a scanning time of approximately 12 minutes. A bare silicon wafer was used as the blank. The IR spectra for polymer bulk were measured with the KBr pellets. The IR spectra were analyzed using the OMNIC 5.0 software.

6.4 Experimental results

We first verified that the hydrolysis of the PtBA using HCl led to the formation of PAA. The FTIR KBr spectra of PtBA prepared using the solution polymerization are shown

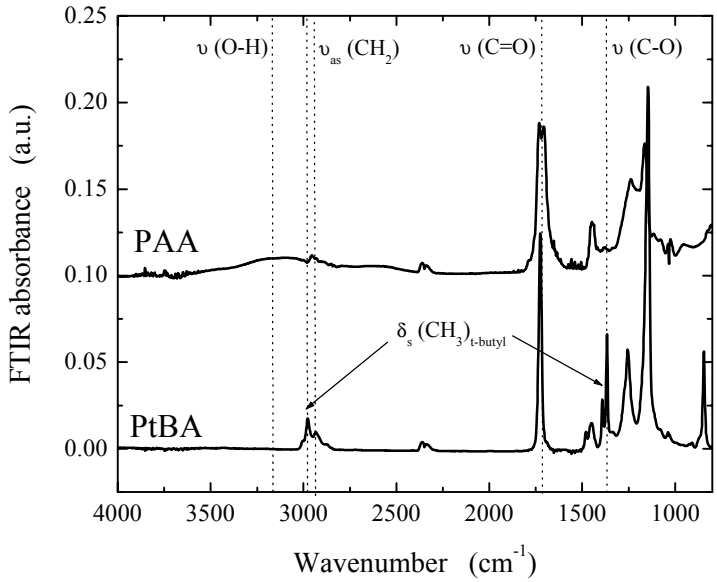

Figure 6.4 The FTIR spectra from the KBr pellets containing PtBA (bottom) and PAA (top) prepared using the solution polymerization.

in the bottom and top parts, respectively, of Figure 6.4. Following previous studies,[27] we can make the following assignments to the FTIR signals: the peak at 1733 cm^{-1} can be assigned to the ester group (-COO), the peaks at 1254 and 1159 cm^{-1} are attributed to C-O, and the weak peaks at 2850 and 2925 cm^{-1} belong to the symmetric and asymmetric vibration modes, respectively, of the $-CH_2-$ groups. The characteristic peaks of *tert*-butyl group, which exist only in PtBA, are at 2979 cm^{-1} ($\nu_{as}(CH_3)$) and 1393/1368 cm^{-1}($\delta_s(CH_3)$). The disappearance of those peaks in PAA IR spectra confirms the completion of the hydrolysis of PtBA. The broad band at 3200 cm^{-1} (ν(OH)) in the PAA IR spectra is attributed to the –OH group formed during the PtBA conversion.

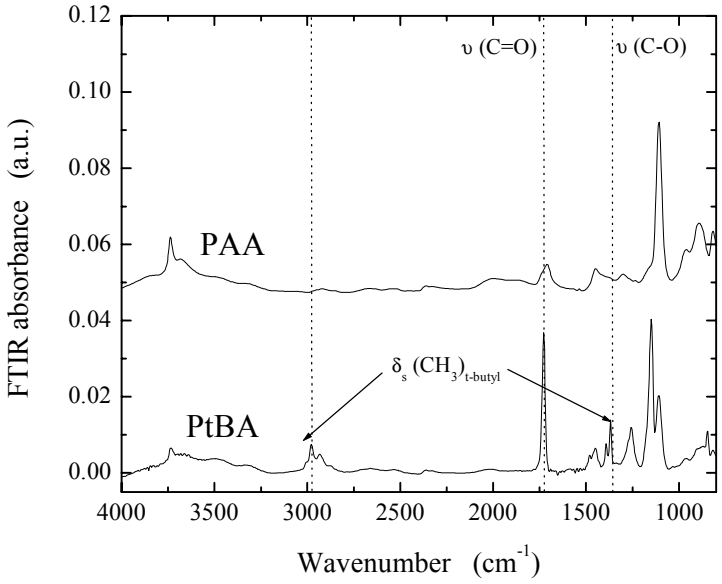

Figure 6.5 FTIR spectra of PtBA and PAA grafted on the Si substrates.

In addition to the PtBA-to-PAA conversion measurements on the polymers prepared in the solution, we have also checked conversion reaction for polymers synthesized on the

surface. PtBA brushes were first grown on Si substrates that were covered homogeneously with the surface-bound initiators. The hydrolysis of PtBA on the Si wafer was performed as a function of the reaction time. In Figure 6.5 we plot the FTIR spectra of PtBA (bottom) and PAA (top) from PtBA polymerized for 24 hrs followed by the hydrolysis reaction for 5 hrs. The spectra for both samples show very similar trends reported earlier for the bulk PtBA and PAA specimens (*cf.* Figure 6.4). As expected, the absolute IR intensities from the latter set of samples were weaker due to the smaller number of polymer chains analyzed. The disappearance of the peaks corresponding to $\nu_{as}(CH_3)$ (at 2979 cm^{-1}) and $\delta_s(CH_3)$ (at 1393 and 1368 cm^{-1}) in the PAA/Si spectra, relative to the PtBA/Si samples, provides evidence that the hydrolysis of poly(*tert*-butyl acrylate) took place.

The PtBA gradient was prepared by applying the polymerization procedure described previously. The polymerization time was 24 hours. The choice for this rather longer polymerization time was motivated by our hope to produce thick PtBA layers that would generate large enough signal for the FTIR measurements. The FTIR spectroscopy experiments were performed in order to verify that a gradient in grafting density of the PtBA was formed on the substrate. In Figure 6.6 we plot the FTIR spectra taken at various positions along the PtBA-covered specimen. The intensities of the two characteristic peaks of PtBA corresponding to $\nu(C=O)$ (at 1733 cm^{-1}) and $\nu(CH_2)$ (at 2850 and 2925 cm^{-1}) are expected to increase while traversing the sample from the OTS-side (small distance along the substrate) towards the PtBA side (larger distance along the substrate). The experimental results confirm the expected trend.

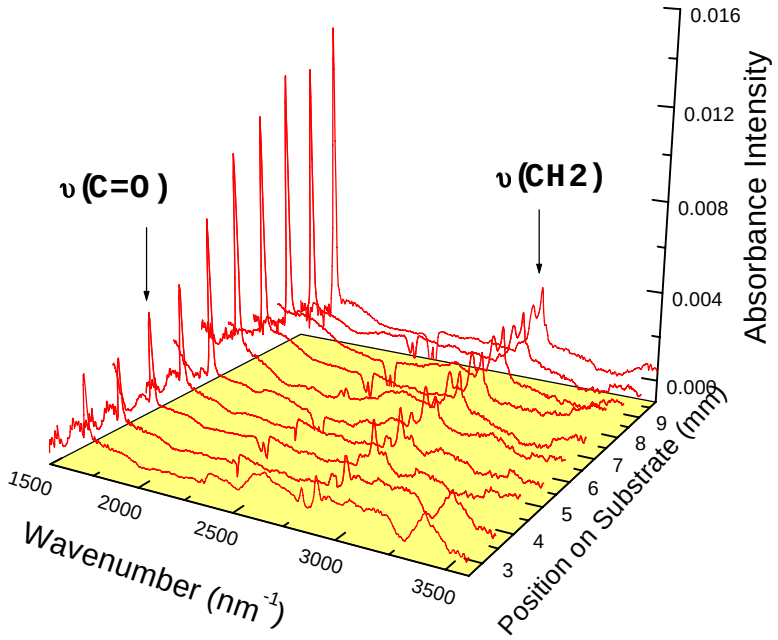

Figure 6.6 FTIR spectra of PtBA grafting density gradient polymerized from the substrate covered with the gradient of the ATRP initiator. The polymerization time was 24 hrs.

While FTIR proved useful in confirming that the conversion of PtBA into PAA took place, it did not provide enough information about the thickness of the polymers on the substrate. Spectroscopic ellipsometry was used to measure the dry thickness of both the PtBA and PAA gradient samples, which were polymerized for 10 hrs and hydrolysis in HCl/dioxane bath for 10 hrs. In Figure 6.7, we plot the dry thickness of PtBA (solid symbols) and PAA (open symbols) as a function of the position on the substrate. The data in Figure 6.7 reveal that the thickness of both PtBA and PAA increases as one moves from the OTS side (small number on the abscissa) of the sample towards the initiator-covered side (large numbers on the abscissa); in both cases the functional form closely resembles that of a backward diffusion-like profile.

Assuming that all chains of both PtBA and PAA have the same degree of polymerization along the substrate (*i.e.*, the polymerization rate was independent of the grafting density of the initiator on the substrate),[35] the increase of the polymer dry thickness can be attributed to the increase of the polymer grafting density on the substrate. Interestingly, there was a rapid decrease in the dry polymer thickness after the hydrolysis. Specifically, the thickness of PtBA decreases 6 fold upon hydrolysis to PAA. The decrease does not seem to be dependent much on the grafting density of the polymer on the substrate. We will return to this point later in our discussion.

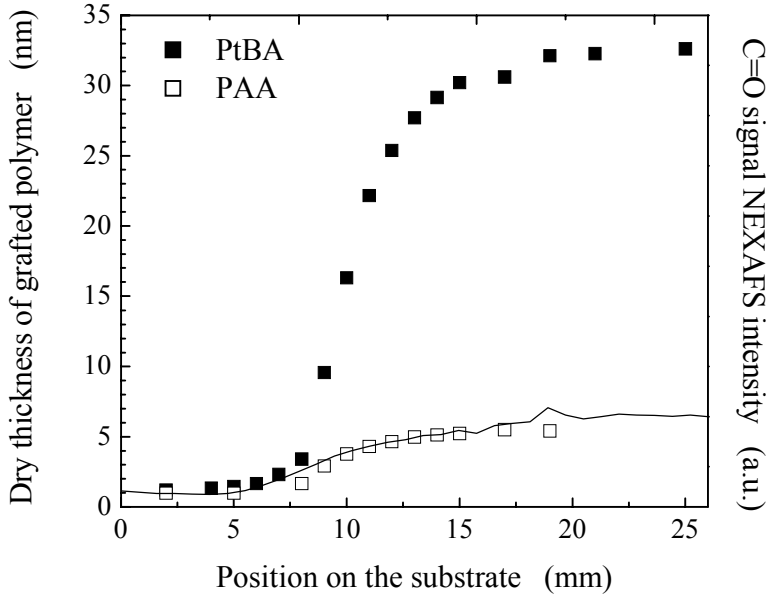

Figure 6.7 Dry thickness of PtBA (solid symbols) and PAA (open symbols) as a function of the position on the substrate. The solid line represents the PEY NEXAFS intensity measured at E=531 eV on the PAA sample as a function of the position on the substrate.

Experiments using NEXAFS were conducted in order to evaluate the density of PAA as a function of the position on the substrate. With the x-ray monochromator set to 531 eV,

which corresponds to the $1s \rightarrow \pi^*_{C=O}$ transition, we collected the partial electron yield (PEY) NEXAFS signal by scanning the x-ray beam along the gradient. The solid line in Figure 6.7 depicts the variation of the PEY NEXAFS intensity corresponding to the C=O bond across the PAA gradient. The NEXAFS results confirm that the C=O intensity, and thus the amount of PAA on the surface, increases as one moves along the gradient. Moreover, the NEXAFS data are in good agreement with the ellipsometric thickness of PAA.

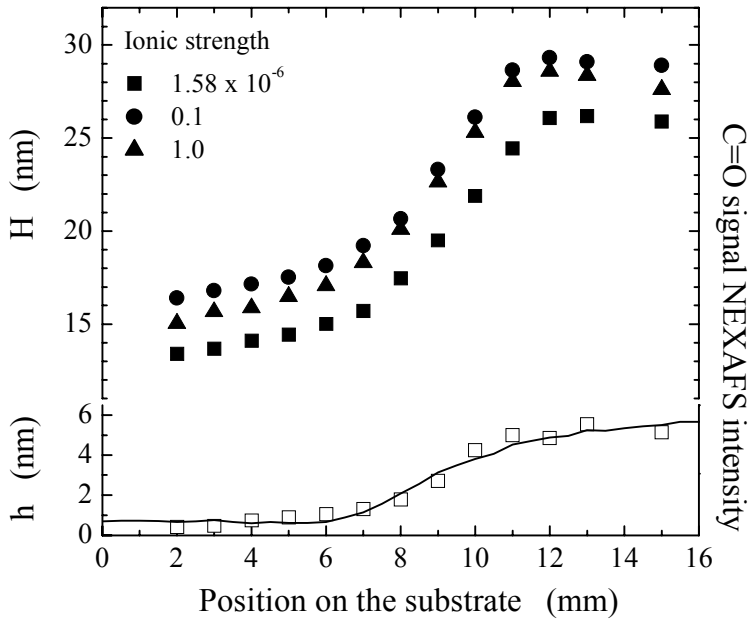

Figure 6.8 Dry (h) and wet (H) thickness of PAA measured as a function of the position on the solid substrate. The wet thickness was evaluated at pH=4 and is plotted as a function of three different ionic strengths. The solid line represents the PEY NEXAFS intensity measured at E=531 eV on the dry PAA sample.

In order to study the solution properties of the surface-grafted PAA, we incubated the PAA gradients under aqueous solutions under the different pH values (4, 5.8, and 10) and a

series of ionic strengths for each pH. Hence, by measuring the wet thickness of PAA along the gradient at different solution condition, we obtained the wet thickness of the grafted polymer layer as a function of the PAA grafting density, pH, and ionic strength. Most of the ellipsometry experiments were carried out on PAA with M_n=4.8 kDa, only a limited series of measurements were done with the M_n=3.34 kDa PAA (see Discussion). In Figure 6.8 we plot an example of a series of measurements performed with the M_n=4.8 kDa PAA. The open symbols represent the dry PAA thickness measured as a function of the position on the substrate. The solid line is the PEY NEXAFS intensity scan at E=531 eV, corresponding to the C=O peak. In the same figure we also plot the wet thickness of PAA (H) measured at pH=4 and three different ionic strengths. The data show that for all ionic strengths, H increases with increasing grafting density of PAA on the substrate. A close inspection of the data in Figure 6.8 reveals that H is a non-monotonous function of the ionic strength. Specifically, as the ionic strength increases, H also increases, reaches a maximum and then decreases. We will address this behavior in the Discussion section that follows.

6.5 Discussion

6.5.1 Surface hydrolysis of PtBA

We studied the kinetics of conversion of PtBA into PAA by measuring the time dependence of the PtBA thickness and contact angle on conversion time on PtBA samples prepared on substrates with a homogeneous distribution of the surface-bound initiator. The results are summarized in Figure 6.9 for several samples with different initial PtBA dry

thicknesses. In Figure 6.9a we plot the dry thickness of PtBA, h, normalized by initial film thickness, h(t=0), as a function of the conversion time. The data show that for all samples studied, the initial thickness decreases rapidly by about 50% within the first two hours, followed by a slower decrease at later times.

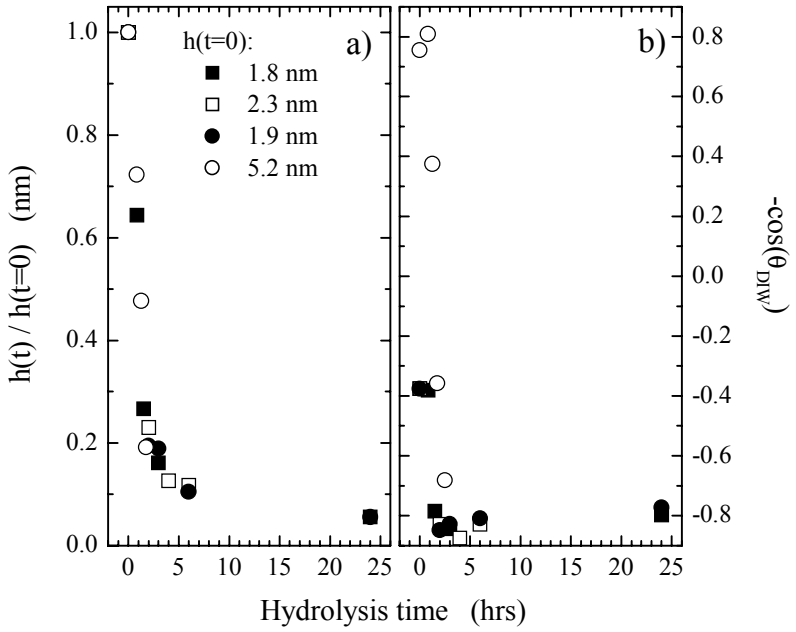

Figure 6.9 Dry thickness (a) and contact angle (b) as a function of the hydrolysis time. The various symbols denote samples with a different initial dry thickness.

We attribute the sharp drop in the film thickness to the decrease of the volume of the polymer, associated with the removal of the bulky *tert*-butyl groups. We note that similar behavior has been observed by others.[27] We speculate that the slower decease in PtBA thickness may be associated with possible cleavage of the polymer from the substrate caused by the hydrolysis of the ester group inside the initiator (a primary ester, *cf.* Figure 6.2).

However, since the reaction rate for *tert*-ester hydrolysis is much faster than that for primary-ester hydrolysis, we can complete the conversion of PtBA to PAA before the polymers are completely cleaved off from the substrate.

We make a simple estimate in order to verify our hypothesis. In Table 6.3 we list the molecular parameters of PtBA and PAA, such as the monomer molecular weight (M_o), the density (ρ), and the volume of the monomer unit (v_o). The latter was calculated by using Eq. (6.4):

$$v_o = \frac{M_o}{\rho N_A} \tag{6.4}$$

where N_A is Avogadro's number.

Table 6.3 Molecular parameters of PtBA and PAA

	PtBA	PAA
M_o (g/mol)	128.17	72.065
ρ (g/cm^3)	1.05 [36]	1.22 [37]
v_o (cm^3)	2.027 x 10^{-22}	9.81 x 10^{-23}

When we assume that the degree of polymerization of PtBA is the same as that of PAA and the total number of polymer chains upon hydrolysis remains constant, we can use the values in Table 6.3 to estimate the change in thickness of the PtBA film associated with complete conversion of the PtBA into PAA as:

$$\frac{\Delta h_{PtBA}}{h_{init,PtBA}} = \frac{\Delta v_o}{v_{o,PtBA}} = 1 - \frac{v_{o,PAA}}{v_{o,PtBA}} \approx 0.52 \tag{6.5}$$

where Δh_{PtBA} and $h_{init,PtBA}$ are the PtBA thickness change upon hydrolysis and the initial PtBA thickness, respectively.

This simple estimate illustrates that complete hydrolysis of PtBA into PAA will result in about 52% decreases of the total PtBA film thickness. It also confirms our earlier hypothesis, namely that the rapid drop in polymer thickness within the first two hours of HCl treatment is associated predominantly with the PtBA to PAA conversion. Based on this estimate, HCl treatment times longer than about 2 hours would result in some cleavage of the polymer from the substrate. For example, based on the data in Figure 6.9, after 5 hours of hydrolysis, the original thickness of PtBA decreases by 85%.

In Figure 6.9b we plot the negative cosine of the DI water contact angle, θ_{DIW}, as a function of the PtBA-to-PAA conversion time. Note that the trend is similar to the PtBA thickness *versus* time behavior. Specifically, θ_{DIW} drops from 88° for a thick PtBA rather rapidly within the first about 4 hours, a behavior that is associated with the conversion of the *tert*-butyl group into the –OH group. The contact angle reaches a minimum at about five hours, after which time is starts to increase again. The latter can be attributed to the surface exposure of the undecyl silane groups that remained grafted to the substrate after the cleavage of the *tert*-ester in the initiator molecule. In our gradient samples, we performed the PtBA hydrolysis for 5 hours in order to ensure the complete removal of *tert*-butyl groups. Although some polymer may have been cleaved off the surface during this extended

hydrolysis, a large enough amount of polymer remained on the surface that was used in further analysis. In fact, NEXAFS experiments on PAA samples prepared by hydrolyzing a PtBA sample for about 10 hours revealed that a significant amount of PAA still remained on the surface.

6.5.2 Dependence of H on ionic strength

In Figure 6.10, we plot the dependence of the PAA wet thickness (H) on the solution ionic strength (IS) at three different pH values for various grafting densities (plotted with the different symbols – see Table 6.4 in the Appendix A.6.2 for details). Since only NaCl, HCl and NaOH were used to change the solution ionic strength, the salt concentration (φ_s) in this case is equal to the solution ionic strength (IS). The data in Figure 6.10 reveal that H depends on IS in a non-monotonous fashion. Specifically, as IS increases, H increases before reaching a maximum at a certain value and then starts to decrease. This behavior, observed for all pH values at all grafting densities (σ), is in accord with the theoretically predicted trends[10] that divide the H vs. IS dependence into three regions (*cf.* Figure 6.1): the osmotic brush (OB), the salted brush (SB), and neutral brush (NB). The ionic strength, at which the transition between the OB and SB regimes occurs (IS_{max}), is related to σ and pH. At pH=4, IS_{max} is nearly constant regardless of the σ (Figure 6.10a). At pH=5.8, IS_{max} remains small at low grafting densities and increases slightly to 0.25 with increasing σ (Figure 6.10b).

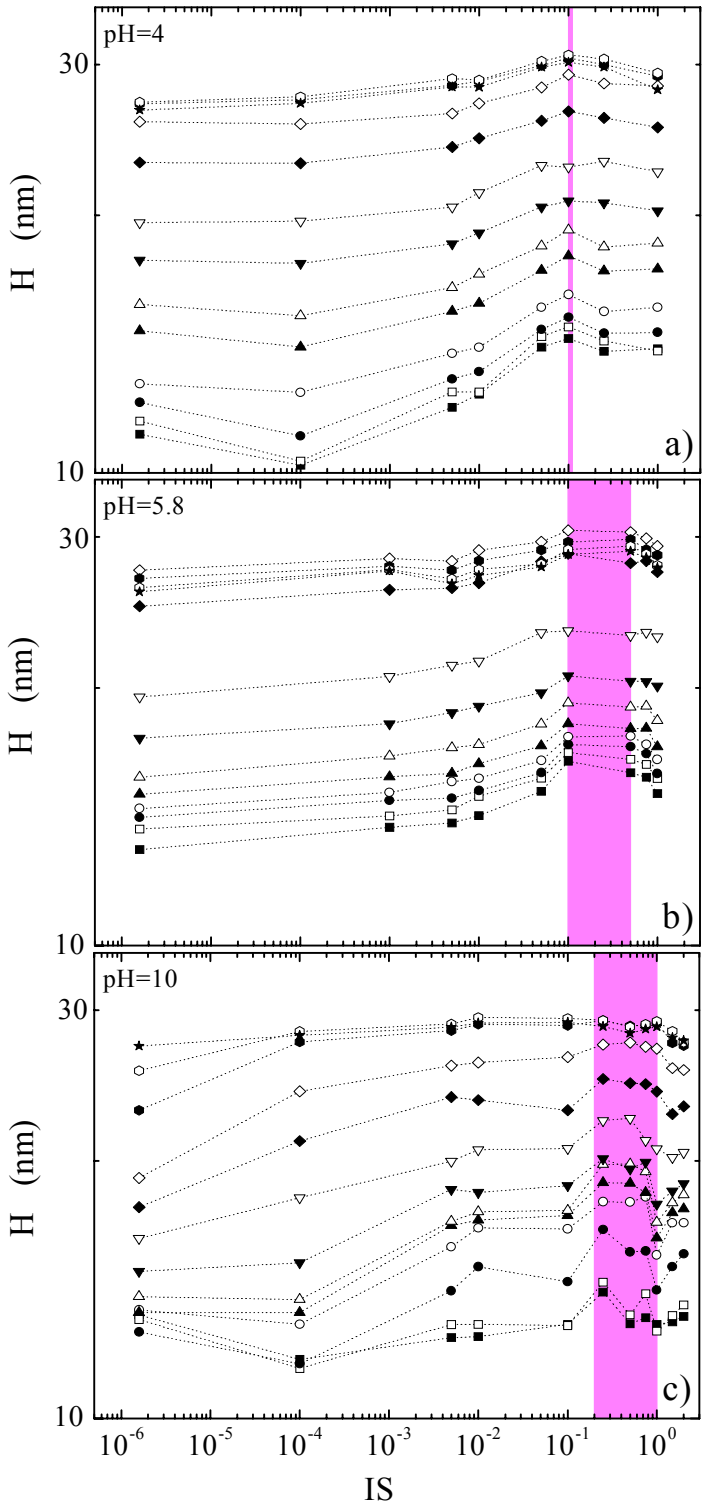

Figure 6.10 Wet thickness of PAA (H) as a function of the solution ionic strength (IS) at pH=4 (a), pH=5.8 (b), pH=10 (c). The symbols represent different grafting densities of PAA. (see Table 6.4 in the Appendix A.6.2 for details).

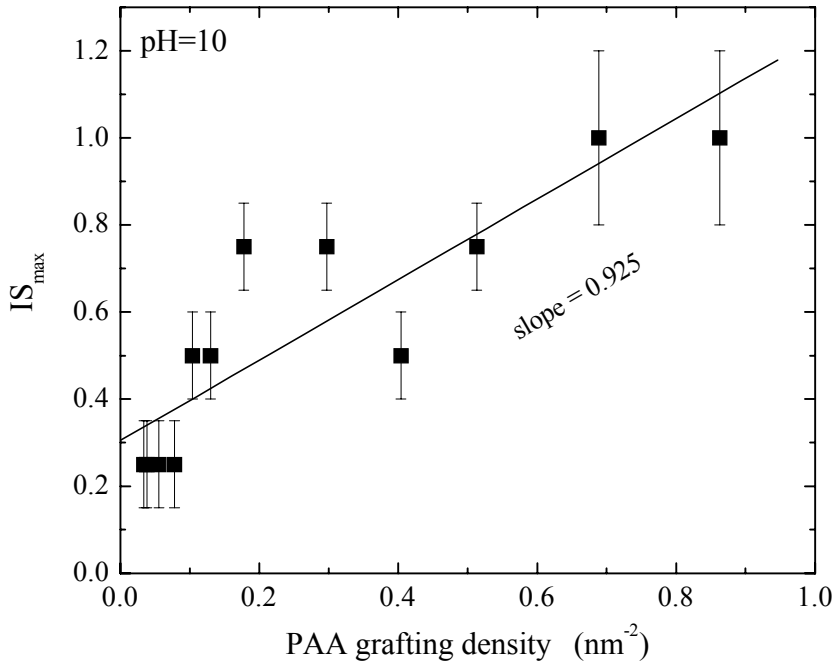

Figure 6.11 IS_{max} as a function of grafting density for the measurements at pH=10

At pH=10, IS_{max} shifts significantly (Figure 6.10c). Specifically, while for low σ (≈0.0381 nm^{-2}) IS_{max}≈0.25, at high σ (≈0.863 nm^{-2}) IS_{max}≈1.

The results are in very good agreement with the theoretical prediction by Israëls et al[10], who proposed that $IS_{max}\sim\sigma(\alpha)^{1/2}$. Clearly, IS_{max} is affected by the solution pH value, which directly influences α. At pH=4, since α is very small, the grafting density change could not produce any obvious change of $\sigma(\alpha)^{1/2}$ or IS_{max}. At pH=10, α is close to 1 (complete ionization), so $IS_{max}\sim\sigma$. In Figure 6.11, we plot the IS_{max} values extracted from Figure 6.10c as a function of σ for the measurements done at pH=10. The slope (=0.925) is close to the expected value of 1. At pH=5.8, α is about 0.5 [21], which explains that the shift in IS_{max} is relatively small, compared to that at pH=10.

6.5.3 Dependence of H on the PAA grafting density

At the beginning of the chapter, we discussed that weak polyelectrolyte wet thickness has a different dependence on the grafting density for polymers in the SB or OB regimes[5]. In the following section we will present the results of the experimentally measure H for each regime separately. Since there is no significant variation in the data for different pH values and molecular weights, we will use the results collected at pH=5.8 and PAA with M_m=4.8kDa.

Salted Brush regime (SB)

In Figure 6.12 we plot H as a function of the PAA grafting density in the SB regime. The various symbols denote data collected at IS ranging from 0.1 to 0.75. At high polymer grafting densities (σ>0.1 nm^{-2}), H increases with increasing σ. This is a typical behavior for the brush conformations. The transition from the brush regime to the mushroom regime occurs at $\sigma\approx$0.08 nm^{-2}. The slope for the brush regime is found to range from 0.29 to 0.31, in a very good agreement with the theoretically predicted value of 1/3. With increasing IS, H decreases and the slope in the H~σ^n dependence increases. The decrease in polymer swelling is largely due to the screening of the electrostatic interactions by the counter ions inside the polymer brush. The increase in the slope suggests that the solution ions move more easily inside the grafted polymer at lower grafting density. With increasing σ, the transport of ions inside the densely packed polymers becomes harder. As a consequence, the screening affects weaken.

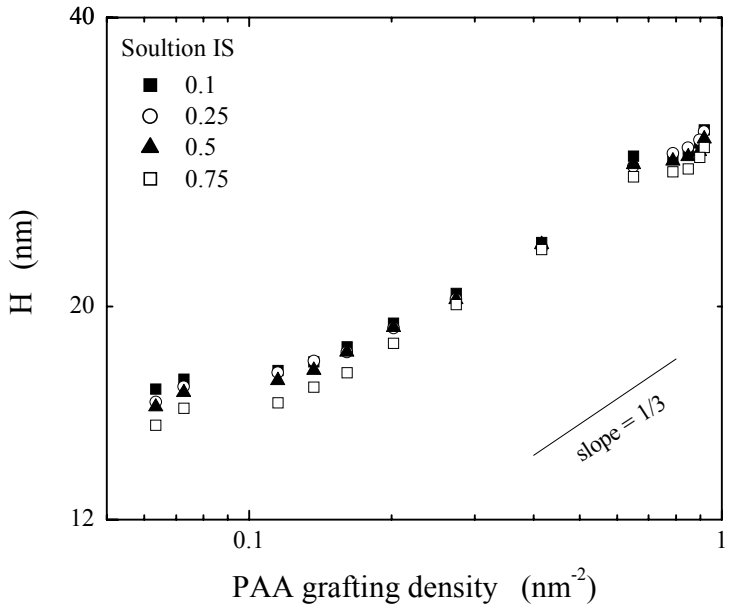

Figure 6.12 Wet thickness at pH=5.8 for PAA (M_n=4.8 kDa) as a function of the grafting density and ionic strength of the aqueous solution in the SB regime.

Osmotic Brush regime (OB)

In Figure 6.13, we plot H as a function of σ for IS ranging from 1.56 x 10^{-6} to 0.1. We have previously identified that at these IS values the system is in the OB regime. Previous theoretical work predicted that in this regime that wet thickness of polymer brush should *decrease* with the grafting density as $H \sim \sigma^{-1/3}$ and should increase with increasing IS[5,10] Based on theoretical studies, at the transition between the OB to SB regimes (at IS_{max}), H is independent of the brush grafting density.

Similar to previous experiments by others,[21] we observe that this scaling relation is somehow flawed. Specifically, by fitting the data in the brush regime to $H \sim N\sigma^n$, we obtain n that ranges from 0.28 to 0.34 instead of the expected value of –1/3.

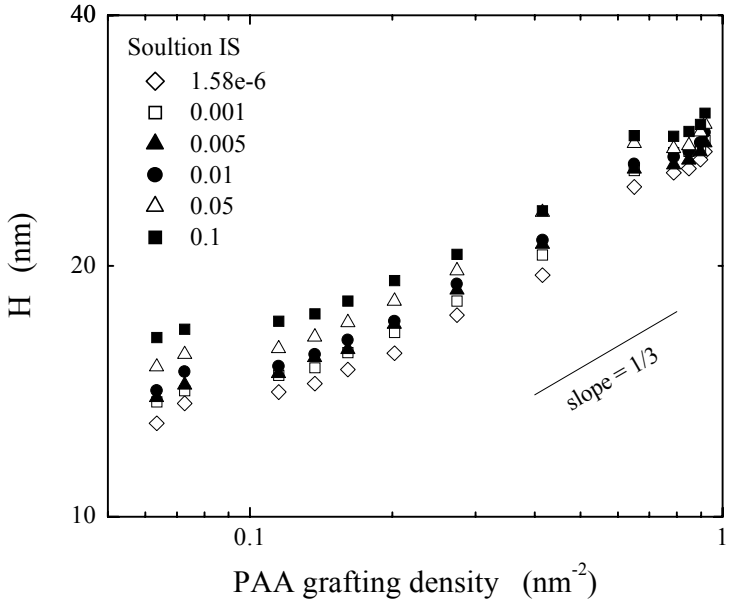

Figure 6.13 Wet thickness at pH=5.8 for PAA (M_n=4.8 kDa) as a function of the grafting density and ionic strength of the aqueous solution in the OB regime.

A close inspection of the data in Figure 6.13 reveals that polymer swelling increases with increasing ionic strength. Interestingly, the value of the exponent n decreases systematically as the solution IS increases. This is in contrast to the performance of PAA in the SB regime, where the value of n increased with increasing IS (*cf.* Figure 6.12). This behavior reveals that when a small amount of salt is added in the OB regime to polymers with a low σ, the grafted polymer swells more relative to PAA at high σ.

In order to quantify this behavior, we define a degree of swelling (DS) of a grafted polymer as:

$$DS = \frac{H(IS) - H_{DIW}}{H(DIW)} x100\% \qquad (6.6)$$

where H(IS) and H_{DIW} are the PAA thicknesses evaluated at a given IS and in "pure" water (IS→0), respectively. In Figure 6.14, we plot the degree of swelling at IS_{max} as a function of the PAA grafting density at different pH values for polymers in the OB regime.

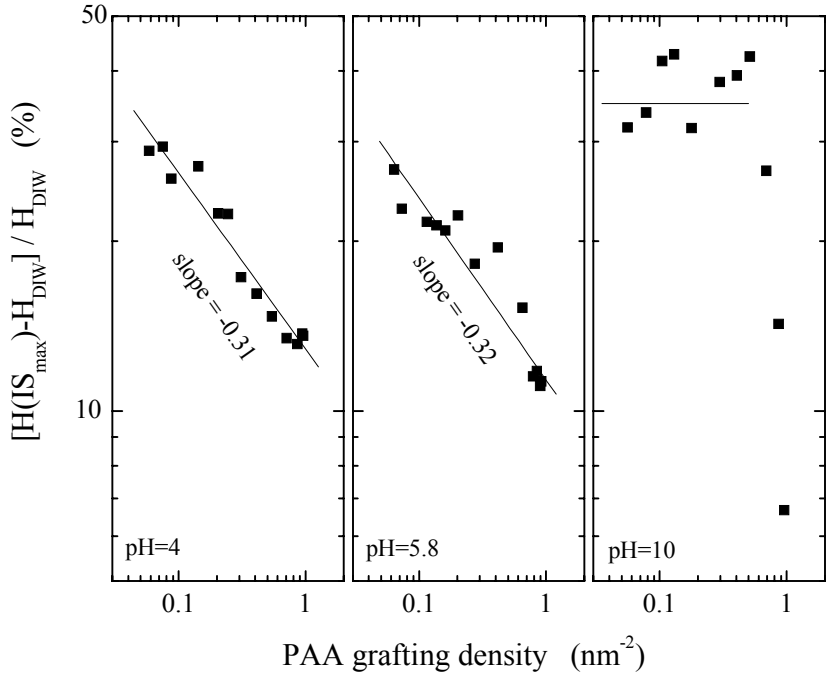

Figure 6.14 Degree of swelling $[H(IS_{max})-H_{DIW}]/H_{DIW}$ for PAA (M_n=4.8 kDa) as a function of the PAA grafting density in the OB regime at different pH values.

By fitting the data to $DS \sim \sigma^n$, we find n to be very close to –1/3 in OB regime for pH=4 and 5.8, and 0 for the pH=10 data. At low pH, PAA behaves as a weak polyelectrolyte, the degree of swelling changes with the σ. At pH=10, almost all charges

along the polymer backbone are activated and present at the backbone. As a consequence, the polymer behavior closely resembles that of a strong polyelectrolyte, whose degree of expansion is independent of the polymer grafting density.

6.5.4 Dependence of H on solution pH value

As mentioned before, the transition from the OB regime to the SB regime depends on the solution pH value. In Figure 6.15, we compare the dependence of the PAA wet thickness

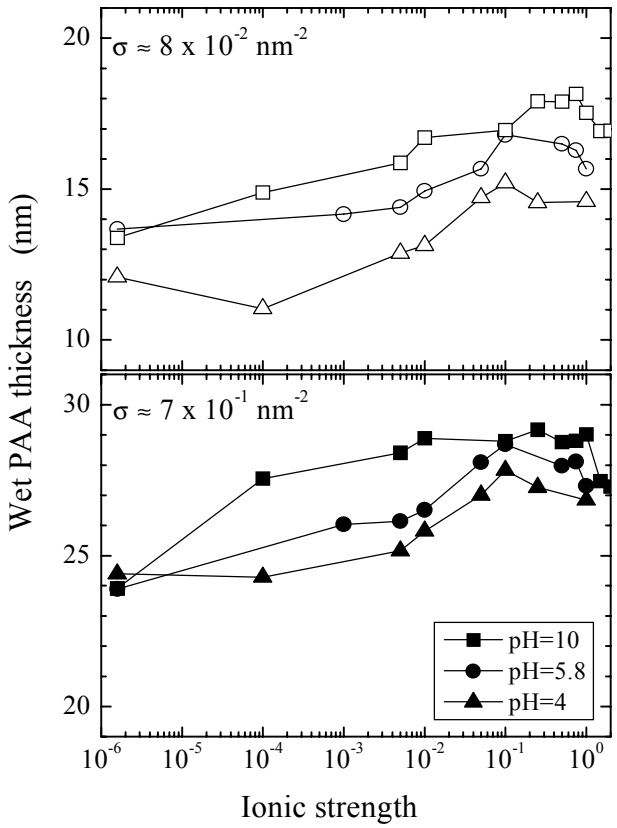

Figure 6.15 Wet thickness of the PAA (M_w=4.8 kDa) with two different values of the grafting density on the solid substrate as a function of the ionic strength in different pH solutions.

on the ionic strength at two representative values of σ under three pH value conditions. For σ≈0.08 nm^{-2} (Figure 6.15a) and σ≈0.7 nm^{-2} (Figure 6.15b), PAA is in the mushroom and brush regimes, respectively. Two trends can be deduced from the data presented in Figure 6.15. First, with increasing grafting density, the height of the polymer brush increases. Second, at both grafting densities, the PAA swelling increases as the solution pH value increases. The latter behavior is associated with the electrostatic charging inside the PAA brush which leads to the increase of the intermolecular repulsions and subsequent brush height increase.

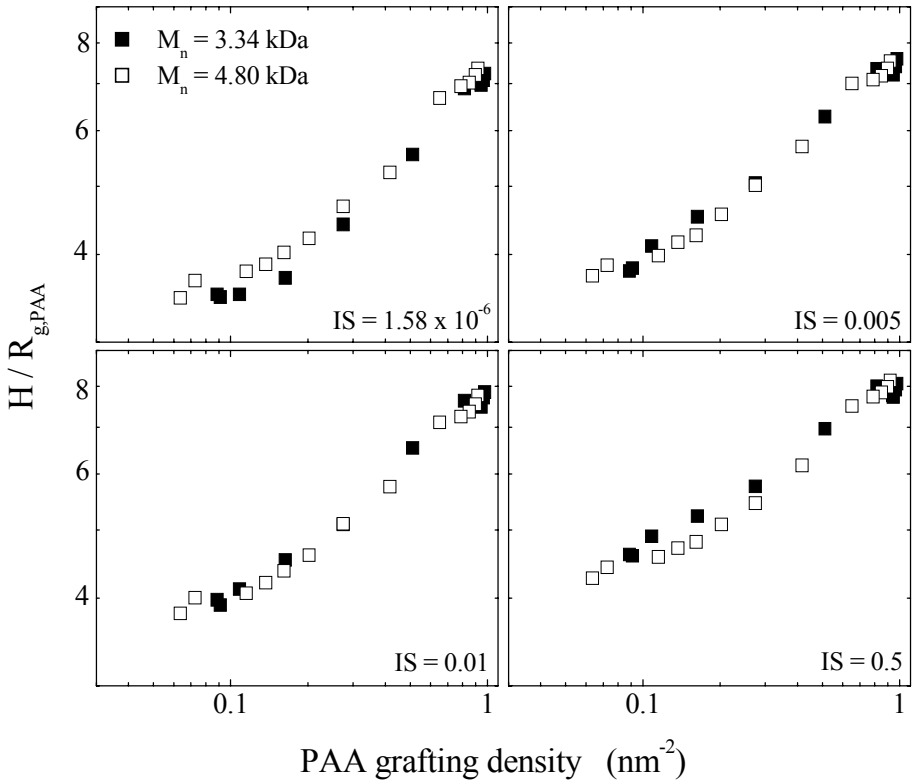

Figure 6.16 H/R_g as a function of the PAA grafting density at pH=5.8 and different ionic strengths of the aqueous solution.

6.5.5 Dependence of H on PAA molecular weight

In Figure 6.16, we plot the PAA wet thickness H normalized by the radius of gyration of PAA for PAA at identical IS and σ values. For each IS value, the normalized thickness can be collapsed on a single master curve. We cannot further rationalize this fining as there still seems to be a controversy in the literature as to whether it is more appropriate to normalize the wet polymer thickness by the number of segments or the radius of gyration of the polymer. Our data seem to be supporting the latter notion. More experiments are needed to further verify this result.

6.6 Summary

In this chapter, we studied the scaling laws of surface grafted polyacrylic acid (PAA) as a function of the polymer grafting density (σ), solution ionic strength (IS), and pH. In order to facilitate the complete exploration of the σ space, we created surface-grafted PAA on flat silica-covered substrate with a spatial variation of the chain grafting density. The surface-bound PAA with a gradual variation of grafting densities was formed by: 1) creating a molecular density gradient of the surface-anchored polymerization initiator, 2) performing ATRP of poly(*tert*-butyl acrylate) (PtBA) from the surface, and 3) converting the PtBA into PAA by hydrolysis. We used spectroscopic ellipsometry to measure the wet thickness of the PAA as a function of σ, IS, and pH.

The wet thickness (H) of the surface-grafted PAA brushes was found to have a non-monotonous dependence on the ionic strength (IS) of the solution. With increasing the

concentration of the external salt, the polymer thickness in solution increased and reached a maximum at a certain ionic strength (IS_{max}), and then further decreased. Guided by the theoretical models of weak polyelectrolyte brushes, we have identified three regimes: the osmotic brush (OB), the salted brush (SB), and the neutral brush (NB) regime. We have discussed how H behaves at different σ in the SB and OB regimes. By comparing the swelling of polymer under different pH solution conditions, we concluded that the expansion of the grafted chain at low pH value was much less than that at high pH solution.

In the SB regime, H was found to increase with increasing σ at high polymer grafting densities, a typical behavior for polymer brushes. The slope for the brush regime ranged from 0.29 to 0.31, in a good agreement with the theoretically predicted 1/3. The transition from the brush to the mushroom regime was found to occur at $\sigma \approx 0.08$ nm^{-2}. We also established that the slope of H increased with increasing IS. This behavior was attributed to the less efficient screening affects from solution ions at higher grafting densities.

At low IS, the system was in the OB regime. Here, the wet PAA thickness was found to depend strongly on σ and pH. Our data revealed that at high σ, H followed the scaling law $H \sim \sigma^n$, with n ranging from 0.28 to 0.34. We commented that this observation was in contrast to the theory, which predicts that in the OB regime $H \sim \sigma^{-1/3}$. We also observed that the degree of polymer swelling increased with increasing IS. The exponent in the $H \sim \sigma^n$ dependence decreased with increasing IS. This behavior was exactly opposite to that detected in the SB regime, where n increased with increasing IS. We defined a degree of swelling (DS) parameter as $[H(IS_{max})-H_{DIW}]/H_{DIW}$, where H(IS) and H_{DIW} are the PAA thicknesses evaluated at a given IS_{max} and in "pure" water ($IS \rightarrow 0$) , respectively. By fitting

the data to $DS \sim \sigma^n$, we found n to be very close to –1/3 in the OB regime for pH=4 and 5.8 and 0 at pH=10. We rationalized that this behavior was a consequence of the conformational changes in the polymer associated with the concentration of the charges along the backbone. At low pH, not all charges were activated and PAA behaved as a typical weak polyelectrolyte and DS increased with decreasing σ. In contrast, at high pH, the whole polymer backbone was decorated with a large number of changes that stayed permanently attached to the backbone. Consequently, PAA behaved like a strong polyelectrolyte, whose degree of expansion is independent of the grafting density.

We also found that the value of the ionic strength at the OB to SB transition (IS_{max}) depends on the polymer grafting density and the solution pH value. At pH=4, IS_{max} is independent of σ. As the solution pH increases, IS_{max} also increases; moreover, IS_{max} also increases with increasing σ. The results are in a good agreement with the theoretical predicted scaling law $IS_{max} \sim \sigma(\alpha)^{1/2}$.

Acknowledgements. This work is supported by the National Science Foundation, Grant No. CTS 0209403, The Camille Dreyfus Teacher-Scholar award, and The 3M Non-Tenured Faculty award. The NEXAFS experiments are carried out at the National Synchrotron Light Source, Brookhaven National Laboratory, which is supported by the U.S. Department of Energy. The author thank Dr. Kirill Efimenko (NCSU) and Dr. Daniel Fischer (NIST) for his assistance during the course of the NEXAFS experiments and Drs. Petr Vlček and Vladimír Šubr (both Institute of Macromolecular Chemistry in Prague) for their assistance with the size exclusion chromatography measurements.

Appendix A.6.1

Glossary

DS	degree of Swelling
h	dry thickness of surface-anchored polymer
H	wet thickness of surface-anchored polymer
$[H^+]$	proton concentration in bulk solution
H_{DIW}	polymer wet thicknesses in "pure" water
H(IS)	polymer wet thicknesses evaluated at a given IS
IS	solution ionic strength
IS_{max}	solution ionic strength at the transition from OB to SB
M_n	average number molecular weight of polymer
M_o	monomer molecular weight
M_w/M_n	polydispersity index
N	degree of polymerization
N_A	Avogadro's number
NB	neutral regime
OB	osmotic regime
R_g	radius of gyration
SB	salted regime
v_o	volume of the monomer unit
α	degree of dissociation in bulk solution
α_o	"internal" degree of dissociation
ν_e	electrostatic excluded volume parameter
ρ	polymer density
σ	grafting density
φ	polymer volume fraction
φ_s	salt concentration in bulk solution
χ	Flory-Huggins interaction parameter

Appendix A.6.2

Table 6.4 Symbols used in Figure 6.10 assigning the different PAA grafting densities

	PAA grafting density (chains/nm^2)		
Symbol	pH=4	pH=5.8	pH=10
·····■·····	0.0635	0.0747	0.0381
·····□·····	0.0727	0.0586	0.0340
·····●·····	0.1150	0.0872	0.0557
·····○·····	0.1370	0.1430	0.0782
·····▲·····	0.1610	0.2040	0.1040
·····△·····	0.2020	0.2450	0.1300
·····▼·····	0.2740	0.3100	0.1780
·····▽·····	0.4160	0.4120	0.2970
·····◆·····	0.6500	0.5420	0.4040
·····◇·····	0.9170	0.7090	0.5130
·····⬢·····	0.8970	0.8620	0.6890
·····⬡·····	0.8480	0.9550	0.8630
·····★·····	0.7880	0.9440	0.9570

References and notes

[1] Halperin, A.; Tirrell, M. and Lodge, T. P. *Adv. Polym. Sci.* **100**, 31 (1991).

[2] Alexander, S. *J. Phys.* 38, 983 (1977); De Gennes, P.-G. *J. Phys.* (Paris) **37**, 1445, (1976); De Gennes, P.-G. *Macromolecules* **13**, 1069 (1980).

[3] Milner S. T. *Science* **251**, 905 (1991).

[4] Pincus, P. *Macromolecules* **24**, 2912 (1991).

[5] Zhulina, E. B.; Birshtein, T. M. and Borisov. O. V. *Macromolecules* **28**, 1491 (1995).

[6] Zhulina, E. B. and Borisov, O. V. *J. Chem. Phys.* **107**, 5952 (1997).

[7] Israëls, R.; Scheutjens, J. M. H. M. and Fleer, G. J. *Macromolecules*, **27**, 3087 (1994).

[8] Israëls, R.; Leermakers, F. A. M., Fleer, G. J., and Zhulina, E. B. *Macromolecules* **27**, 3249 (1994).

[9] Fleer, G. J. Ber. Bunsenges, *Phys. Chem.* **100**, 936 (1996).

[10] Israëls, R.; Leermakers, F. A. M., and Fleer, G. J. *Macromolecules* **27**, 3087 (1994).

[11] Israëls, R.; Leermakers, F. A. M., and Fleer, G. J. *Macromolecules* **28**, 1626 (1995).

[12] Lyatskaya, Yu. V.; Leemarkers, F. A. M.; Fleer, G. J.; Zhulina, E. B. and Birshtein, T. M. *Macromolecules* **28**, 3562 (1995).

[13] Kelly, T. W.; Schorr, P. A.; Johnson, K. D.; Tirrell, M. and Frisbie, D. C. *Macromolecules* **31**, 4297 (1998).

[14] Mir, Y.; Auroy, P. and Auvray, L. *Phys. Rev. Lett.*, **75**, 2863 (1995).

[15] Guenoun, P.; et al. *Phys. Rev. Lett.* **81**, 3872 (1998).

[16] Biesalski, M. and Rühe J. *Macromolecules* **32**, 2309 (1999).

[17] Biesalski, M. and Rühe J. *Langmuir*, **16**, 1943 (2000).

[18] Biesalski, M. and Rühe J. *Macromolecules*, **35**, 499 (2002).

[19] Kurihara, K.; Kunitake, T.; Higashi, N. and Niwa, M. *Langmuir* **8**, 2087 (1992).

[20] Currie, E. P. K.; Sieval, A. B.; Fleer, G. J. and Cohen Stuart, M. A. *Langmuir* **15**, 7116 (1999).

[21] Currie, E. P. K.; Sieval, A. B.; Fleer, G. J. and Cohen Stuart, M. A. *Langmuir* **16**, 8324 (2000).

[22] Patter, T. E.; Xia, J.; Abernathy, T. and Matyjaszewski, K. *Science* **272**, 866 (1996).

[23] Coessens, V.; Pintauer, T. and Matyjaszewski, K. *Prog. Polym. Sci*, **26**, 337 (2001).

[24] Wu, T.; Efimenko, K. and Genzer, J. *J. Am. Chem. Soc.* **124**, 9394 (2002).

[25] Matyjaszewski, K.; Miller, P. J.; Shukla, N.; Immaraporn, B.; Gelman, A.; Luokala, B. B.; Siclovan, T. M.; Kickelbick, G.; Vallant, T.; Hoffmann, H. and Pakula, T. *Macromolecules* **32**, 8716 (1999).

[26] Davis, K. A. and Matyjaszewski, K. *Macromolecules* **33**, 4039 (2000).

[27] Matyjaszewski, K.; Miller, P. J.; Shukla, N.; Immaraporn, B.; Gelman, A.; Luokala, B. B.; Siclovan, T. M.; Kickelbick, G.; Vallant, T.; Hoffmann, H. and Pakula, T. *Macromolecules* **32**, 8716 (1999).

[28] Efimenko, K.; Wallace, W. E. and Genzer, J., *J. Colloid Interface Sci.* **254**, 306 (2002).

[29] M. K. Chaudhury, G. M. Whitesides, Science **256**, 1539 (1992).

[30] Davis, K. A. and Matyjaszewski, K. *Macromolecules* **33**, 4039 (2000).

[31] L. Mrkvickova, J. Danhelka. *J. Appl. Polym. Sci.* **41**, 1929 (1990).

[32] It is value for poly(n-butyl acrylate) from *Polymer Handbook*; Brandrup, J.; Immergut, E. H., Eds; (Wiley & Sons: New York, 1999).

[33] Brandrup, J., Immergut, E. H. and Grulke, E. A. (Editors): *Polymer handbook* (Wiley, New York, 1999).

[34] Stöhr, J. *NEXAFS Spectroscopy* (Springer-Verlag, Berlin, 1992).

[35] A detailed argument for this assumption could be found in chapter 5 of this Thesis.

[36] It is value for poly(sec-butyl acrylate) from *Polymer Handbook*; Brandrup, J.; Immergut, E. H., Eds; (Wiley & Sons: New York, 1999).

[37] Brandrup, J., Immergut, E. H. and Grulke, E. A. (Editors): *Polymer handbook* (Wiley, New York, 1999).

Chapter 7

Preparing high-density polymer brushes by mechanically assisted polymer assembly (MAPA)

7.1 Abstract

This chapter describes a novel method of fine-tuning some physico-chemical (wetting, barrier) properties of grafted macromolecules on elastic surface by varying the grafting density and the chemical structure of the grafts at the surface. To accomplish this, we utilize "mechanically assisted polymer assembly" (MAPA). MAPA is based on depositing the polymerization initiator using the mechanically-assembled monolayers (MAMs) technology, developed recently in the Genzer group, and subsequently growing the polymer from the substrate using living-radical polymerization technique. By using this simple (and yet extremely powerful) strategy, we not only will produce materials with unique surface properties but also be able to explore a variety of interesting and important physico-chemical phenomena.

7.2 Motivation

It is well known that when polymers are end-anchored in a sufficient concentration to a substrate, they form a so-called polymer "brush" whereby the chains are stretched with respect to their preferred configuration away from the interface. The characteristics of polymer brushes have been analyzed using a variety of theoretical methods and experimental probes and are now fairly well established.[1,2,3,4] For example, the thickness of the brush layer, H, is known to depend linearly on the number of repeat units of the polymer, N, and on the power law of the brush grafting density at the substrate, σ, with the exponent of 1/3 or 1,

depending on the surface coverage.[1,2] In order to fine-tune the polymer brush properties one needs to have a good control over H and σ. While H can be adjusted by simply varying the polymerization time or/and monomer concentration, σ depends on the methods by which polymer brushes are formed.

Previous reports established that polymer brushes with moderately high grafting densities can be prepared by harnessing the "grafting from" principle in which the polymer chains are synthesized using radical initiators that are covalently bound to the substrate. A vast majority of experiments involved classical radical growth methods with either azo- (*e.g.*, AIBN) or peroxide-based initiators that were either created directly on the substrate or were attached to the substrate via self-assembly.[5,6,7,8,9,10,11] While the advantage of such methods is their ease of use and the ability to prepare brushes from a variety of monomers, a major disadvantage is a hard-to-control polymerization process, which usually leads to brushes with broad molecular weight distributions. Recently several reports appeared that described the formation of polymer brushes using surface-initiated "living" radical polymerization,[12] such as the atom transfer radical polymerization (ATRP).[13,14]. Because of its simplicity, robustness and the ability to synthesize polymers with narrow molecular weight distributions, ATRP has been the method of choice for most surface-initiated "living" radical polymerization processes. A recent review by Matyjaszewski and Xia[15] summarized the research activity in the field of ATRP, since the first reports in 1995 to the end of 2000. Various functional monomers including styrenes, methacrylates, methacrylamides and others were (co)polymerized in a controlled fashion, resulting in well-defined polymers with a good control over molecular weight and low polydispersities.

As mentioned previously, one of the crucial parameters governing the behavior of polymer brushes is their grafting density at the polymer/substrate interface. The "grafting from" techniques offer a fairly good control over the grafting density of the polymer brush - in the ideal case σ is simply equal to the surface density of the polymerization initiators. While a relatively high density of initiators can be achieved by assembling the molecules on the surface by means of Langmuir-Blodgett (LB) techniques[16,,17] or by forming organized self-assembled monolayers (SAMs),[18] tailoring the grafting density of the SAM chains is not an easy task. SAMs are usually formed through self-assembly processes that are governed by the chemical and structural nature of the SAM molecules and the means of their attachment to the substrate. To overcome this limitation, one would need to seek another way of controlling the grafting density of the surface initiators that is independent of the system thermodynamics.

Recently, Genzer and Efimenko[19] have demonstrated that one can fine-tune the grafting density of molecules on surfaces by fabricating MAMs (="mechanically assembled monolayers"), structures that are based on the combination of natural self-assembly and mechanical manipulation of the grafted molecules on surfaces. In this work we utilize the MAMs to adjust the surface density of the initiators and consequently that of polymer brushes grown by surface-initiated ATRP. Following the steps involved in the preparation procedure (see below), we call this technique MAPA (="mechanically assisted polymer assembly").

7.3 Description of MAPA

Figure 7.1 shows schematically how PAAm-MAPA works. First, a pristine PDMS network film is prepared (*cf.* Fig. 7.1a) by casting a mixture of PDMS and a cross-linker into a thin (≈1 mm) film and curing it at 70°C for about two hours. The film is then cut into small strips (≈1 x 5 cm^2) and uniaxially mechanically elongated by Δx (*cf.* Fig. 7.1b). Subsequent exposure to UV/ozone (UVO) treatment (*cf.* Fig. 7.1c) produces hydrophilic PDMS surfaces (PDMS-UVO) composed mainly of hydroxyl groups ($HO\text{-}[Si]_{surface}$)[20] that serve as attachments points for chlorosilane-based ATRP initiators. Following previous work on PAAm brushes, we use 1-trichlorosilyl-2-(m/p-chloro-methylphenyl)ethane (CMPE) (United Chemical Technologies, Inc.) as the initiator. The CMPE molecules are deposited from vapor onto this stretched substrate (*cf.* Fig. 7.1d) and form an organized CMEP-SAM following the well-known set of reactions:

$$CMPE - SiCl_3 + 3H_2O \xrightarrow{-3HCl} CMPE - Si(OH)_3 \tag{7.1}$$

$$CMPE - Si(OH)_3 + HO - [Si]_{substrate} \xrightarrow{-3H_2O} CMPE - Si \equiv O - [Si]_{substrate} \tag{7.2}$$

After the CMPE-SAM deposition, any physisorbed CMPE molecules are removed by thoroughly washing the substrates with warm deionized water (75°C, > 16 MΩ·m) for several minutes. The flask is sealed under N_2, placed into an oil bath, and the mixture is reacted at 130°C for 45 hours to form PAAm brushes on PDMS-UVO substrates (*cf.* Fig. 1e). After the reaction, the strain is released from the PDMS-UVO substrate, which

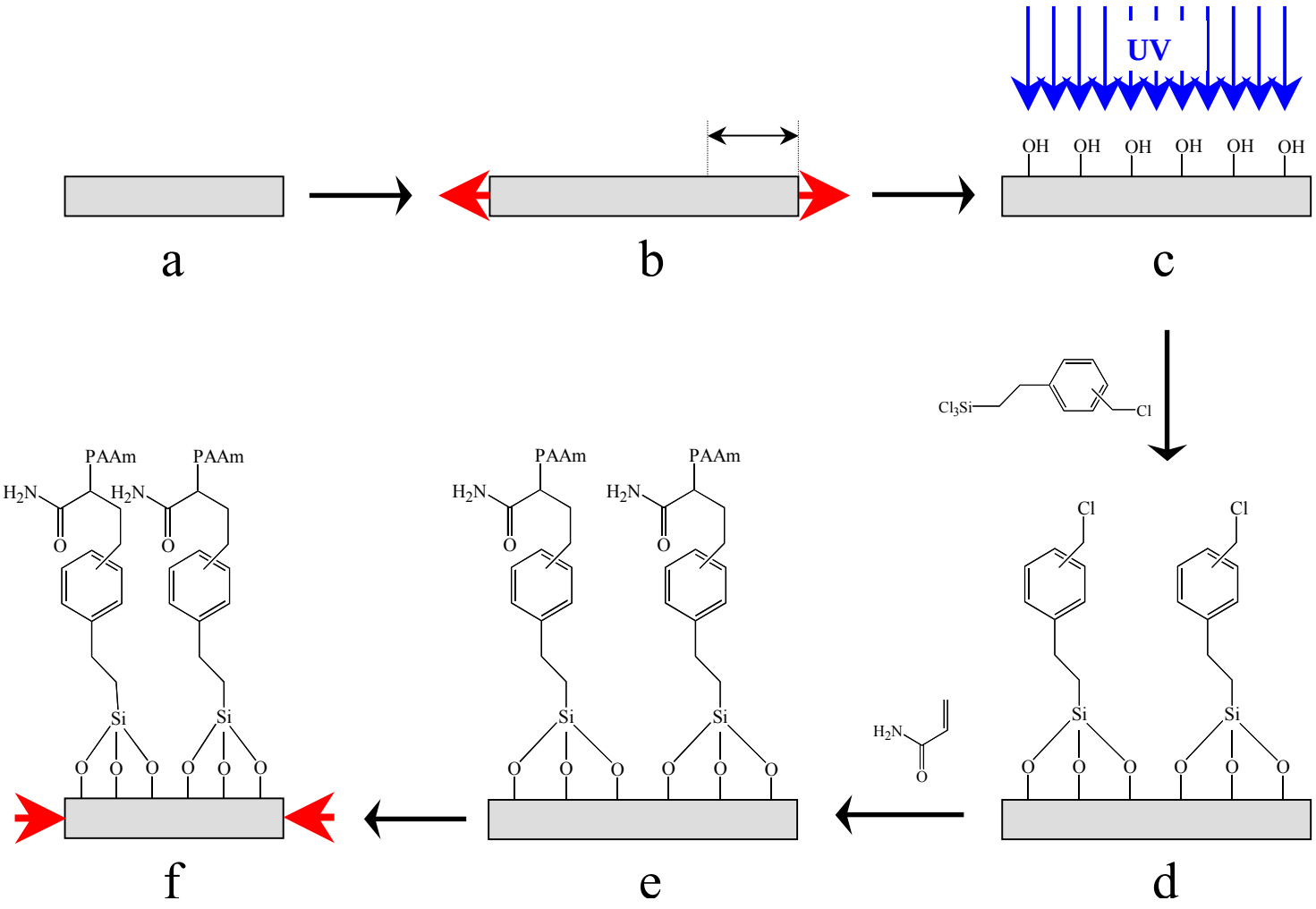

Figure 7.1 Schematic illustrating the principle of preparing high-density polyacrylamide bushes using MAPA ("=mechanically assisted polymer assembly").

returns to its original size (*cf.* Fig. 1f), causing the grafted PAAm polymers to form a densely organized brush. Any physisorbed monomeric and polymeric acrylamide is removed by Soxhlet extraction with deionized water for 48 hours.

Following is the detailed description of each step:

PDMS film preparation. The PDMS networks are prepared from the commercial PDMS Sylgard 184 and the curing agent 184 (Dow Corning Chemical). The PDMS:curing agent ratio is 10:1, as recommend by the recipe provided by the manufacturer. After a complete mixing of the two components, weak vacuum (≈1 torr) is applied to remove the air bubbles trapped in the mixture. About 5 g of the mixture is poured into a Petri-dish to form ≈1 mm thick film. The mixture is allowed to settle horizontally for about half an hour at room temperature and then cured it at 70°C for about two hours.

PDMS stretching. As shown in Fig. 7.2, three pieces of PDMS with certain lengths (equal or different) could be placed in the stretching apparatus at the same time. The samples are then stretched to produce the elongation Δx.

UVO treatment. The ultraviolet/ozone (UVO) treatment of the PDMS surface is carried out in a commercial UVO chamber (Jelight Company, Inc., Model 42). UVO treatment is a photo-sensitized oxidation process, in which the molecules of the treated material are excited and/or dissociated by the absorption of short-wavelength UV radiation. Atomic oxygen is simultaneously generated when molecular oxygen is dissociated by λ_1=184.9 nm and ozone by λ_2=253.7 nm. The 253.7 nm radiation is absorbed by most hydrocarbons and also by ozone. The organic products of this excitation react with atomic

oxygen to form simpler, volatile molecules, which desorb from the surface. Therefore, when both wavelengths are present, atomic oxygen is continuously generated, and ozone is continually formed and destroyed. We carried out the UVO treatment using one low-pressure mercury vapor grid lamp, or Standard Fused Quartz lamp. This lamp has an output of 28 mW/cm^2 at the distance 6 mm, as reported by the manufacturer, and has emission intensity 65% at 184.9 nm and 35% at 253.7 nm. The Stretched PDMS samples are placed into the UVO cleaner tray at a distance of about 5 mm from the UV source and exposed to the radiation from one side only for 35 minutes. The pressure, temperature, and relative humidity in the chamber were maintained at 1 atm, 20°C, and 50–60%, respectively.

Initiator deposition. The CMPE-SAM deposition experiments are done in a desiccator that is connected to a mechanical vacuum pump. The vacuum level in the deposition chamber is approximately 50 mmHg, so that there is still sufficient amount of water molecules needed for the reaction (1). Contact angle experiments indicate that a dense monolayer of CMPE forms in approximately 2 hours on the PDMS-UVO substrates placed 3 cm upside-down above the diffusion source, which consists of a mixture of CMPE and paraffin oil. Because the paraffin oil does not mix with the chlorosilane molecules, it provides a convenient diluting medium for the diffusion source; the flux of the CMPE molecules can be adjusted by simply varying the CMPE:paraffin oil ratio. In these experiments we used CMPE:paraffin oil ratio equal to 1:1.

Polymerization of PAAm. The surface polymerization of PAAm on PDMS is performed in a specially designed experimental chamber, as shown in figure 7.2. The PAAm ATRP on the PDMS-UVO/CMPE substrates was performed as described previously[21] by

placing the samples into 120 mL of N,N'-dimethylformamide and by adding 0.3 g of CuCl, 1.0 g of bipyridine, and 16.0 g of acrylamide (all obtained from Aldrich and used as received).

To verify that PAAm could be grown from PDMS surface by attaching initiator on UVO treated surface first and then following "grafting from" polymerization, PAAm was first synthesized on unstretched PDMS samples with different polymerization time. The reaction times are 12hr, 24hr and 48hr. For polymerization on stretched samples, surfaces of PDMS prestretched to Δx equal to 0%, 10%, and 20%; the ATRP of PAAm for 48 hrs is carried out on all sample at the same time.

Sample strain release. After polymerization, the strain is released slowly from the sample and then samples are cut off at both ends.

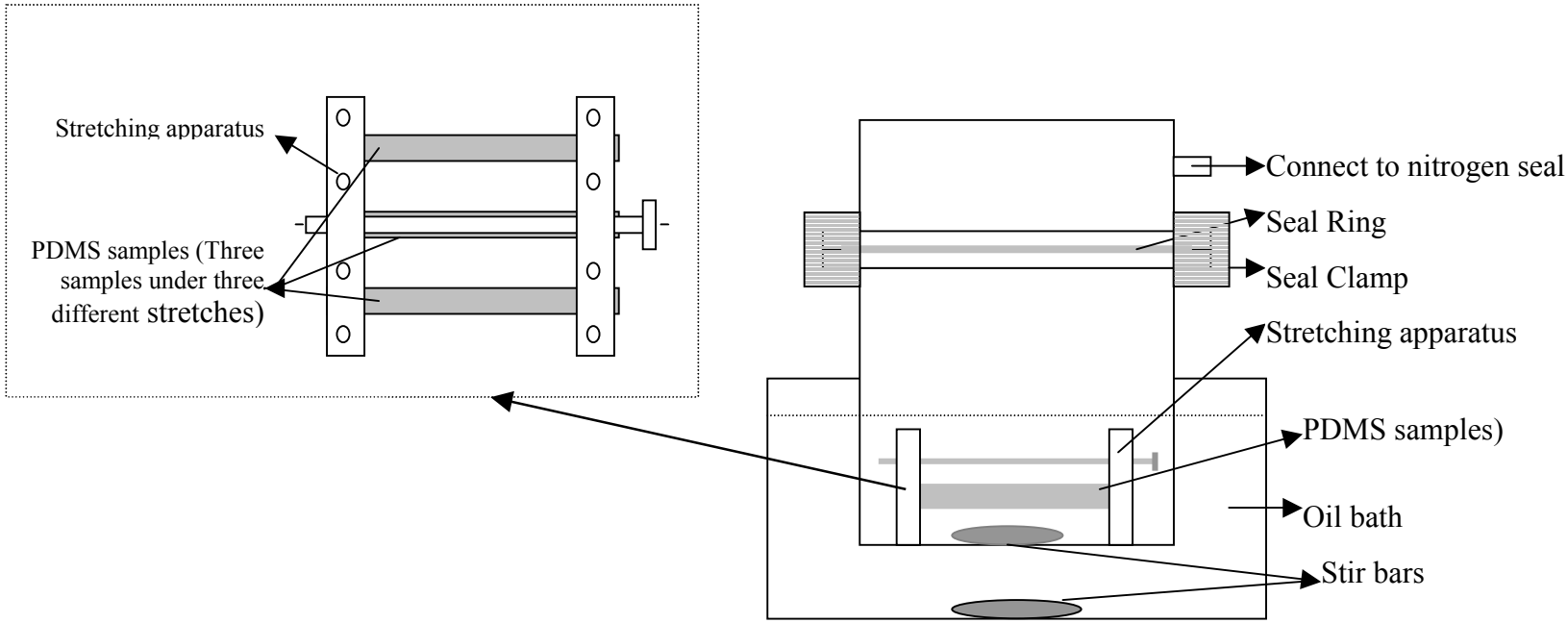

Figure 7.2 Experimental apparatus for surface ATRP polymerization of PAAM on stretched PDMS

7.4 Experimental techniques

7.4.1 NEXAFS measurement

NEXAFS is used to examine the surface and bulk chemistry (including bond densities) of the samples. NEXAFS involves the resonant soft x-ray excitation of a K or L shell electron to an unoccupied low-lying antibonding molecular orbital of σ symmetry, σ*, or π symmetry, π*.[22] The initial state K shell excitation gives NEXAFS its element specificity, while the final-state unoccupied molecular orbitals provide NEXAFS with its bonding or chemical selectivity. A measurement of the intensity of NEXAFS spectral features thus allows for the identification of chemical bonds and determination of their relative population density within the sample. The NEXAFS experiments were carried out on the NIST/Dow materials characterization end-station at the National Synchrotron Light Source at Brookhaven National Laboratory (NSLS BNL).[23] The set up at NSLS BNL is capable of detecting both the partial electron yield (PEY) and the fluorescence yield (FY) NEXAFS spectra. Thus by simultaneously collecting both the PEY and FY NEXAFS signals, whose probing depths are ≈2 and ≈100 nm, respectively, the surface and bulk chemical compositions of the sample can be probed in a single experiment.

7.4.2 FTIR-ATR measurement

Fourier transform infrared spectrometry in the attenuated total reflection (FTIR-ATR) is measured with a Digilab UMA-500 spectrometer equipped with a liquid nitrogen cooled MCT detector, Germanium Crystal and a mirror speed of 0.3 cm/s. Constant dry air flux is

applied to remove moisture in the air bag. A total of 1024 scans for each sample are collected at a resolution of 4 cm^{-1}. The IR spectra data are analyzed by the `BioRad-IR software.`

7.5 Experimental results

In Figure 7.3 we plot the PEY NEXAFS spectra taken at the nitrogen K-edge (left) and oxygen K-edge (right) of PDMS-UVO and PAAm-MAPA samples. The absence of any nitrogen signal for PDMS-UVO and strong absorption peaks detected at the nitrogen K-edge of the PAAm-MAPA samples verify that PAAm brushes are formed during the MAPA process. This finding is further supported by exploring the PEY NEXAFS spectra collected at the oxygen K-edge. While the broad peaks in the oxygen K-edge between 534 – 548 eV that are present in all spectra can be associated with various bonding environments of Si-O,[24] the peak at 531 eV corresponding to the $1s \rightarrow \pi^*_{C=O}$ transition is detected only in the PAAm-MAPA samples, providing an additional evidence for the presence of PAAm. A close inspection of the data in Fig. 7.3 reveals that the intensity of the $1s \rightarrow \pi^*_{C=O}$ transition increases with increasing Δx indicating that the density of the C=O bonds and thus the PAAm chains increases with increasing Δx, as expected. Furthermore, because no measurable nitrogen signal could be detected in the nitrogen K-edge FY NEXAFS spectra and also because the carbon K-edge and oxygen K-edge FY NEXAFS spectra are almost

indistinguishable from that of bare PDMS, the NEXAFS measurements confirmed that the PAAm brushes were present only on the sample surface and not in the bulk.

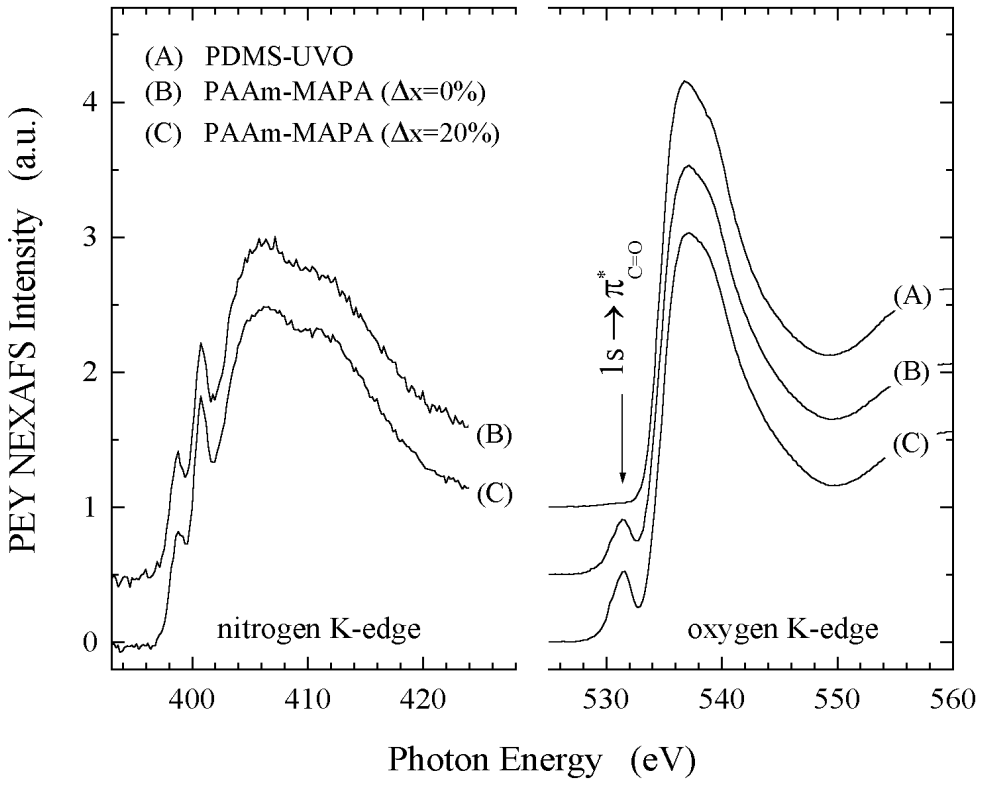

Figure 7.3 PEY NEXAFS spectra from PDMS-UVO (A), PAAm-MAPA (Δx=0%) (B), and PAAm-MAPA (Δx=20%) (C) samples. The spectra were collected at the nitrogen (left) and oxygen (right) K-edge. The arrow in the oxygen K-edge spectra indicates the position of the $1s \rightarrow \pi^*_{C=O}$ transition.

Further information about the nature of the MAPA-grown brushes can be obtained from FTIR-ATR spectra. Figure 7.4 shows FTIR-ATR spectra of collected from unstretched samples with different polymerization times (12 hr, 24 hr, and 48 hr). PDMS treated with UVO is used for comparison. Figure 7.5 shows the measurements on PDMS-UVO and MAPA-PAAm samples prepared by "MAPA" with Δx equal to 0%, 10% and 20% (top to bottom). All FTIR-ATR spectra were normalized to the Si-CH_3 deformation mode at 1414 cm^{-1}.[25] Inspection of the data reveals that there are several characteristic peaks in the FTIR-ATR spectra. Following previous studies on PAAm, we attribute the 1668 cm^{-1} and 1616 cm^{-1} signals to the symmetric anhydride C=O stretching mode, and the combination of the C-N stretching/N-H deformation modes, respectively.[25] Moreover, the bands at 3335, 3200 cm^{-1} are assigned to the asymmetric and symmetric N-H stretching modes of the amide functionality, respectively.[25]

From Fig. 7.4, the strong intensities at 1668 cm^{-1} and 1616 cm^{-1} and the appearances of the bands at 3335, 3200 cm^{-1} are attributed from PAAm formed on PDMS surface. It illustrates that initiator CMPE can be chemically bonded onto a UVO treated PDMS surface and followed by success growth of PAAm brush on PDMS surface by using the "grafting from" technique. In addition, the intensity of both the C=O and N-H stretching modes increases with increasing polymerization time, which is due to the increase of PAAm molecular weight. It further confirms that this ATRP reaction system is applicable for PAAm polymerization on PDMS surface.

The spectra of PDMS-MAPA samples with Δx = 0%, 10%, 20% also clearly show the strong characteristic peaks of PAAm, as shown in Fig. 7.5, which confirm the exists of

polymer. And the intensity of both the C=O and N-H stretching modes increases with increasing Δx. This result thus demonstrates unambiguously that the polyacrylamide grafting density at the PDMS-UVO substrate increases with increasing elongation on the untreated elastic substrate.

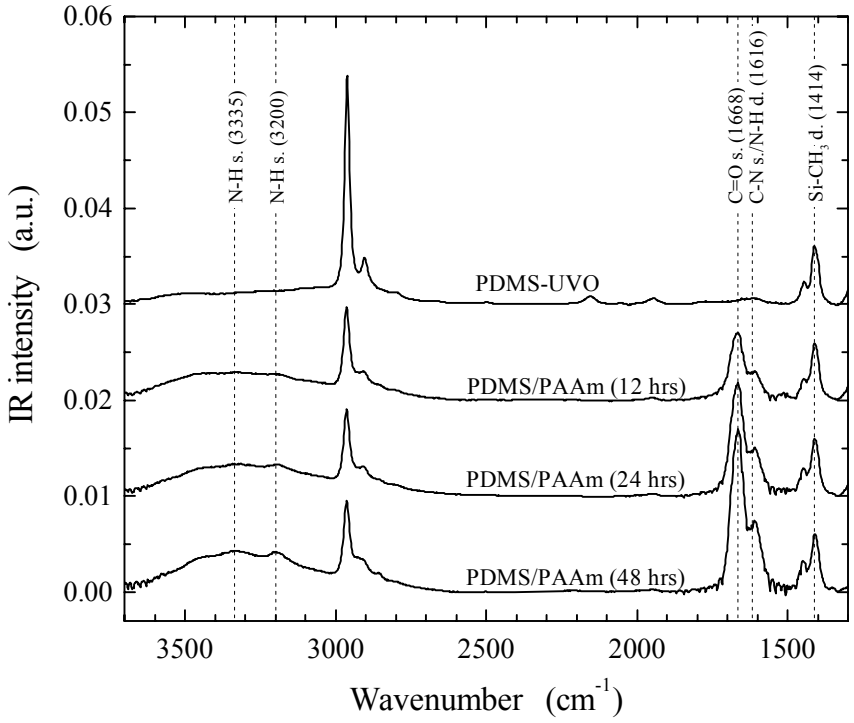

Figure 7.4 ATR-FTIR spectra from PDMS-UVO and PAAm-PDMS (Δx=0%) at reaction time 12hr, 24hr and 48hr. A total of 1024 ATR-FTIR scans was collected with a resolution of 4 cm^{-1} and normalized to the Si-CH_3 deformation signal at 1414 cm^{-1}.

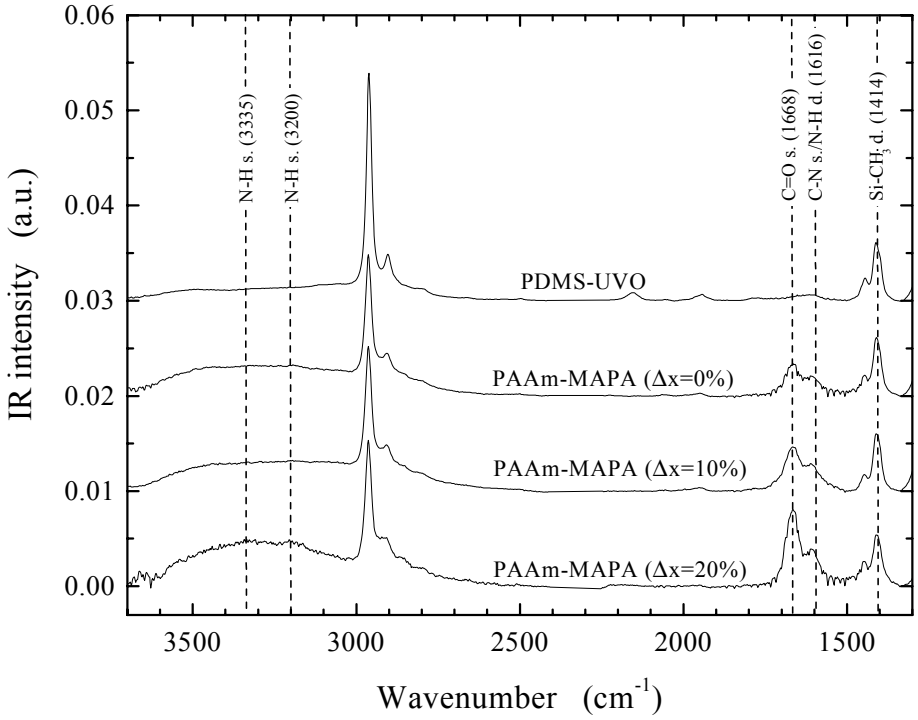

Figure 7.5 ATR-FTIR spectra from PDMS-UVO, PAAm-MAPA (Δx=0%), PAAm-MAPA (Δx=10%), and PAAm-MAPA (Δx=20%) samples. A total of 1024 ATR-FTIR scans was collected with a resolution of 4 cm^{-1} and normalized to the Si-CH_3 deformation signal at 1414 cm^{-1}.

7.6 Discussion

While more work is needed to further characterize the physico-chemical characteristics of polymer brushes grown by MAPA, the results clearly indicate that the MAPA method offers a unique and extremely simple means of tailoring the molecular

properties of polymer brushes. Realizing that PDMS behaves as an ideal elastic material, the grafting density of the initiators, and thus the polymer brush grafting density is directly proportional to Δx and can be varied smoothly (and with high precision) over a wide range. We predict that polymer brushes with extremely high grafting densities, higher than can be achieved using any other technique, can be successfully prepared by MAPA.

In summary, this part of work illustrates the principles of MAPA on preparing dense polymer brushes of polyacrylamide (PAAm). FTIR-ATR and NEXAFS results show that PAAm has been synthesized on PDMS surface with ATRP graft from technique. Grafting density of polymers on substrate increases with increasing the elongation amount Δx of the substrate.

Acknowledgements. This research was supported by the NCSU COE start-up funds and the NSF CAREER award, Grant No. DMR98-75256. NEXAFS experiments were carried out at the National Synchrotron Light Source, Brookhaven National Laboratory, which is supported by the U. S. Department of Energy, Division of Materials Sciences and Division of Chemical Sciences. The authors thank Dr. Daniel Fischer (NIST/BNL) for his assistance during the course of the NEXAFS experiments. We also thank Professor Stefan Franzen (NCSU, Chemistry) for allowing us to use his FTIR-ATR spectrometer.

References and notes

[1] deGennes, P. G., *J. Physique* **37**, 1445 (1976); *Macromolecules* **13**, 1069 (1980)**,** Alexander, S., *J. Physique* **38**, 983 **(**1977).

[2] Milner, S. T., *Science* **251**, 905 (1991).

[3] Halperin, A.; Tirrell, M. and Lodge, T. P., *Adv. Polym. Sci.* **100**, 31 (1992).

[4] Fleer, G. J.; Cohen Stuart, M. A.; Scheutjens, J. M. H. M.; Cosgrove, T. and Vincent, B. *Polymers at interfaces*; Chapman & Hall: London, 1993.

[5] Tsubokawa, N., Shirai, Y. and Hashimoto, K., *Colloid Polym. Sci.* **273**, 1049 (1995), Tsubokawa, N. and Satoh, M., *J. Appl. Polym. Sci.* **65**, 2165 (1997).

[6] Zaremski, M. Y. et al*., J. Macromol. Sci. Pure* **A33**, 237 (1996).

[7] Luzinov, I. et al., *Macromolecules* **31**, 3945 (1998).

[8] Prucker, O. and Rühe, J., *Macromolecules* **31**, 592 (1998); *Langmuir* **14**, 6893; (1998) Biesalski, M. and Rühe, J., *Macromolecules* **32**, 2309 (1999), Stohr, T. and Rühe, J., *Macromolecules* **33**, 4501 (2000).

[9] Velten, U. et al., *Macromolecules* **32**, 3590 (1999).

[10] Fujiki, K. et al., *J. Polym. Sci. Pol. Chem.* **37**, 2121 (1999).

[11] Minko, S. et al., *Macromolecules* **32**, 4525 (1999); *ibid* **32**, 4532 (1999).

[12] Matyjaszewski, K., *Controlled radical polymerization*: ACS Symposium Series 685, American Chemical Society: Washington, D.C, 1998,.

[13] Patten, T. E. et al., *Science* **272**, 866 (1996).

[14] Patten, T. E. and Matyjaszewski, K., *Adv. Mater,* **10**, 901 (1998).

[15] Matyjaszeswski, K. and Xia, J. Chem. Rev. **101**, 2921 (2001).

[16] Ejaz, M. et al., *Macromolecules* **31**, 5934 (1998).

[17] Yamamoto, S. et al., *Macromolecules* **33**, 5602 (2000).

[18] Shah, R. R. et al., *Macromolecules* **33**, 597 (2000).

[19] Genzer, J. and Efimenko, K. *Science* **290**, 2130 (2000).

[20] Efimenko, K.; Wallace, W. E. and Genzer, J., *J. Colloid and Interface Sci.* **254,** 306 (2002).

[21] Huang, X.; Doneski, L. J. and Wirth, M. J., *Chemtech* **Dec 1998**, 19; *Anal. Chem*., **70**, 4023 (1998); Huang, X. and Wirth, M. J., *Macromolecules*, **32**, 1694 (1999).

[22] Stöhr, J. *NEXAFS Spectroscopy*; Springer-Verlag: Berlin, (1992).

[23] For the description of the NSLS BNL U7A beamline see: Genzer, J. et al., *Langmuir* **16**, 1993 (2000); *Macromolecules* **33**, 1882 (2000).

[24] Urquhart, S. et al., *Organometalics* **16**, 2080 (1997).

[25] Gaboury, S. R. and Urban, M. W., *Langmuir* **3**, 3225 (1993).

Chapter 8

Outlook

8.1 Future work on for surface polymer gradients

The major theme of this Thesis was to develop methodologies leading to production of surface-anchored polymer assemblies on solid substrates. We have demonstrated that one can create 3-dimensional polymeric structures on substrates and that the gradual variation of the grafting density offers a convenient alternative to the existing traditional patterning technologies, such a soft lithography. In Chapters 5 and 6, we have also shown that the multivariant nature of the substrate can be conveniently suited to explore the behavior of surface-grafted neutral (polyacryamide) and weak polyelectrolyte (polyacrylic acid) polymers.

While the techniques as developed are quite robust and provide reproducible data, there are several aspects of the preparation procedures that can still be improved upon. First, we suggest modifying the vapor phase diffusion technique that was used to create the molecular gradients of the ATRP initiator on the silica surface. Those experiments were carried in a Petri-dish under ambient conditions. Both the humidity and temperature are known to affect the molecular diffusion and grafting of the silane molecules to the substrate. Hence, controlling the grafting conditions by performing the experiments in a chamber that maintains the humidity, temperature and pressure constant would improve the repeatability and further tunability of gradient profiles.

The next suggestion pertains to the measurement of the polymer thickness on the substrate. Both dry and wet polymer thicknesses were measured along the substrate by manually moving the sample after each measurement. This procedure is quite tedious and it limits the precise determination of the position on the sample (particularly for the wet

thickness measurements that have to be performed in a solution cell). If a moving stage with a precise motion control were installed, it would enhance the accuracy of the position measurements. Moreover, the ellipsometry measurements could be processed continuously along the substrate, which will provide more detailed information about the gradient properties and will ultimately simplify the data analysis.

When analyzing the properties of the polymer gradient substrates, we always assumed that all the polymers along the gradient have the same molecular weight. Jones and coworkers recently reported on studies of grafting from polymerization of poly(methyl methacrylate) using ATRP from substrates having various surface densities of the polymerization initiator, ω-mercaptoundecyl bromoisobutyrate.[1] Their study revealed that the grafting density of the polymer depends on the grafting density of the initiator. However, based on the data presented in Ref. 1 it is uneasy to discern whether the kinetics of the polymerization also depends on the grafting density of the initiator. Right now, we do not have a good method to directly measure the polymer weight on the substrate because the amount of polymer on the substrate is insufficient for analysis even using mass spectrometry (MALDI-TOF), which typically requires only minute amounts of the analyzed material. Huck and coworkers offered to solve the problem by synthesizing the polymer on multiple large (4" diameter) silica wafers and analyzing the polymer molecular weight using the SEC. We fear that such an approach would be a big challenge and will possibly introduce severe errors into the data analysis. Another way to proceed is to use flat porous silica as a substrate. Such substrates can be conveniently prepared by photochemical etching of silicon.[2,3] The polymer brush gradient will then be created using the same methodology as outlined in this Thesis. However, due to the enlarged area below the substrate, one should be

able to synthesize a sufficient amount of polymer that can subsequently be analyzed using MALDI-TOF.

8.2 Applications of surface polymer gradients

The dual nature of molecular gradients (discrete on a microscale and continuous on a macroscale) endows them with unique properties that can and will be further exploited in other scientific and industrial applications, such as in nanotechnology and biology study. The following are two application examples, which would use these 3-dimension polymer gradient structures as the templates.

8.2.1 Study of nanoparticle organization inside polymer brushes

The production of structures comprising organized arrays of nanoparticles embedded in material matrices represents one of the most important challenges facing today's materials scientists and engineers. The macroscopic properties of the nanoparticle-based composites will reflect both the physical characteristics which are specific to nanoobjects (*e.g.*, the ability to form ferromagnetic monodomains, optical microcavities or to generate third order harmonic optical waves) and those which are characteristic of large mesh periodic structure of the nanoparticles in the matrix (*e.g.*, a possible coherent response to electromagnetic radiation). From a technological point of view, the unusual optical, electric, magnetic, adsorption, and other important materials characteristics of nanoparticle/matrix hybrids can

be utilized in a large variety of applications, including high-density information storage media, magnetic fluids, medical diagnostics, molecular semiconductors, selective membranes and catalysts, *etc*

Recent reports shown that polymer brushes could be used to direct organization of nanoparticles on the surface.[4,5] The combination of poly(ethylene oxide) brush and silica particles was used as an interesting model system to study the brush-particle interaction.[4] Organization of gold nanocrystal in polymer brushes was investigated to explore the new approaches for modification of macroscopic surface with nanoscopic particles.[5] While some initial experiments have appeared, lot of work remains to be done. Due to the growing interest in nanotechnology, more basic scientific understanding about the structure and properties of nanoparticles in polymer brushes is needed.

With our new technique, we would be able to prepare 3D polymer/nanoparticle composites in which the particle density and their spatial distribution is controlled by adjusting the molecular properties of the polymer on the surface (grafting density) and the length of the polymer. Recent theoretical work[6] provides some guidance about the conditions under which the polymer brushes can be "doped" with nanoparticles. Based on Kim and O'Shaughnessy's prediction, the particles would either have to be relatively small in order to overcome the unfavorable entropic barrier imposed by the brush, or the particle/polymer interaction would have to be increased dramatically. We envision that the latter route can be conveniently achieved by using charged particles and polyelectrolyte brushes. If weak polyelectrolytes are used, additional tunability can be achieved as the behavior in such system is expected to depend strongly on the pH and the amount of the

external salt. We believe that such nanoparticle/polymer composite gradients will soon be generated and that such structures will find potential uses as, for example, sensors.

8.2.2 Applications in biology and medical study

A recent review summarizes the progress in the application of gradient substrates in studies of cellular interaction phenomena up until 1997.[7] Gradient surfaces are especially useful to study biological interactions along their lengths, as the influence of the entire wettability spectrum upon protein adsorption or cellular interactions can be obtained in one single experiment, therewith minimizing biological variations.

Most experiments are limited to the gradient surfaces created by small molecules with different chemistry. It has been recognized that immobilization of proteins and peptides on the surface of a material offers a powerful method of probing cell response and migration, biodetection, and activity control. The need for such well-defined surfaces as well as the requirement of reducing the number of specimens necessary for these studies has stimulated the development of methodologies providing gradients of biological macromolecules. Our technique could provide a convenient way to prepare such gradients.

This technique also could be applied to drug discovery and drug delivery. Drugs coated with biodegradable polymers would be more effective, if they could target the specific cell or human body part, which requires information about the coated polymer layer structures responding to the cell absorption or need synthesis of new biomaterials. Utilizing macromolecular gradients also will provide simple means of mimicking molecular and biomolecular transport.

8.3 MAPA further research and applications

Future work on MAPA could involve switching from the uniaxial stretching of the PDMS substrate to biaxial stretching, or even using different elastic substrates, such as polyisoprene networks. Also the possibility of using a solvent as the swelling ("stretching") agent could be explored. One way to directly prove that MAPA could produce higher density of polymer on surface is to measure the amount of the grafted polymer, so it could be compared to the amount prepared from traditional methods.

For the applications of the MAPA technique, coating would be one of the areas where MAPA technique could be applied. With the higher grafting density, coated polymer layer would provide better anti-corrosion and protection for the substrate surface. Biology and biomedical researchers can also use this technique for cell adsorption or molecular recognition. For example, study of the grafting density effects on cell absorption could be easily carried out by simply stretching or releasing the substrates on which the polymers were grafted.

References

[1] Jones, D. M.; Brown, A. A. and Huck W. T. S. *Langmuir* **18**, 1265 (2002).

[2] Smith, R. L.; Chuang, S. F. and Collins, S. D. *Sensors and Actuators: Part A - Physical Sensors* **23**, 825, (1990).

[3] Zangooie, S.; Jansson, R. and Arwin, H. *Appl. Surf. Sci.* **136**, 123 (1998).

[4] Gage, R. A.; Currie, E. P. K., and Cohen Stuart, M. A. *Macromolecules*, **34**, 5078 (2001).

[5] Liu, Z.; Pappacena, K.; Cerise, J.; Kim, J. Durning, C. J.; O'Shaughnessy, B. and Levicky, R. *Nano Lett.* **2**, 219 (2002).

[6] Kim, J. and O'Shaughnessy, B. O., *Phys. Rev. Lett.* **89**, 238301 (2002).

[7] Ruardy, T. G.; Schakenraad, J. M.; van der Mei, H. C.; Busscher, H. J. *Surf. Sci. Rep.* **29**, 1 (1997).